

AD-A265 274



October 1992

THESIS

Modeling Present and Future River Runoff Using Global
Atmospheric Models

Captain Scott C. Van Blarcum

AFIT Student Attending: State University of New Jersey AFIT/CI/CIA-92115

AFIT/CI
Wright-Patterson AFB OH 45433-6583

Approved for Public Release IAW 190-1
Distributed Unlimited
ERNEST A. HAYGOOD, Captain, USAF
Executive Officer

S DTIC
ELECTE
MAY 28 1993
E D

**MODELING PRESENT AND FUTURE RIVER RUNOFF USING
GLOBAL ATMOSPHERIC MODELS**

BY SCOTT C. VAN BLARCUM

A thesis submitted to the

Graduate School-New Brunswick

Rutgers, The State University of New Jersey

in partial fulfillment of the requirements

for the degree of

Master of Science

Graduate Program in Meteorology and Physical Oceanography

Written under the direction of

Dr. James Miller

and approved by

James R. Miller
David A. Robinson

New Brunswick, New Jersey

October, 1992

Accession For	
NTIS CRA&I	<input checked="" type="checkbox"/>
DTIC TAB	<input type="checkbox"/>
Unannounced	<input type="checkbox"/>
Justification
By	
Distribution /	
Availability Codes	
Dist	Avail and/or Special
A-1	

DTIC QUALITY INSPECTED

93 6 03 020

93-12509



ABSTRACT OF THE THESIS

**Modeling Present and Future River Runoff Using
Global Atmospheric Models**

by **SCOTT C. VAN BLARCUM**

Thesis Director:
Dr. James Miller

A global atmospheric model is used to calculate the monthly river runoff for 30 of the world's major rivers for the present climate and for a doubled CO₂ climate. The model has a horizontal resolution of 4° X 5°, but the runoff from each model box is quartered and added to the appropriate river drainage basin on a 2° X 2.5° resolution. A new routing scheme is used to allow runoff calculated for a particular grid box to flow to an adjacent downstream grid box and ultimately to the mouth of the river. The total instantaneous runoff leads runoff at the mouth by one to two months. The model-generated runoff at the mouth is compared to observations for several different simulations. The runoff peaks of high-latitude rivers are due to spring snow melt and there is a time lag between when the snow melts and when the melt water reaches the mouth. The new routing scheme allows the calculation of runoff at any location in the river basin. Model-generated river runoff and precipitation for the Mississippi River and its tributaries are analyzed for the present climate, where annual precipitation is within 5% of the observed precipitation. However, model-generated monthly precipitation is too high in the spring and too low in the summer and fall. In a model simulation with doubled CO₂, river runoff increases for 27 of the 30 rivers and in most cases coincides with increased precipitation. All high-latitude rivers show an increase in precipitation and runoff with a shift in the runoff maximum, approximately one month earlier, due to an earlier snow melt season. In a doubled CO₂ climate, snow mass decreases for mid and high-latitude rivers in North America and northwestern Asia, but increases for rivers in northeastern Asia, where observed winter temperatures average -30° to -50° C.

ACKNOWLEDGMENTS

I want to thank Dr. James Miller of Rutgers University, for his guidance and support throughout the course of this study. I also would like to thank Dr. Roni Avissar and Dr. David Robinson of Rutgers University for their support and many useful suggestions. I wish to extend my thanks to Gary Russell of the Goddard Institute for Space Studies for providing the model-generated runoff and precipitation. Finally, I would like to thank my family and especially my wife Louann, son Gregory, and daughter Amy, for their love and support throughout my course of study and career in the United States Air Force.

This study is dedicated to my mother and father.

Table of Contents

Title Page.....	i
Abstract of Thesis.....	ii
Acknowledgments.....	iii
Table of Contents.....	iv
List of Tables.....	v
List of Figures.....	vi
1. Introduction.....	1
2. Atmospheric and Hydrologic Models.....	5
a. Model description.....	5
b. River routing scheme.....	9
3. Monthly River Runoff and Precipitation.....	12
a. Observed runoff and precipitation.....	13
b. River runoff for the world's major rivers.....	14
4. Mississippi River Basin.....	34
5. Changes in Monthly River Runoff in a Doubled CO ₂ Climate.....	44
6. Summary and Conclusions.....	78
Appendix: Tables of monthly statistics for each river basin.....	83
References.....	114

List of Tables

Table Number	Page Number
3.1. Comparison of the different model simulations. In the text, model simulations are referred to by the model number in the first column.	12
3.2. Annual observed and model-generated runoff (Km^3/yr) and precipitation (Km^3/yr) for the world's major rivers for several different model simulations.	19
4.1. Model and observed drainage basin areas (Km^3) for the Mississippi River and its tributaries. The last column is the ratio of the model to the observed drainage area.	35
4.2. Seasonal model-generated snow mass (Km^3) averaged over fall, winter, and spring for the Mississippi River and its tributaries for the present climate.	38
5.1. Annual observed and model-generated runoff (Km^3/yr) and precipitation (Km^3/yr) for the world's major rivers for the present climate (1XCO_2) and the doubled CO_2 climate (2XCO_2). Change from 1XCO_2 to 2XCO_2 is given by the % change column.	52
5.2. Model and observed drainage basin areas (Km^2) for the world's major rivers. The ratio is defined as the model to observed ratio.	53
5.3. Seasonal model-generated snow mass (Km^3) averaged over fall, winter, and spring for the world's major rivers for the present climate (1XCO_2). Change from 1XCO_2 to 2XCO_2 is given by the % change column.	54

List of Figures

Figure Number	Page Number
3.1. Drainage basin locations of the rivers used in this study. Black dots indicate the approximate location of the river basin's mouth.	20
3.2. Observed monthly precipitation from <i>Legates and Willmott</i> [1990] and <i>Shea</i> [1986] for the (a) Amazon, (b) Congo, (c) Orinoco, (d) Mekong, (e) Magdalena, and (f) Sao Francisco rivers.	21
3.3. Observed monthly precipitation from <i>Legates and Willmott</i> [1990] and <i>Shea</i> [1986] for the (a) Yangtze, (b) Zambesi, (c) Mississippi, (d) Nile, (e) LaPlata (Parana), and (f) Niger rivers.	22
3.4. Observed monthly precipitation from <i>Legates and Willmott</i> [1990] and <i>Shea</i> [1986] for the (a) Indus, (b) Yellow, (c) Tigris-Euphrates, (d) Murray, and (e) Colorado rivers.	23
3.5. Observed monthly precipitation from <i>Legates and Willmott</i> [1990] and <i>Shea</i> [1986] for the (a) Mackenzie, (b) Severnaya Dvina, (c) Ob, (d) Amur, (e) Lena, and (f) Yenesei rivers.	24
3.6. Model-generated (M) and observed (O) precipitation and river runoff for the (a) Congo and (b) Mekong rivers. R_{tot} is model river runoff averaged over the entire river basin while R_m is model river runoff at the mouth using the new routing scheme. Observed precipitation is from <i>Legates and Willmott</i> [1990] and observed runoff is from <i>UNESCO</i> [1969, 1974, 1985].	25
3.7. Model-generated (M) and observed (O) precipitation and river runoff for the (a) Mississippi and (b) Yangtze rivers. R_{tot} is model river runoff averaged over the entire river basin while R_m is model river runoff at the mouth using the new routing scheme. Observed precipitation is from <i>Legates and Willmott</i> [1990] and observed runoff is from <i>UNESCO</i> [1969, 1974, 1985].	26

- 3.8. Model-generated (M) and observed (O) precipitation and river runoff for the (a) Indus and (b) Yellow rivers. R_{tot} is model river runoff averaged over the entire river basin while R_m is model river runoff at the mouth using the new routing scheme. Observed precipitation is from *Legates and Willmott* [1990] and observed runoff is from *UNESCO* [1969, 1974, 1985]. 27
- 3.9. Model-generated (M) and observed (O) precipitation and river runoff for the (a) Yenesei and (b) Amur rivers. R_{tot} is model river runoff averaged over the entire river basin while R_m is model river runoff at the mouth using the new routing scheme. Observed precipitation is from *Legates and Willmott* [1990] and observed runoff is from *UNESCO* [1969, 1974, 1985]. 28
- 3.10. Model-generated (A51, B100, C003, 848) and observed precipitation and river runoff for the Congo River. Observed precipitation is from *Legates and Willmott* [1990] and observed runoff is from *UNESCO* [1969, 1974, 1985]. A51, B100, C003, and 848 refer to the simulations shown in Table 3.1. River runoff, R_{tot} , is averaged over the entire river basin. 29
- 3.11. Model-generated (A51, B100, C003, 848) and observed precipitation and river runoff for the Mississippi River. Observed precipitation is from *Legates and Willmott* [1990] and observed runoff is from *UNESCO* [1969, 1974, 1985]. A51, B100, C003, and 848 refer to the simulations shown in Table 3.1. River runoff, R_{tot} , is averaged over the entire river basin. 30
- 3.12. Model-generated (A51, B100, C003, 848) and observed precipitation and river runoff for the Indus River. Observed precipitation is from *Legates and Willmott* [1990] and observed runoff is from *UNESCO* [1969, 1974, 1985]. A51, B100, C003, and 848 refer to the simulations shown in Table 3.1. River runoff, R_{tot} , is averaged over the entire river basin. 31
- 3.13. Model-generated (A51, B100, C003, 848) and observed precipitation and river runoff for the Yenesei River. Observed precipitation is from *Legates and Willmott* [1990] and observed runoff is from *UNESCO* [1969, 1974, 1985]. A51, B100, C003, and 848 refer to the simulations shown in Table 3.1. River runoff, R_{tot} , is averaged over the entire river basin. 32
- 3.14. Monthly model-generated (M) and observed (O) precipitation and river runoff and cumulative model-generated (M_c) and observed (O_c) precipitation and river runoff for the (a) Mississippi and (b) Lena rivers. Observed precipitation is from *Legates and Willmott* [1990] and observed runoff is from *UNESCO* [1969, 1974, 1985]. River runoff, R_m , is measured at the mouth. 33

4.1. A 2° X 2.5° grid map of the Mississippi River basin and its tributaries, Missouri, Illinois, Ohio, and Arkansas rivers. The arrows indicate the downstream flow of the river runoff and the numbers are latitude and longitude.	40
4.2. Observed and model-generated monthly precipitation and runoff for the (a) Mississippi River at Keokuk, Iowa, (b) Illinois River, and (c) Missouri River. Observed precipitation is from <i>Legates and Willmott</i> [1990] and observed runoff is from the <i>US Geological Survey</i> .	41
4.3. Observed and model-generated monthly precipitation and runoff for the (a) Mississippi River at St Louis, Missouri, (b) Ohio River, and (c) Arkansas River. Observed precipitation is from <i>Legates and Willmott</i> [1990] and observed runoff is from the <i>US Geological Survey</i> .	42
4.4. Observed and model-generated monthly precipitation and runoff for the Mississippi River at Vicksburg, Mississippi. Observed precipitation is from <i>Legates and Willmott</i> [1990] and observed runoff is from the <i>US Geological Survey</i> .	43
5.1. Comparison between model-generated mean annual precipitation and runoff for the present and doubled CO ₂ climates and the observed precipitation from <i>Legates and Willmott</i> [1990] and runoff from <i>UNESCO</i> [1969, 1974, 1985] for (a) wet river basins and (b) moderately wet river basins.	55
5.2. Comparison between model-generated mean annual precipitation and runoff for the present and doubled CO ₂ climates and the observed precipitation from <i>Legates and Willmott</i> [1990] and runoff from <i>UNESCO</i> [1969, 1974, 1985] for (a) dry and (b) high-latitude dry river basins.	56
5.3a. Model-generated precipitation and runoff seasonal changes for the wet river basins in the doubled CO ₂ climate for Dec, Jan, Feb (DJF), Mar, Apr, May (MAM), Jun, Jul, Aug (JJA), and Sep, Oct, Nov (SON).	57
5.3b. Model-generated precipitation and runoff seasonal changes for the moderately wet river basins in the doubled CO ₂ climate for Dec, Jan, Feb (DJF), Mar, Apr, May (MAM), Jun, Jul, Aug (JJA), and Sep, Oct, Nov (SON).	58
5.3c. Model-generated precipitation and runoff seasonal changes for the dry river basins in the doubled CO ₂ climate for Dec, Jan, Feb (DJF), Mar, Apr, May (MAM), Jun, Jul, Aug (JJA), and Sep, Oct, Nov (SON).	59

5.3d. Model-generated precipitation and runoff seasonal changes for the high-latitude dry river basins in the doubled CO ₂ climate for Dec, Jan, Feb (DJF), Mar, Apr, May (MAM), Jun, Jul, Aug (JJA), and Sep, Oct, Nov (SON).	60
5.4. Model-generated monthly precipitation and runoff for the present [M(1)] and doubled CO ₂ [M(2)] climates and observed [O] precipitation from <i>Legates and Willmott</i> [1990] and runoff from <i>UNESCO</i> [1969, 1974, 1985] for the (a) Amazon and (b) Congo rivers.	61
5.5. Model-generated monthly precipitation and runoff for the present [M(1)] and doubled CO ₂ [M(2)] climates and observed [O] precipitation from <i>Legates and Willmott</i> [1990] and runoff from <i>UNESCO</i> [1969, 1974, 1985] for the (a) Orinoco and (b) Sao Francisco rivers.	62
5.6. Model-generated monthly precipitation, runoff, and averaged snow mass during the snow season for the present [M(1)] and doubled CO ₂ [M(2)] climates and observed [O] precipitation from <i>Legates and Willmott</i> [1990] and runoff from <i>UNESCO</i> [1969, 1974, 1985] for the Mekong River.	63
5.7. Model-generated monthly precipitation, runoff, and averaged snow mass during the snow season for the present [M(1)] and doubled CO ₂ [M(2)] climates and observed [O] precipitation from <i>Legates and Willmott</i> [1990] and runoff from <i>UNESCO</i> [1969, 1974, 1985] for the (a) Mississippi and (b) Yangtze rivers.	64
5.8. Model-generated monthly precipitation and runoff for the present [M(1)] and doubled CO ₂ [M(2)] climates and observed [O] precipitation from <i>Legates and Willmott</i> [1990] and runoff from <i>UNESCO</i> [1969, 1974, 1985] for the (a) Niger and (b) La Plata (Parana) rivers. Observed runoff stations are not near the mouth of the river.	65
5.9. Model-generated monthly precipitation and runoff for the present [M(1)] and doubled CO ₂ [M(2)] climates and observed [O] precipitation from <i>Legates and Willmott</i> [1990] and runoff from <i>UNESCO</i> [1969, 1974, 1985] for the (a) Zambesi and (b) Nile rivers. Observed runoff station for the Nile is not near the mouth of the river.	66

5.10. Model-generated monthly precipitation, runoff, and averaged snow mass during the snow season for the present [M(1)] and doubled CO ₂ [M(2)] climates and observed [O] precipitation from <i>Legates and Willmott</i> [1990] and runoff from <i>UNESCO</i> [1969, 1974, 1985] for the (a) Yellow and (b) Colorado rivers.	67
5.11. Model-generated monthly precipitation and runoff for the present [M(1)] and doubled CO ₂ [M(2)] climates and observed [O] precipitation from <i>Legates and Willmott</i> [1990] and runoff from <i>UNESCO</i> [1969, 1974, 1985] for the (a) Tigris-Euphrates and (b) Murray rivers. Observed runoff station for the Tigris-Euphrates is not near the mouth of the river.	68
5.12. Model-generated monthly precipitation, runoff, and averaged snow mass during the snow season for the present [M(1)] and doubled CO ₂ [M(2)] climates and observed [O] precipitation from <i>Legates and Willmott</i> [1990] and runoff from <i>UNESCO</i> [1969, 1974, 1985] for the (a) Yukon and (b) Mackenzie rivers.	69
5.13. Model-generated monthly precipitation, runoff, and averaged snow mass during the snow season for the present [M(1)] and doubled CO ₂ [M(2)] climates and observed [O] precipitation from <i>Legates and Willmott</i> [1990] and runoff from <i>UNESCO</i> [1969, 1974, 1985] for the (a) Severnaya Dvina and (b) Ob rivers.	70
5.14. Model-generated monthly precipitation, runoff, and averaged snow mass during the snow season for the present [M(1)] and doubled CO ₂ [M(2)] climates and observed [O] precipitation from <i>Legates and Willmott</i> [1990] and runoff from <i>UNESCO</i> [1969, 1974, 1985] for the (a) Yenesei and (b) Lena rivers.	71
5.15. Model-generated monthly precipitation, runoff, and averaged snow mass during the snow season for the present [M(1)] and doubled CO ₂ [M(2)] climates and observed [O] precipitation from <i>Legates and Willmott</i> [1990] and runoff from <i>UNESCO</i> [1969, 1974, 1985] for the (a) Kolyma and (b) Indigirka rivers.	72
5.16. Model-generated monthly precipitation, runoff, and averaged snow mass during the snow season for the present [M(1)] and doubled CO ₂ [M(2)] climates and observed [O] precipitation from <i>Legates and Willmott</i> [1990] and runoff from <i>UNESCO</i> [1969, 1974, 1985] for the Amur River.	73

5.17. Model-generated monthly precipitation, runoff, and averaged snow mass during the snow season for the present [M(1)] and doubled CO ₂ [M(2)] climates and observed [O] precipitation from <i>Legates and Willmott</i> [1990] and runoff from the <i>US Geological Survey</i> for the Mississippi river at Keokuk, Iowa.	74
5.18. Model-generated monthly precipitation, runoff, and averaged snow mass during the snow season for the present [M(1)] and doubled CO ₂ [M(2)] climates and observed [O] precipitation from <i>Legates and Willmott</i> [1990] and runoff from the <i>US Geological Survey</i> for the Mississippi river at St Louis, Missouri and Vicksburg, Mississippi.	75
5.19. Model-generated monthly precipitation, runoff, and averaged snow mass during the snow season for the present [M(1)] and doubled CO ₂ [M(2)] climates and observed [O] precipitation from <i>Legates and Willmott</i> [1990] and runoff from the <i>US Geological Survey</i> for the Missouri and Arkansas rivers	76
5.20. Model-generated monthly precipitation, runoff, and averaged snow mass during the snow season for the present [M(1)] and doubled CO ₂ [M(2)] climates and observed [O] precipitation from <i>Legates and Willmott</i> [1990] and runoff from the <i>US Geological Survey</i> for the Illinois and Ohio rivers.	77

Chapter 1. Introduction

Global warming associated with the increase in greenhouse gases, such as carbon dioxide (CO₂), continues to be a major topic within the scientific and political fields. Most people associate temperature change with global warming, however, the earth's hydrologic cycle will also be affected by the increase of CO₂. Over land, the major components of the hydrologic cycle include precipitation, ground water, evapotranspiration, ice, and runoff. Runoff is generated by precipitation and snow melt. Because evaporation exceeds precipitation over the oceans, it is runoff from the land to the ocean that keeps the hydrologic cycle in equilibrium. River runoff depends on precipitation, moisture storage within the soil (dependent on evaporation, soil type, and vegetation cover), and flow rate due to topography [Thornthwaite, 1955]. The world's 20 largest rivers account for about 40% of the total continental runoff [Baumgartner and Reichel, 1975].

Several atmospheric general circulation models (GCMs) have been developed to allow detailed scientific studies of the hydrologic cycle [Hansen et al., 1983; Gordon and Stern, 1982; Manabe and Hahn, 1981; Pitcher et al., 1983; and Williamson, 1983]. Russell and Miller [1990] compared mean annual river runoff from a four-year GCM simulation with observations. Kuhl and Miller [1992] extended that work to examine monthly river runoff statistics for wet, dry, and moderately wet river basins. Potential changes in the hydrologic cycle (specifically river runoff) due to global warming will affect many areas, including agriculture, water resources, and hydroelectric power.

Potential changes in river runoff have caused hydrologists to generally focus on calculating river runoff at smaller scales (about 1 kilometer) than those considered by global atmospheric modelers. Most studies are centered around specific river basins and assess the potential changes in river runoff due to global warming. Vörösmarty et al [1989] have developed a continental drainage basin runoff scheme and applied it to the Amazon River basin using observed data as input. This is one of the first attempts to

model river runoff over much larger scales. The model allows the calculation of water volume from one grid box to another, however, the model is based on observed data and can not be used directly to calculate potential changes in river runoff due to global warming.

There are two primary methods used to study effects of global warming on river runoff using GCMs. The first method uses temperature and precipitation variables from doubled CO₂ simulations as input to a hydrologic model to produce runoff statistics. This is referred to as an off-line method. Regional river runoff changes due to global warming using the off-line method are discussed in *Gleick* [1987] and *Lettenmaier and Gan* [1990]. The off-line method can also be used to input temperature and precipitation based on scenarios from other models and studies. Several scenario studies have been developed which focus on specific river basins around the world [*Ayers et al.*, 1990; *Flasehko et al.*, 1987; and *Roos*, 1989]. The second method, which computes river runoff as part of the GCM simulation, is referred to as an on-line method. Changes in river runoff using this method are discussed in *Miller and Russell* [1992]. *Rind et al.* [1990] analyze both on-line and off-line methods with respect to drought conditions using potential evapotranspiration. They suggest that drought intensification is understated in most GCM simulations because they lack realistic land surface parameterizations.

The purpose of this thesis is to obtain a better understanding of land surface hydrology, particularly river runoff, as it is modeled in global atmospheric GCMs and examine potential changes in river runoff due to global warming using the on-line method with river runoff calculated from the Goddard Institute for Space Studies (GISS) GCM of *Hansen et al.* [1983]. This study will utilize the version of the GISS model which has a horizontal resolution of 4° latitude by 5° longitude and nine vertical layers. River runoff is calculated from several different three to five year simulations. Each of the 4° X 5° grid boxes overlays four 2° X 2.5° grid boxes which are assigned to river basins. The observed river runoff is defined as the flow rate at a certain location within the river basin. A new

river routing scheme is used to obtain runoff at various sites within the river basin. A description of the hydrology scheme used in the model and the new routing scheme will be given. The objectives follow:

1. Apply a new river routing scheme with the GISS two-layer grid point hydrology scheme and examine the monthly runoff for approximately 30 major river basins. In particular, high latitude river basins will be examined to determine how snow melt affects monthly runoff and dry river basins will be examined to learn why the runoff is poorly simulated by the model.
2. The new routing scheme which allows flow from one grid box to another will be used to simulate the runoff of the Mississippi river basin by examining the runoff of its major tributaries (Missouri, Illinois, Arkansas, and Ohio rivers).
3. Examine how monthly river runoff responds to the doubling of atmospheric carbon dioxide by examining model simulations with an emphasis on high latitude rivers dominated by spring snow melt.

River runoff and precipitation from approximately 30 river basins throughout the world representing dry, wet, and moderately wet climates as well as high, middle, and low latitudes will be examined based on several GCM simulations of the GISS model. Results discussed in *Russell and Miller* [1990], *Miller and Russell* [1992], and *Kuhl and Miller* [1992] will be extended by allowing river runoff to be routed between grid boxes within a river's drainage basin. These simulations will be used to analyze the similarities and differences between monthly runoff calculated with this new routing scheme and compared with the total monthly runoff into a river basin as in *Kuhl and Miller* [1992].

With this routing scheme in place, the components of the Mississippi river basin will be studied separately. These include the upper Mississippi River, Illinois River,

Missouri River, Ohio River, and Arkansas River. The basin will be separated into 2° X 2.5° grid boxes. The Mississippi River and its tributaries will be examined in detail by comparing model-generated and observed river runoff and precipitation at several locations.

The last objective of this thesis is to examine the effects of doubling the current atmospheric CO₂ level and to determine how this changes monthly river runoff for wet, dry, and moderately wet river basins throughout the world, particularly the impact on snow fall and snow melt for high latitude rivers. The annual results of *Miller and Russell* [1992] will be extended to examine potential seasonal changes in future runoff due to the doubled CO₂ climate. The emphasis will be on the high latitude river basins and how spring runoff, due to snow melt, changes in the doubled CO₂ climate and how the different modeling schemes simulate the peak runoff season.

For the 30 river basins in this study, precipitation and river runoff, from several different simulations will be examined. The emphasis is on the new routing scheme and climate change, particularly for high latitude rivers. The results are analyzed in the context of several other studies [*Gleick*, 1987; *Russell and Miller*, 1990; and *Kuhl and Miller*, 1992], which use both the on-line and off-line methods to calculate river runoff. Suggested improvements on how the model generates precipitation and river runoff are given.

Chapter 2. Monthly river runoff calculated from an atmospheric model

2a. Model description and hydrology

The atmospheric model used to calculate the river runoff and precipitation was developed at the NASA/Goddard Institute for Space Studies and is described by *Hansen et. al*, [1983]. This model has a horizontal resolution of 4° X 5° in latitude and longitude respectively, and a vertical resolution of nine atmospheric layers. The model simultaneously solves the equations for the conservation of mass, energy and momentum, and the equation of state on a spherical grid. Atmospheric parameters such as radiation, atmospheric gases and aerosols, cloud cover, convection, and heat and momentum are computed. Other parameters include ground temperatures, snow depth and albedo, and ground hydrology. The primitive equations, conservation of momentum (Newton's 2nd law of motion) [Eqn 2.1], conservation of mass (continuity equation) [Eqn 2.2], conservation of energy (1st law of thermodynamics) [Eqn 2.3], and the ideal gas law [Eqn 2.4], describing the state and motion of the atmosphere are solved numerically.

$$\frac{d\mathbf{V}}{dt} = -2\boldsymbol{\Omega} \times \mathbf{V} - \rho^{-1} \nabla p + \mathbf{g} + \mathbf{F} \quad (2.1)$$

$$\frac{d\rho}{dt} = -\rho \nabla \cdot \mathbf{V} + C - D \quad (2.2)$$

$$\frac{dl}{dt} = -p \frac{d\rho^{-1}}{dt} + Q \quad (2.3)$$

$$p = \rho RT \quad (2.4)$$

where \mathbf{V} is the velocity relative to the rotating earth, t is time, $\boldsymbol{\Omega}$ is the planet's angular rotation vector, ρ is the atmospheric density, \mathbf{g} is the apparent gravity [true gravity - $\boldsymbol{\Omega} \times (\boldsymbol{\Omega} \times \mathbf{r})$], \mathbf{r} is the position relative to the planet's center, \mathbf{F} is the force per unit mass, C is the rate of creation of (gaseous) atmosphere, D is the rate of destruction of atmosphere, I is the internal energy per unit mass [$c_v T$], Q is the heating rate per unit mass, R is the gas constant, T is the temperature, and $c_v T$ is the specific heat at constant volume.

The top of the dynamical atmosphere is fixed at 10mb. In the model, the nine vertical layers include two in the boundary layer, five in the troposphere, and two in the stratosphere. At the surface, grid boxes are divided into land and ocean fractions, except for the model-simulation C003, in which grid boxes are all water or all land (see Table 3.1). The land distribution and continental topography are from a corrected version of *Gates and Nelson* [1975]. Interactions between the surface and atmosphere are computed separately for each surface type.

The atmospheric model separates the soil-moisture storage into two layers described by *Hansen et al* [1983]. The upper layer responds immediately to evaporation and precipitation while the lower layer acts as a seasonal reservoir. The rate of change of moisture in the upper layer is given by

$$\frac{\partial W_1}{\partial t} = \frac{P - E - R}{f_1} + \frac{W_2 - W_1}{\tau} \quad (2.5)$$

where W_i ($i = 1$ or 2), is the ratio of available water to the field capacity (available water at saturation) of each layer, P is precipitation, E is evaporation, and R is runoff. τ is the time constant for the diffusion of moisture between the two soil layers and f_i is the field capacity. The rate of change of soil moisture storage in the lower layer is given by

$$\frac{\partial W_2}{\partial t} = \frac{f_1}{f_2} \frac{W_1 - W_2}{\tau} \quad (2.6)$$

There is a 2-day time constant for diffusion of water between the two layers, except during the growing season in which upward diffusion occurs instantly over vegetated areas. The water field capacities of the two layers depend on vegetation characteristics taken from *Matthews* [1983]. A more physically realistic formulation of the surface hydrology has been developed by *Abramopoulos et al* [1988] and will be used in future simulations with the GISS model.

The computed runoff in each grid box depends on the precipitation, evapotranspiration, and water storage within the land portion of each grid box. The evapotranspiration is calculated as the product

$$E = \beta \rho C V (q_s - q_A) \quad (2.7)$$

where β is a dimensionless efficiency factor for evapotranspiration, ρ is the surface air density, C is a dimensionless drag coefficient that depends on stability, V is the surface wind speed, q_s is the surface saturation specific humidity that depends on ground temperature and the surface pressure, and q_A is the surface air specific humidity at 10m above the surface. The partition of rainwater or meltwater between the fraction that enters and remains in the soil and the fraction moving out of the grid box depends on the soil water holding capacity and the soil moisture. The water leaving the grid box is the runoff [*Miller*, 1977]. Runoff R is calculated as

$$R = \text{maximum} \left(\frac{1}{2} P W / W_c, P + W - W_c \right) \quad (2.8)$$

where P is the precipitation, W is the water and ice in the first layer, and W_C is the water field capacity. The factor β in (2.7) is assumed to equal W/W_C unless the ground is snow covered, in which case, $\beta = 1$. The coefficient of one-half in (2.8) was chosen so that the computed mean annual global runoff is consistent with that observed [Hansen *et al*, 1983]. In the parameterization given in (2.8), no distinction is made between surface runoff and ground water runoff that leaves each grid box. Since (2.8) represents the total water removed from a grid box, it combines the water lost from the two components of runoff but without any time lag, thus, runoff occurs during precipitation and stops when the precipitation stops. Runoff is a continuous function of precipitation. In the model precipitation can be in the form of rain or snow. The snow depth for any given area is computed as the balance of snowfall, melting and sublimation [Hansen *et al*, 1983]. If the air temperature is less than 0°C, precipitation falls as snow. If the temperature of the upper layer of soil is less than or equal to 0°C, the snow depth will increase, otherwise the snow melts and the upper soil temperature decreases. The snow melt is then included in the runoff.

The drainage basins for this study were defined by Russell and Miller [1990] using the maps of Korzoun *et al* [1977] and the *Times Atlas of the World* [1967]. The model's 4° X 5° grid boxes were divided into four 2.5° X 2° grid boxes with the total area of the river drainage basin equal to the sum of the areas of the 2.5° X 2° grid boxes. If a particular grid box was assigned to a river basin, all the runoff from that grid box was assigned to the river flow. In Kuhl and Miller [1992], computed monthly runoff was defined as the sum of the runoff from each grid box within the river basin during the month. This is not the same as observed runoff, which is defined as the monthly water flow at the mouth of the river. Comparisons between model-generated runoff and observed runoff are discussed in Miller and Russell [1992] and Kuhl and Miller [1992].

2b. River routing scheme.

A river routing scheme has been developed to simulate water flow from one grid box to another. This allows a time lag in the routing of river runoff, in particular it allows one to calculate river runoff at the mouth of the river basin and more easily compare it with the observed data. The calculation of the monthly runoff in the routing scheme requires directed paths connecting grid boxes within the river basin to grid boxes which are successfully closer to the river's mouth. This is discussed in *Miller et al.* [1992]. The rate at which water moves between grid boxes depends on many factors such as the slope, the volume of the water in the river, bottom composition, shape, width, depth, and distanced traveled, of which only slope, river volume, and distanced traveled are included in the model simulations.

River direction files were created using the 2.5° X 2° resolution described in the previous section. Each grid box contains a value from 0 through 8 defining the direction of flow within a grid box. A value of zero means no flow out of the grid box. Values greater than zero means water flows out of the grid box via other rivers to an adjacent grid box downstream. A value of one represents water flow downstream to the northeast, and values from 2 through 8 represent water flow downstream to the north, northwest, west, southwest, south, southeast, and east, respectively. Direction files were extracted from world maps [*Korzoun et al.*, 1977].

Once the direction files have been established, the next step is to determine the volume of the river water in each grid box and the flow rate between each grid box. This approach is modeled after continuous streamflow simulation models discussed by *Singh* [1989]. The volume of water in a grid box after a time step Δt is given by

$$V(t + \Delta t) = V(t) + (F_{in} - F_{out})\Delta t + K_s R_s \Delta t + K_g R_g \Delta t \quad (2.9)$$

where F_{in} and F_{out} are the flow rates into and out of the grid box, K_s and K_g are rate constants for surface and ground water runoff, respectively, and R_s and R_g are reservoirs of surface and groundwater runoff. For each grid box, flow into the box can be from all directions, however, flow out of a grid box can only be in one direction and is assumed to be of the form

$$F_j = \Omega_j f(i_j) V_j \Delta y / \Delta s_j \quad (2.10)$$

where i_j is the slope of the grid box, f is a function of i_j , Ω_j (s^{-1}) is a rate coefficient, Δy is the north-south width of the grid box, and Δs_j is the distanced traveled by the river across the grid box. The subscripts indicate that the variables may differ from grid box to grid box.

The rate coefficient, Ω_j , depends on soil type and depth, characteristics of the drainage basin network, and vegetation cover, however, Ω_j will be taken as a constant independent of these variables. Equation 2.10 is based on the Muskingum method [Linsley *et al.*, 1982] and represents a simplified form of the runoff routing scheme used by Vorosmarty *et al.* [1989]. As discussed in Miller *et al.* [1992], Ω_j is dependent on grid resolution. If the grid size increases than Ω_j will decrease. Miller *et al.* [1992] have given an alternative formulation to Eqn. 2.10 in which they define a basinwide turnover rate which is independent of grid resolution.

The slope, i_j , is dimensionless and is calculated as the ratio of the height difference between the upstream and downstream grid boxes and the distanced traveled. The distanced traveled depends on the direction of flow in a grid box, east-west, north-south, or diagonally, which is found on a directional map file discussed before. If the river flows in the north-south direction, then $\Delta s_j = \Delta y$, and equation 2.10 reduces to $F_j = \Omega f(i_j) V_j$. If the flow is east-west, than the distanced traveled will decrease as one moves northward

due to the converging meridians. If the river flows diagonally, then $\Delta s_j^2 = (\Delta x_j^2 + \Delta y_j^2)$. *Miller and Russell* [1992] discuss the effects of grid box size and the direction and distance traveled.

The next step in the routing scheme is to include topography. Grid boxes with steeper channel slopes are assumed to flow faster. Variations in topography are shown in *Miller et al* [1992] for four of the rivers discussed in this paper. In this work

$$f(i_j) = \sqrt{(i_j) i_{min}} \quad (2.11)$$

where i_{min} is the minimum slope allowed for a grid box, hence, $i_{min} \leq i_j \leq i_{max}$ and $i_{min} = 20\text{m}/\Delta s$ and $i_{max} = 200\text{m}/\Delta s$.

The routing scheme described in equations 2.9 and 2.10 allows river water to move more realistically from its origin to the mouth of the river basin. It also allows one to calculate the runoff at any location on the river, the total volume of water in each grid box and in the entire river basin, and the total instantaneous runoff into the river. *Kuhl and Miller* [1992] examined monthly runoff variation of the total runoff (sum over all grid boxes) for 16 river basins. The next chapter will extend their work and compare runoff at the river mouth with the total runoff.

Chapter 3. Monthly River Runoff and Precipitation

In this chapter, monthly river runoff and precipitation generated by several different simulations with the GISS GCM are compared for several major river basins. Table 3.1 shows how the horizontal grid, sea surface temperature, and run length for the different simulations. The purpose of the comparison is to provide some insight into the sensitivity and variability of the model.

Table 3.1. Comparison of the different model simulations used in this paper. For simplicity, model simulations will be referred to by the model number shown in the first column.

Model	Horizontal Grid ¹	CO ₂ Level		Simulation Length	Climatological Sea surface temps		Fractional Grid	
		Present	Doubled		Yes	No	Yes	No
848	B	✓		5 yr	✓		✓	
B100	B	✓		5 yr	✓		✓	
C003	C	✓		5 yr	✓			✓ ²
A51	B	✓		3 yr		✓ ³	✓	
947	B		✓	3 yr		✓ ³	✓	

1. Horizontal grid system used based on *Hansen et al.* [1983]

2. Non-fractional grid. Each grid box is either all water or all land.

3. Sea surface temperatures are interpolated from equilibrium simulations at 8° X 10° resolution, in which SST were predicted in *Hansen et al.* [1984].

Several different three-year and five-year simulations are available with somewhat different model formulations for the present climate. Because of the relatively short simulations, it's not certain that the models represent long term climatology for runoff and precipitation. If all the simulations are in agreement with each other, than runoff and precipitation for the present climate should be representative of the long term ciimatology. However, if the simulaions differ, there would be less confidence in the results for that basin.

3a. Observed river runoff and precipitation

Figure 3.1 shows the location of the mouth of all rivers used for this study. The observed monthly river runoff in this study is the flow at the location nearest the mouth within the river basin and is based on UNESCO data. During the 1960's, the thirteenth General Conference of UNESCO launched the International Hydrological Decade, (IHD) 1965-1974. Part of the program focused on recording and collecting rates of river runoff at various locations within the drainage basin. The number of years used for river runoff averages vary between river basins. The majority of the river basins have more than 20 years of data, while the remaining basins contain only four years of data. The observed precipitation accumulated over the model's drainage basin area is taken from two studies, *Shea* [1986] and *Legates and Willmott* [1990].

In previous studies of *Russell and Miller* [1990], *Kuhl* [1990], *Miller and Russell* [1992], and *Kuhl and Miller* [1992], the observed precipitation was based on *Shea* [1986]. Figures 3.2-3.5 show comparisons of observed monthly precipitation between *Legates and Willmott* [1990] and *Shea* [1986] for several of the world's major river basins. For the majority of the river basins, annual precipitation between the two studies is within 10% with *Legates and Willmott* [1990] averaging slightly higher annual amounts. The greatest disparity between the two observed studies occurs in the wet climates (Figure 3.2), however, despite an increase in precipitation amounts of 30% for several of the rivers, the overall monthly variation in precipitation is similar for *Legates and Willmott* [1990] and *Shea* [1986]. This is true for all the rivers in Figures 3.2-3.5, thus, observed precipitation in the remainder of this study was taken from *Legates and Willmott* [1990], which is the more recent of the two studies and contains more observed data.

3b. River runoff for the world's major rivers

Model-generated monthly river runoff, R_{tot} , discussed in *Kuhl and Miller* [1992] was calculated by summing the runoff from each grid box over the river basin, as discussed in the previous chapter. This is different from observed runoff at the mouth of the river basin, R_m , which represents the flow of water at the mouth after the water has moved through the entire river basin, thus R_{tot} should lead R_m . A time dependent river routing scheme has been developed by *Miller et al.* [1992] to allow the calculation of model-generated river runoff anywhere in the river basin, as discussed in chapter 2. To better understand how the new routing scheme works, the B100 model was used to calculate R_m and R_{tot} . Figures 3.6-3.9 show model-generated and observed precipitation and runoff for several of the world's major river basins. The remainder of this paper will refer to river runoff at the mouth as R_m and the sum of river runoff basinwide as R_{tot} .

The timing of the model-generated runoff without the routing scheme, R_{tot} , is primarily based on the model's precipitation. As explained in chapter 2, runoff continues as long as the precipitation continues and when precipitation stops runoff stops. A good example of how the model acts without the routing scheme is in the wet climates (Figure 3.6) where there is no snowfall. Figure 3.6a shows that the variation of the precipitation for the Congo River is similar to that of R_{tot} , although precipitation is too large. Figure 3.6a shows that the maximum model-generated precipitation occurs in March and minimum model-generated precipitation occurs in July. The model-generated runoff, R_{tot} , follows the same pattern. However, for the model-generated runoff, R_m , the river runoff in March is lower and the runoff from April through July is higher at the mouth which indicates that the water contributing to the March peak in R_{tot} reaches the mouth in the following months. The opposite is true for the period August through October, the period between the minimum and next maximum precipitation, in which R_{tot} follows the same pattern as the precipitation curve, however, R_m shows the river runoff lagging behind

slowly building up for a maximum in January. The model-generated river runoff, R_m , follows the general patterns of the observed runoff. Similar results are shown in Figures 3.6b through 3.8 for the Mekong and other rivers.

The effect of the new routing scheme is illustrated best in the higher latitude river basins where snow occurs and snow melt is a major contributor to river runoff. Where snow accumulates during the winter, river runoff maxima usually occur when the snow melts during the spring and early summer. Figure 3.9 shows monthly precipitation and runoff from the Yenesei and Amur river basins located in northeastern Siberia. Although the annual variation of the model-generated precipitation is in good agreement with the observed, for both rivers, it is too high in the spring. Precipitation peaks in July the Yenesei Rivers, however, unlike the wet climates discussed before, the runoff maximum occurs prior to the precipitation maximum. This is due to the snow melt in spring and early summer. In the model the maximum snow melt occurs in March and April, with model-generated runoff peaks occurring during the same months for R_{tot} . Results are similar for the other high latitude rivers. With the routing scheme in place, model-generated runoff is allowed to flow downstream towards the mouth of the river throughout the snow melt season peaking in late spring and R_m is in reasonably good agreement with the observed

The new routing scheme simulates water moving downstream and enables modeler's to simulate the magnitude and timing of the runoff peak. The new routing scheme also allows modeler's to choose any location within the river basin and analyze the instantaneous runoff flow at that specific location. The routing scheme does not deal directly with movement of water within each grid box. This is done using the grid box hydrology scheme discussed in chapter 2. It should be noted that although the new routing scheme produces changes in the timing of the runoff peak, only monthly data exist. If daily data were available, the timing of runoff peaks would be further resolved giving modeler's a more precise tool for forecasting the magnitude and timing of river runoff.

Also of note is that the routing coefficients are constant and have not been tuned for individual river basins. There is some variation of flow rates based on topography. Optimal results may not be possible until the routing coefficients are tuned to individual basins.

The different model simulations for the present climate used in this study were listed in Table 3.1. Table 3.2 shows model-generated precipitation and runoff for 30 river basins comparing the different model simulations used in this paper along with the observed precipitation and runoff. As discussed before, longer simulations would be better for comparing model-generated river runoff with observed river runoff. Overall, all four model simulations produce too much precipitation and are in general agreement with each other more than with the observed precipitation. With the exception of the wet climate river basins, river runoff is too high for all four simulations.

The four simulations use two of the three horizontal grid schemes described in *Hansen et al.*, [1983], scheme B and scheme C. In the B and C grid schemes, the pressure gradient and velocity divergence are computed over ΔX , resulting in more accurate representation of the geostrophic adjustment [*Arakawa*, 1972]. The difference between the B and C scheme is that the winds are directly computed on grid C, but on grid B it is necessary to average the winds. Less averaging of the winds should lead to more accurate transports of heat and water with the C grid scheme. More detailed explanations on the different grid schemes are in *Hansen et al.* [1983].

Figures 3.10 through 3.13 show comparisons of model-generated precipitation and runoff for four river basins. Model generated runoff shown is R_{tot} . One interesting case is the Indus River (Fig 3.12) in which the model C003 is the only one to show a summer maximum in precipitation due to the monsoon season. The three other models have precipitation maxima in the winter months. Model C003 is the only model simulation to use a non-fractional grid. Each grid box is either water or land. Model C003 also uses the C horizontal grid scheme discussed above. These two factors may cause the difference in

the monthly precipitation in the Indus River basin. Overall, the annual model-generated precipitation and river runoff for all four simulations are within 8% and 13%, respectively, of each other. The monthly precipitation and river runoff are for the most part in agreement with one another. The only difference is the amount of precipitation and river runoff flow. The largest discrepancies occur in the dry basins, as seen with the Indus River, in which the four simulations differ in precipitation and river runoff by 50% and 235%, respectively.

Throughout this paper comparisons of annual and monthly precipitation and runoff are discussed. Annual model-generated precipitation and runoff may be within 5% of the annual observed precipitation and runoff, as in the case of the Mississippi River (within 2% of the observed precipitation) and Lena River (within 4% of the observed runoff), however, monthly precipitation and river runoff could be incorrect as shown for the Mississippi and Lena rivers (Fig 3.14). The Lena River, though within 4% of the annual observed river runoff, peaks too soon in the model-generated river runoff, R_m . The Mississippi River has too much model-generated precipitation in the spring and too little model-generated precipitation in the fall. These are examples of cases in which annual precipitation and runoff are simulated well, but monthly precipitation and runoff are not as well simulated.

The factor Ω in Eqn. 2.10 is a key variable in calculating the runoff at a rivers mouth. In that equation Ω was taken to be constant globally. As Ω continues to increase, and if the time step is relatively short, the variation of runoff at the mouth will approach that of R_{tot} . As Ω gets small, water will build up in the grid box smoothing the flow rate over time. The runoff rates given by Eqn. 2.10 for individual grid boxes could be modified further by allowing Ω to vary depending on the physical characteristics of a particular grid box. These might include soil type and depth, vegetation type, and topography or other characteristics of the river basin.

Another problem which may exist in analyzing individual river basins is that the precipitation and runoff are occurring in the correct part of the river basin. With the new routing scheme, it is possible to examine runoff for separate components of a larger river basin. For example, the Mississippi River can be divided into its components, the Missouri, Ohio, Illinois, and Arkansas Rivers for further analysis. The new routing scheme allows us to choose any location within the basin and simulate runoff there. The next chapter will discuss the precipitation and runoff for the Mississippi River and its components.

Table 3.2. Annual observed and model-generated runoff (Km³/yr) and precipitation (Km³/yr) for the world's major rivers for several different model simulations.

<i>Climate Type</i>	<i>Precipitation</i>					<i>Runoff</i>					
	<i>River</i>	<i>OBS</i>	<i>848</i>	<i>B100</i>	<i>C003</i>	<i>A51</i>	<i>OBS</i>	<i>848</i>	<i>B100</i>	<i>C003</i>	<i>A51</i>
<i>Wet</i>											
Amazon	13942	12296	12842	13241	14224	4886	2338	2479	4055	3079	
Congo	5516	8841	7635	6446	8470	1398	2170	1574	1643	2094	
Orinoco	2193	2173	2221	2040	2005	794	475	615	707	466	
Mekong	1477	1996	2112	1758	2133	449	712	709	410	710	
Magdalena	758	863	1176	1095	1056	213	314	520	581	304	
Sao Francisco	799	1160	987	821	1273	83	211	178	189	272	
Average	4114	4555	4496	4234	4861	1304	1037	1013	1264	1154	
<i>Moderately Wet</i>											
Yangtze	1985	3436	3167	2787	3465	792	1304	1239	898	1499	
Mississippi	3039	2645	2965	2127	2981	498	517	646	395	660	
LaPlata (Parana)	3662	2955	2629	3905	3164	---	(407)	(369)	(1444)	(474)	
St Lawrence	1070	1204	1144	1053	1102	214	462	361	505	322	
Danube	1192	995	1349	1289	1683	---	(298)	(352)	(309)	(516)	
Columbia	507	753	660	669	774	172	304	227	258	248	
Zambesi	1218	1600	1319	1058	1356	105	256	177	204	198	
Fraser	179	288	278	362	307	87	159	127	215	134	
Nile	1960	3508	3601	3228	3659	---	(587)	(634)	(758)	(656)	
Niger	1618	1917	2306	2136	2116	---	(350)	(403)	(418)	(331)	
Average	1643	1930	1942	1861	2061	311	500	463	413	510	
<i>Dry</i>											
Indus	392	660	314	543	592	76	302	116	198	204	
Tigris-Euphrates	497	500	503	442	497	---	(79)	(86)	(126)	(75)	
Yellow	541	1403	1347	1088	1454	---	(514)	(497)	(275)	(563)	
Colorado	205	418	408	198	339	12	83	87	33	70	
Murray	528	727	639	336	585	8	117	98	44	97	
Average	433	742	642	521	693	32	219	177	135	202	
<i>High Latitude Dry</i>											
Yenesei	1126	1480	1646	1788	1371	558	499	586	710	461	
Lena	926	1407	1590	1839	1486	516	540	638	779	535	
Ob	1354	1248	1131	1440	1066	388	503	455	605	464	
Amur	1120	1364	1484	1635	1394	309	316	357	475	273	
Mackenzie	607	1172	1159	1134	1242	264	560	514	599	644	
Yukon	333	779	707	886	715	197	492	519	713	510	
Severnay Dvina	206	224	237	284	241	107	118	117	152	132	
Kolyma	258	470	559	514	506	71	337	434	411	366	
Indigirka	100	205	233	214	228	49	119	146	135	134	
Average	670	928	972	1082	917	273	387	418	509	391	
Total Average	1644	1956	1945	1879	2050	510	550	538	621	578	

Observed precipitation is from *Legates and Willmott* [1990]. Observed runoff is from *UNESCO* [1969,1974,1985]. (- - -) Indicates river basins in which observed runoff station is not near the mouth of the river. Values in () are not included in climate type and total runoff averages.

MAJOR RIVER DRAINAGE BASINS

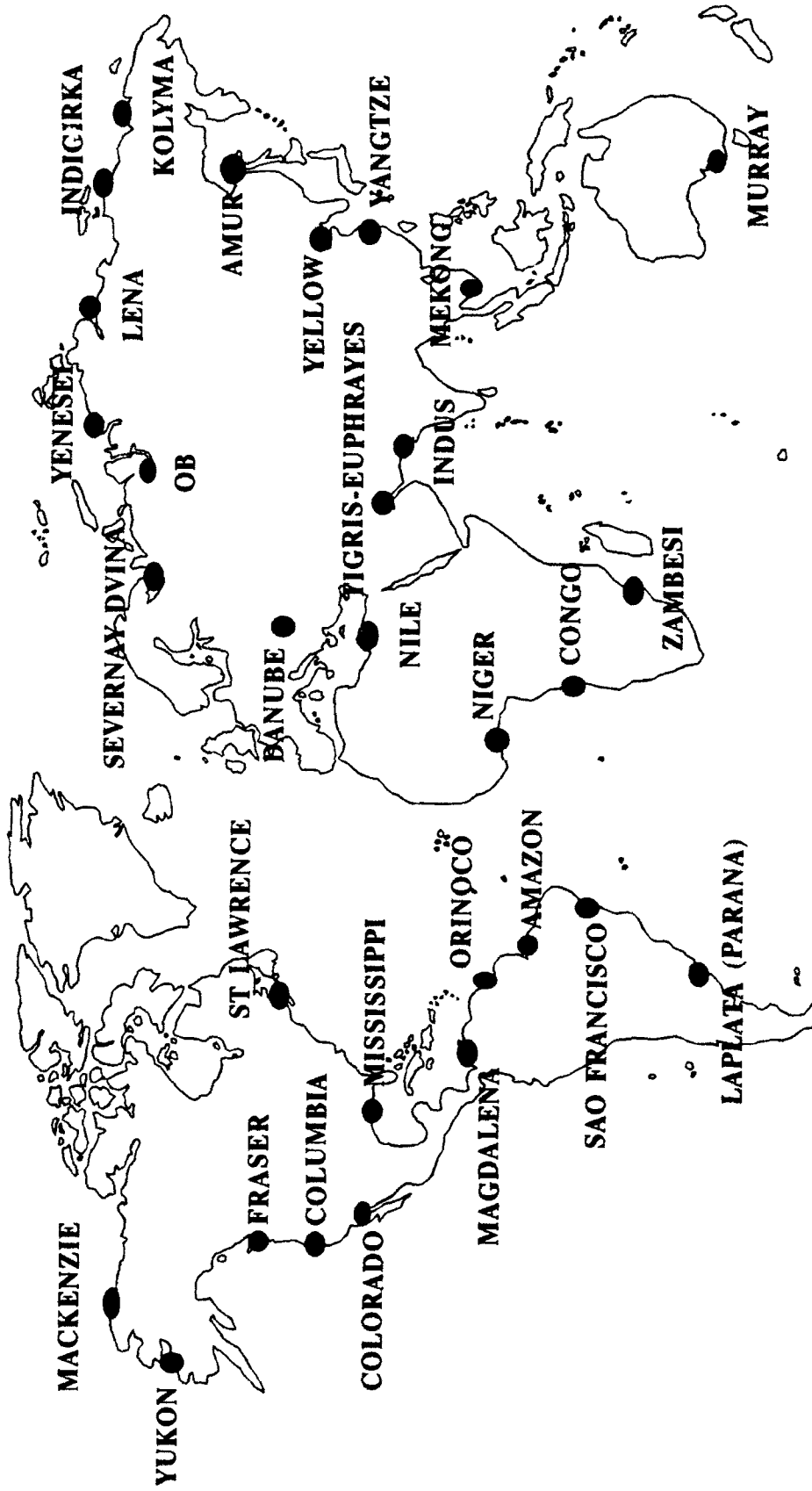


Figure 3.1. Drainage basin locations of the rivers used in this study. Black dots indicate the approximate location of the river basin's mouth.

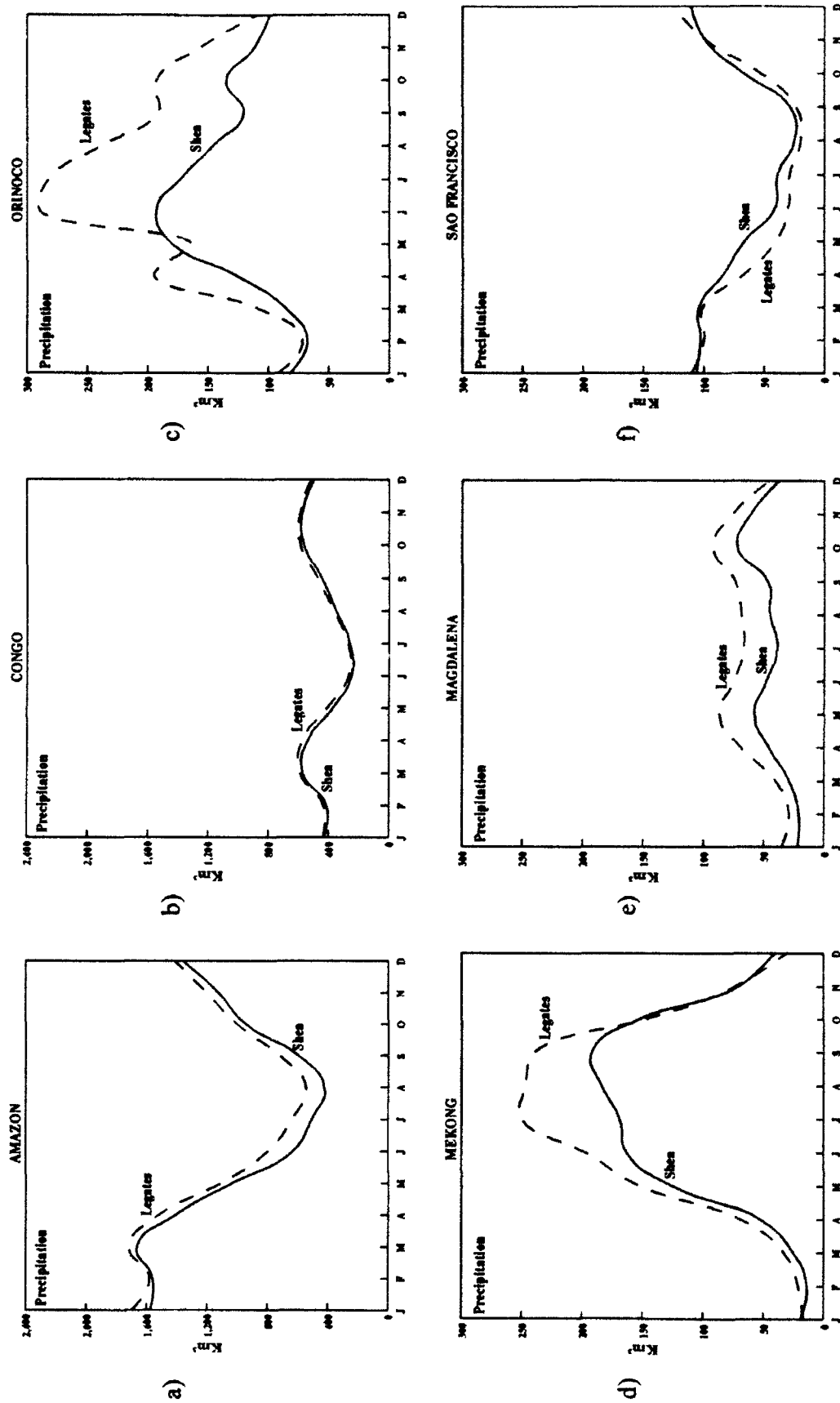


Figure 3.2. Observed monthly precipitation from Legates and Willmott [1990] and Shea [1986] for the (a) Amazon, (b) Congo, (c) Orinoco, (d) Mekong, (e) Magdalena, and (f) Sao Francisco rivers.

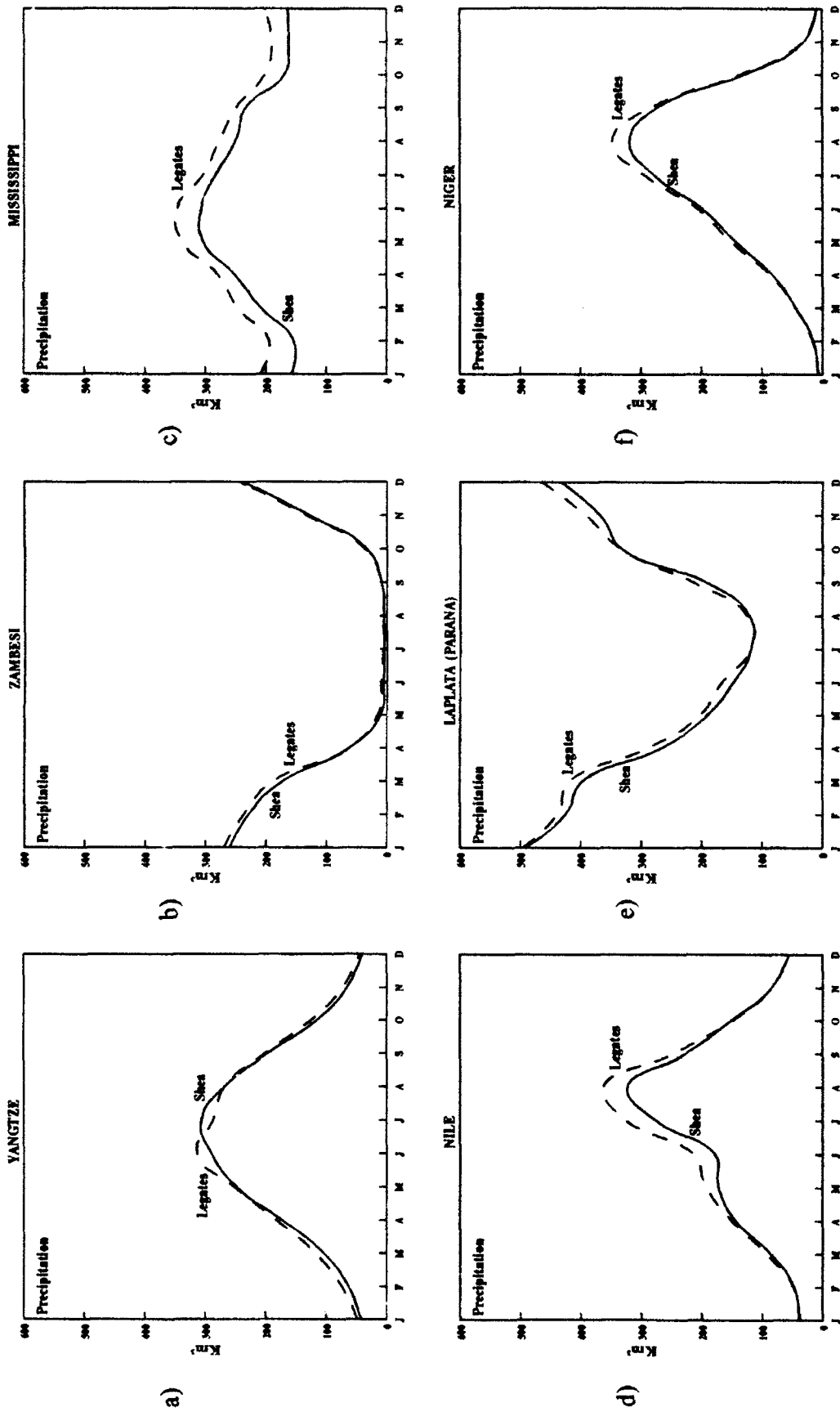


Figure 3.3. Observed monthly precipitation from Legates and Willmott [1990] and Shea [1986] for the (a) Yangtze, (b) Zambesi, (c) Mississippi, (d) Nile, (e) LaPlata (Parana), and (f) Niger rivers.

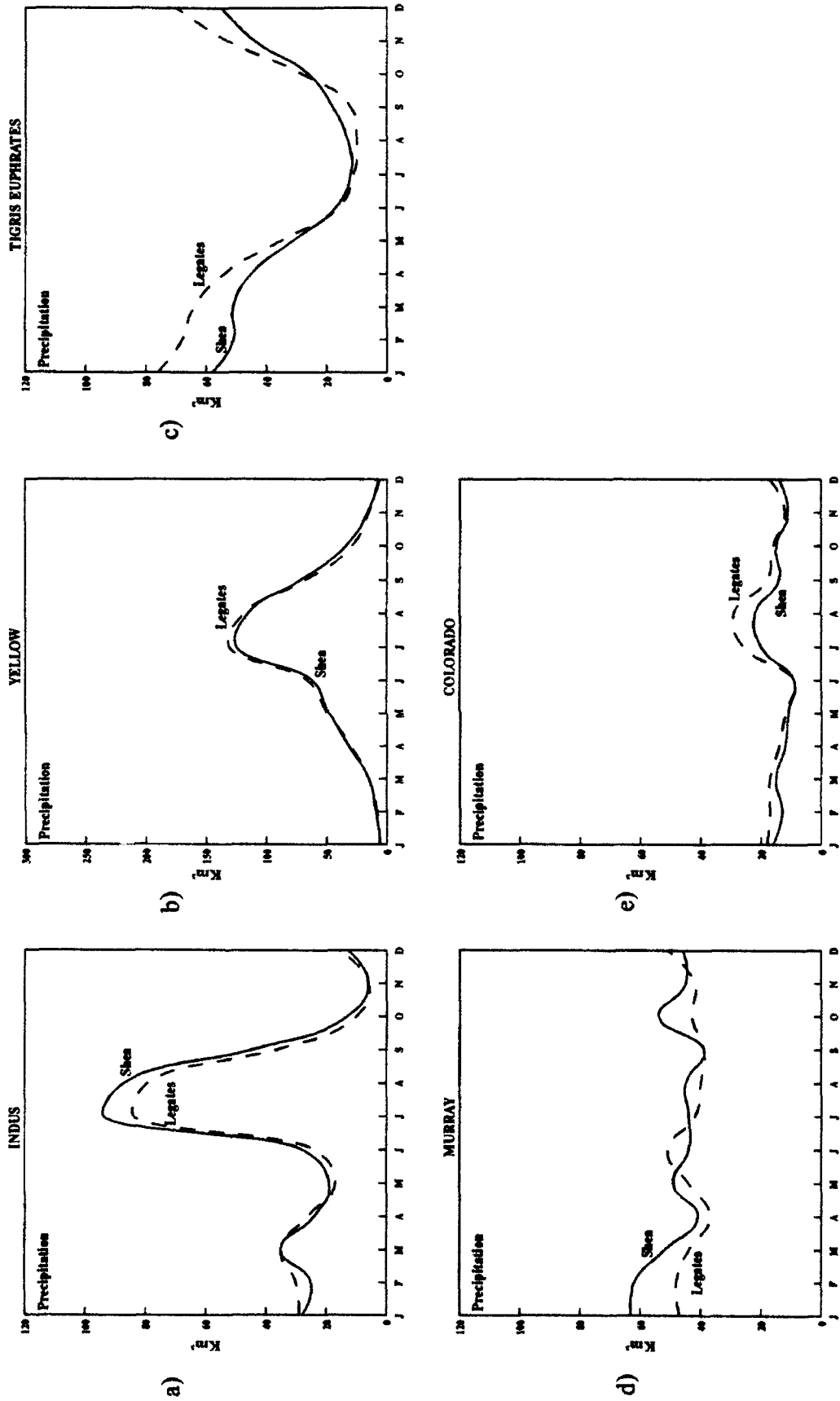


Figure 3.4. Observed monthly precipitation from Legates and Willmott [1990] and Shea [1986] for the (a) Indus, (b) Yellow, (c) Tigris-Euphrates, (d) Murray, and (e) Colorado rivers.

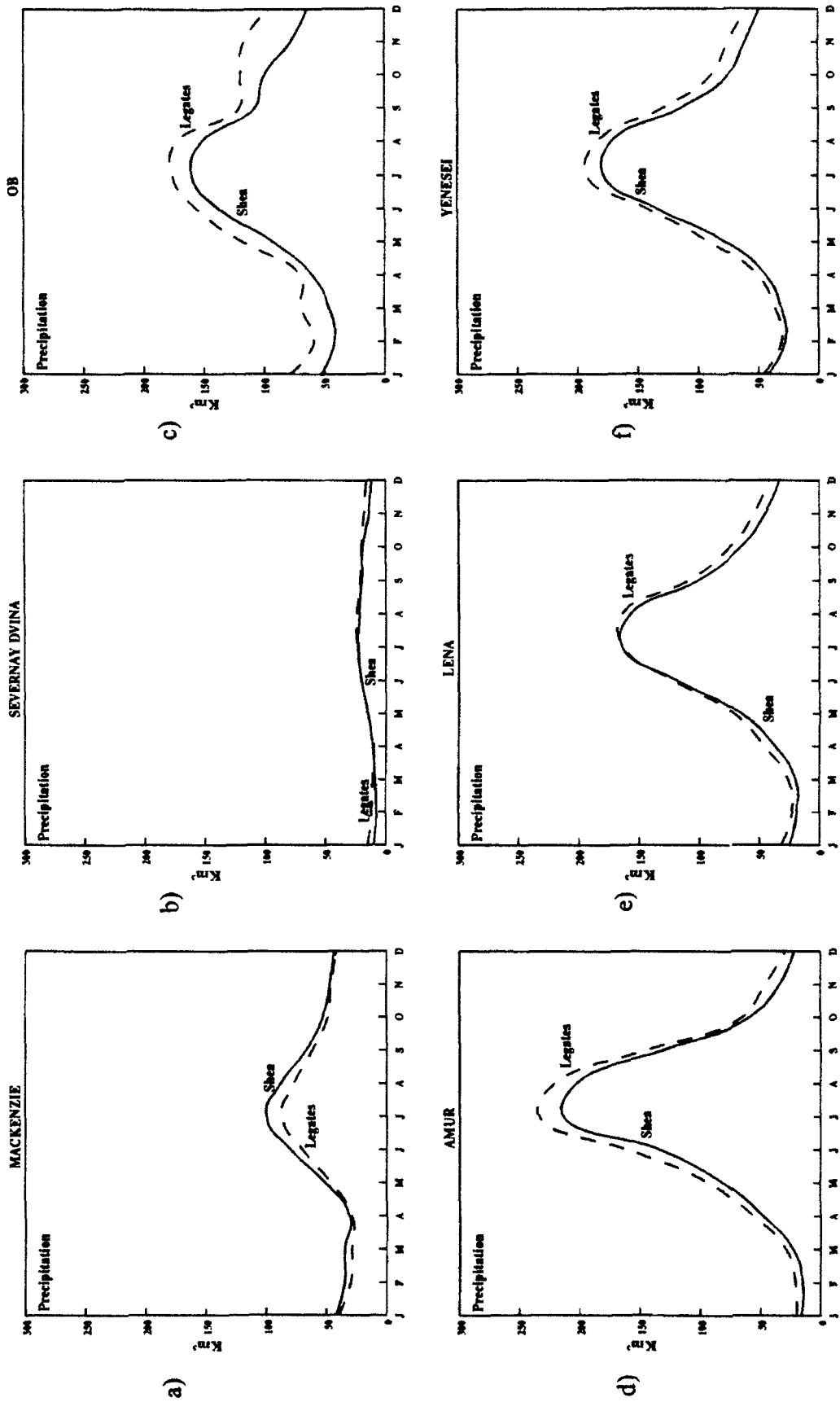


Figure 3.5. Observed monthly precipitation from *Legates and Willmott* [1990] and *Shea* [1986] for the (a) Mackenzie, (b) Severnaya Dvina, (c) Ob, (d) Amur, (e) Lena, and (f) Yenesei rivers.

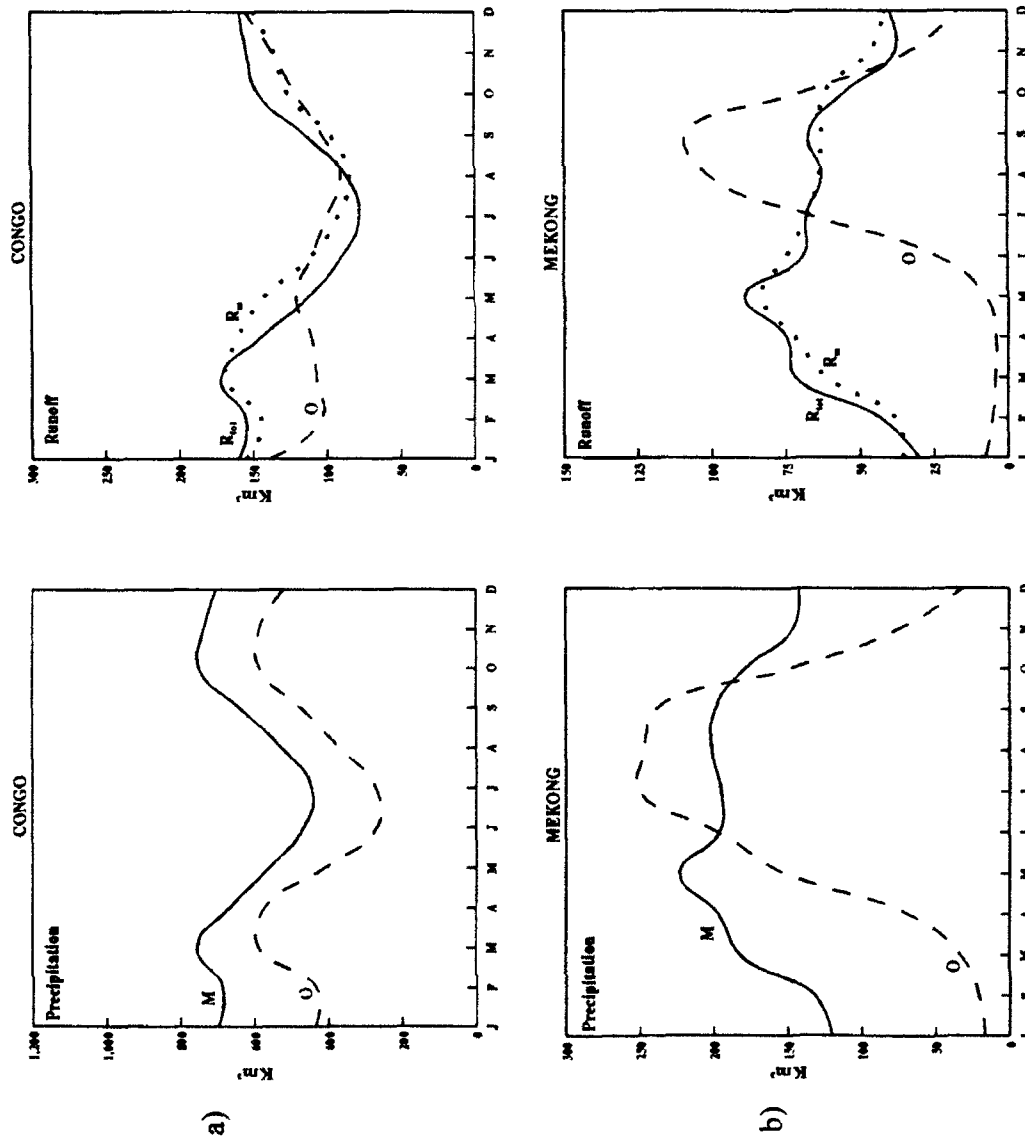


Figure 3.6. Model-generated (M) and observed (O) precipitation and river runoff for the (a) Congo and (b) Mekong rivers. R_{tot} is model river runoff averaged over the entire river basin while R_m is model river runoff at the mouth using the new routing scheme. Observed precipitation is from *Legates and Willmott* [1969, 1974, 1985].

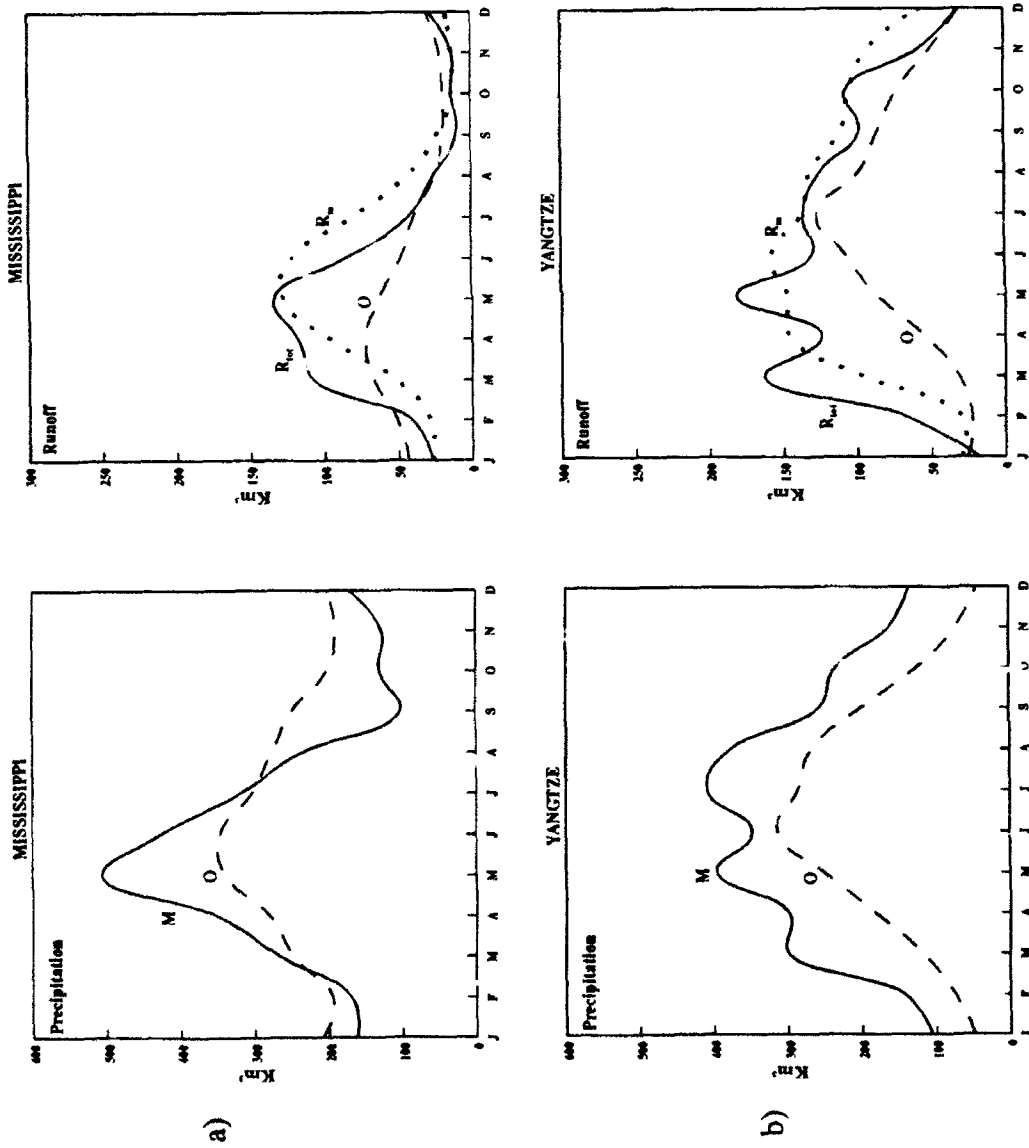


Figure 3.7. Model-generated (M) and observed (O) precipitation and river runoff for the (a) Mississippi and (b) Yangtze rivers. R_{tot} is model river runoff averaged over the entire river basin while R_m is model river runoff at the mouth using the new routing scheme. Observed precipitation is from *Legates and Willmott* [1990] and observed runoff is from *UNESCO* [1969, 1974, 1985].

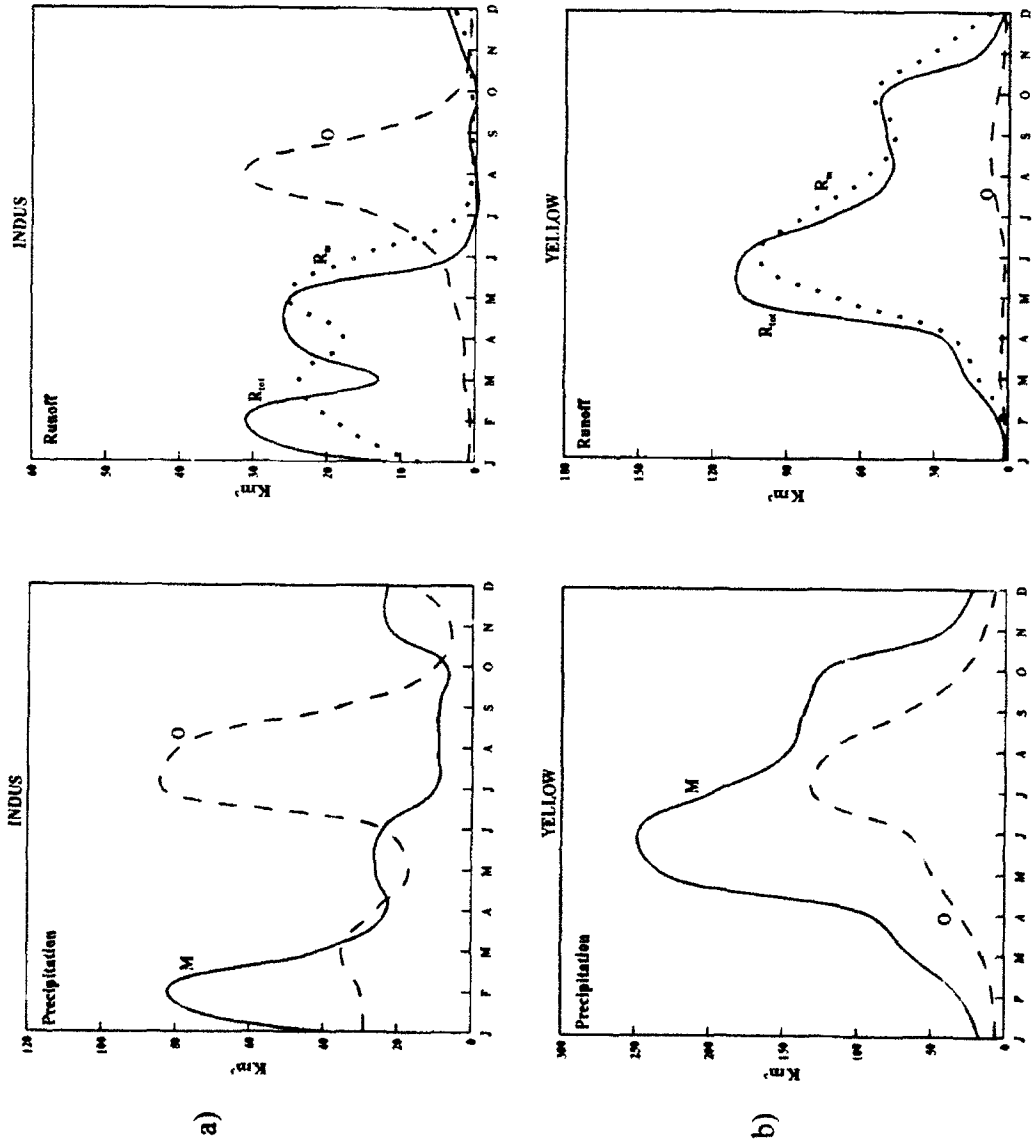


Figure 3.8. Model-generated (M) and observed (O) precipitation and river runoff for the (a) Indus and (b) Yellow rivers. R_{tot} is model river runoff averaged over the entire river basin while R_m is model river runoff at the mouth using the new routing scheme. Observed precipitation is from *Legates and Willmott* [1990] and observed runoff is from *UNESCO* [1969, 1974, 1985].

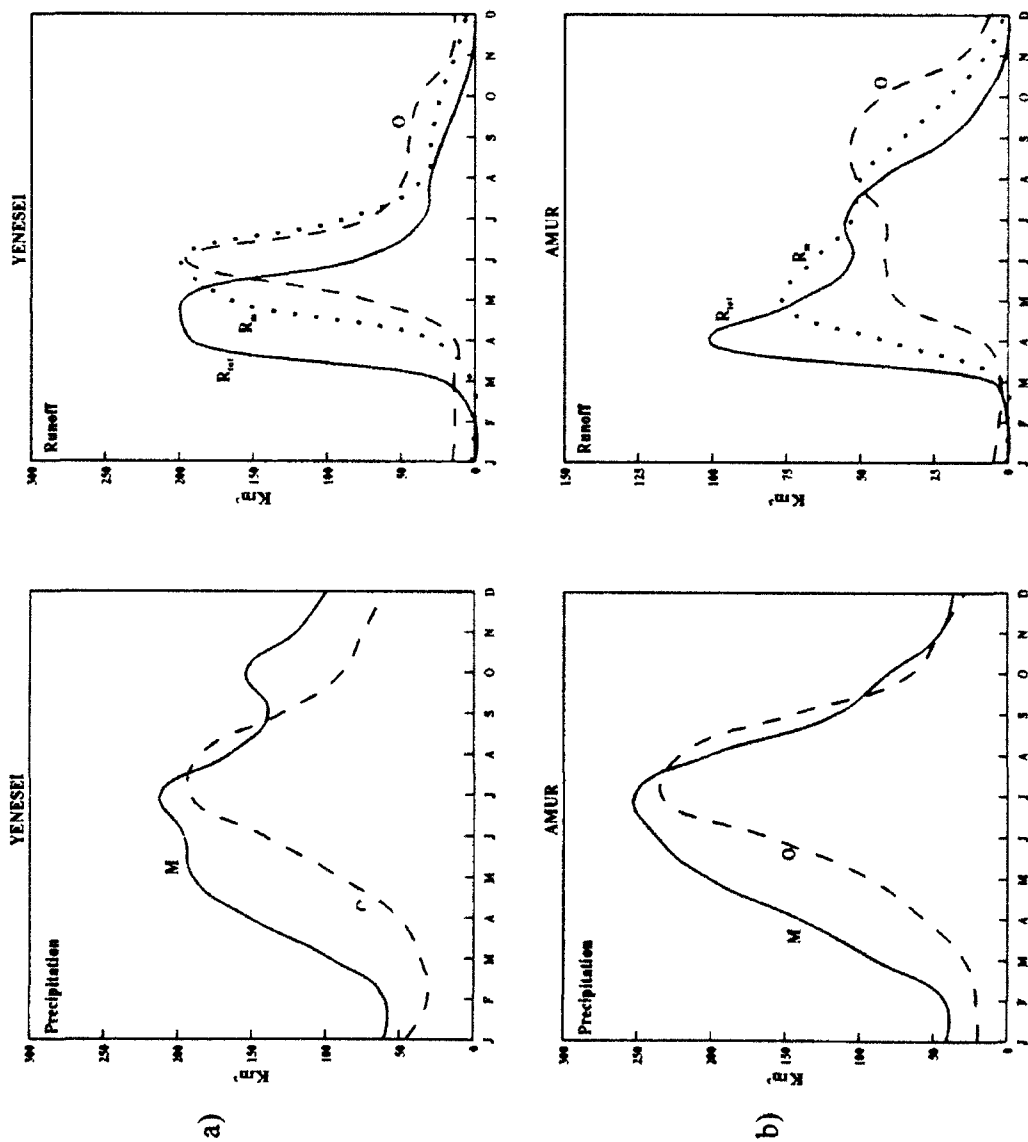


Figure 3.9. Model-generated (M) and observed (O) precipitation and river runoff for the (a) Yenesei and (b) Amur rivers. R_{tot} is model river runoff averaged over the entire river basin while R_m is model river runoff at the mouth using the new routing scheme. Observed precipitation is from *Legates and Willmott* [1990] and observed runoff is from *INESCO* [1969, 1974, 1985].

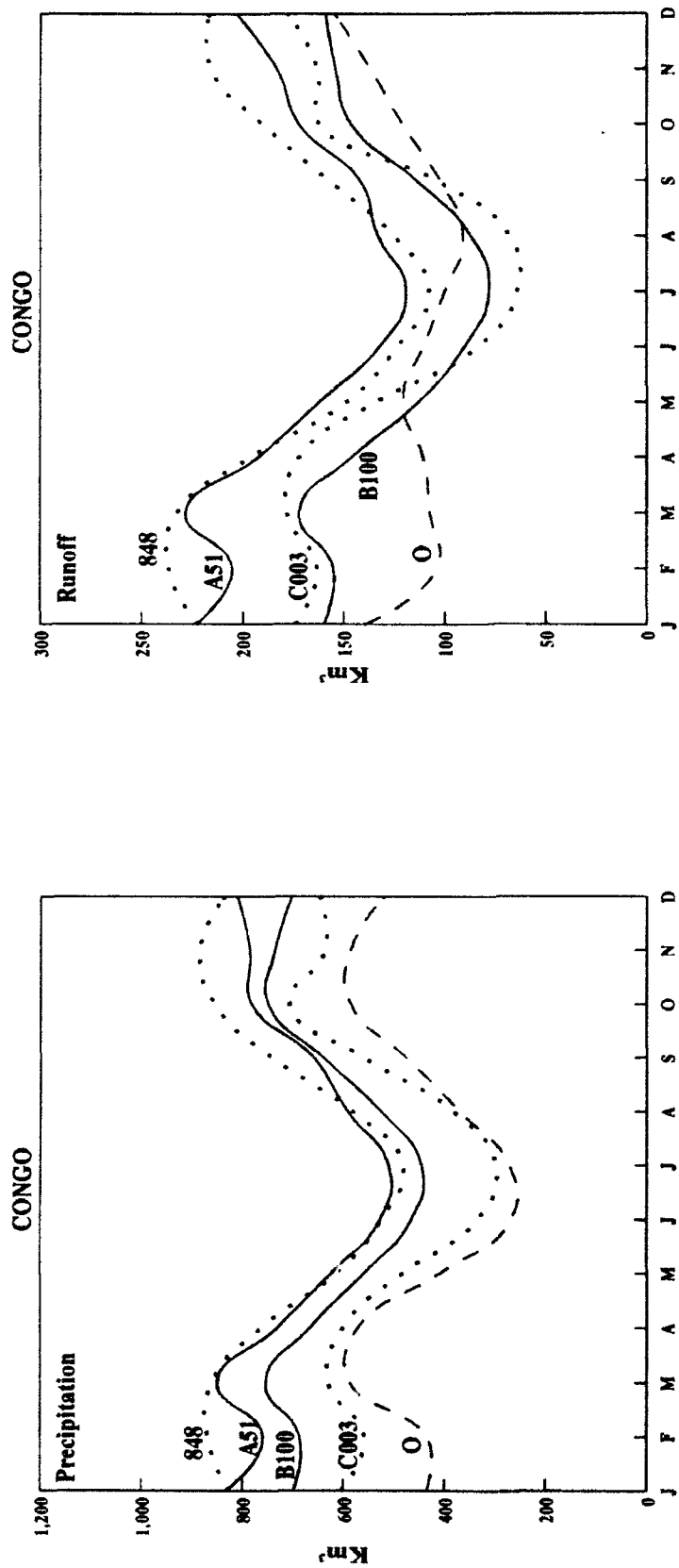


Figure 3.10. Model-generated (A51, B100, C003, 848) and observed (O) precipitation and river runoff for the Congo River. Observed precipitation is from *Legates and Willmott* [1990] and observed runoff is from *UNESCO* [1969, 1974, 1985]. A51, B100, C003, and 848 refer to the simulations shown in Table 3.1. River runoff, R_{tot} , is averaged over the entire river basin.

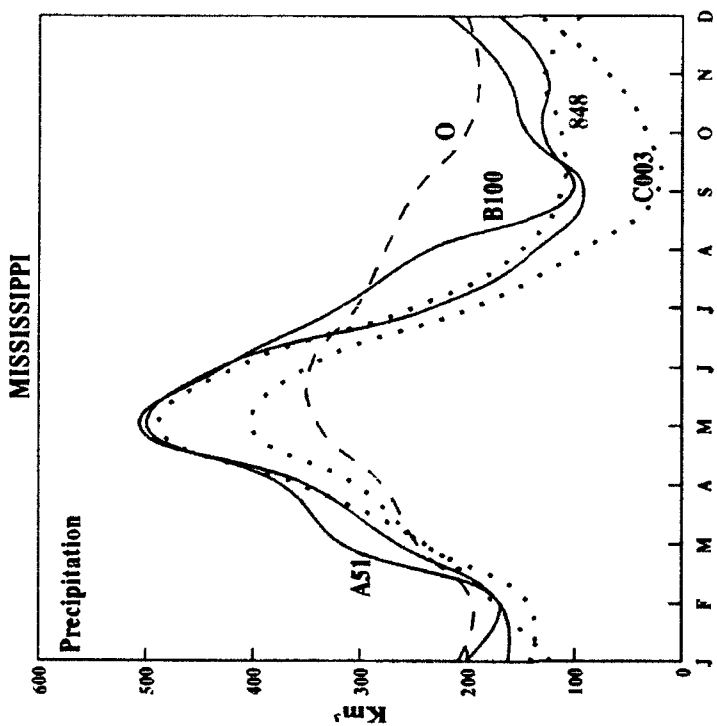
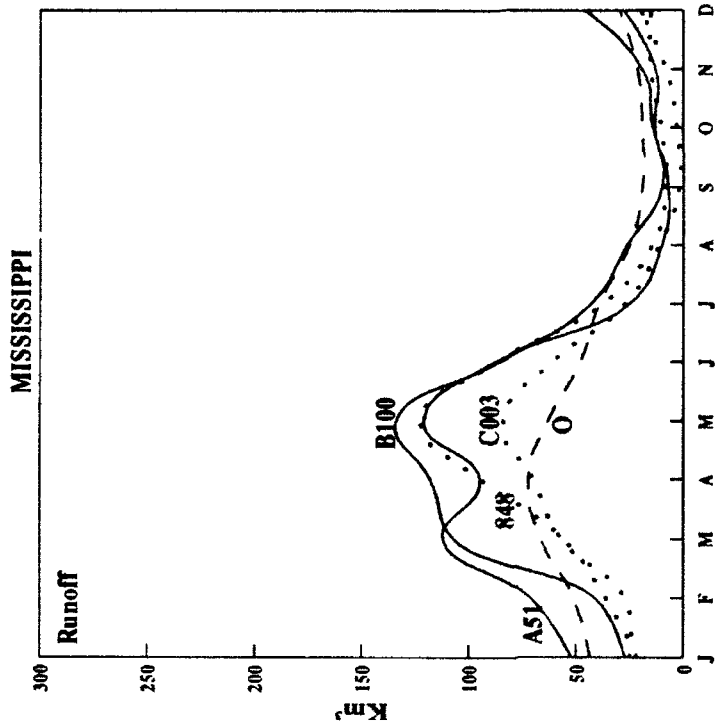


Figure 3.11. Model-generated (A51, B100, C003, 848) and observed (O) precipitation and river runoff for the Mississippi River. Observed precipitation is from *Legates and Willmott* [1990] and observed runoff is from *UNESCO* [1969, 1974, 1985]. A51, B100, C003, and 848 refer to the simulations shown in Table 3.1. River runoff, R_{tot} , is averaged over the entire river basin.

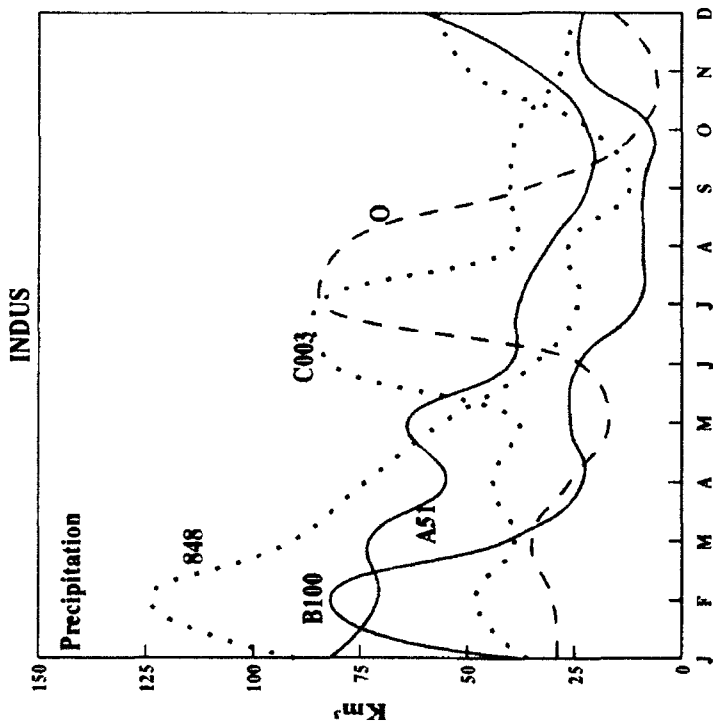
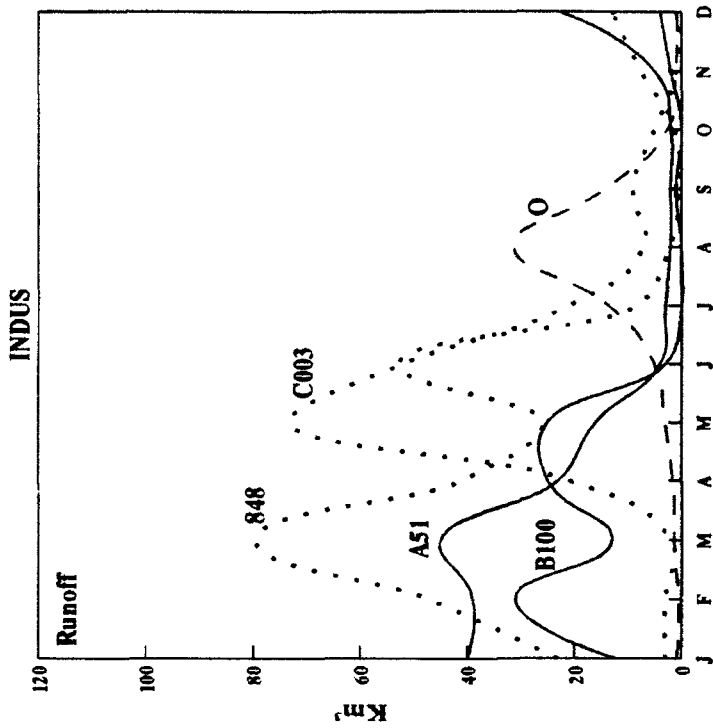


Figure 3.12. Model-generated (A51, B100, C003, 848) and observed (O) precipitation and river runoff for the Indus River. Observed precipitation is from *Legates and Willmott* [1990] and observed runoff is from *UNESCO* [1969, 1974, 1985]. A51, B100, C003, and 848 refer to the simulations shown in Table 3.1. River runoff, R_{tot} , is averaged over the entire river basin.

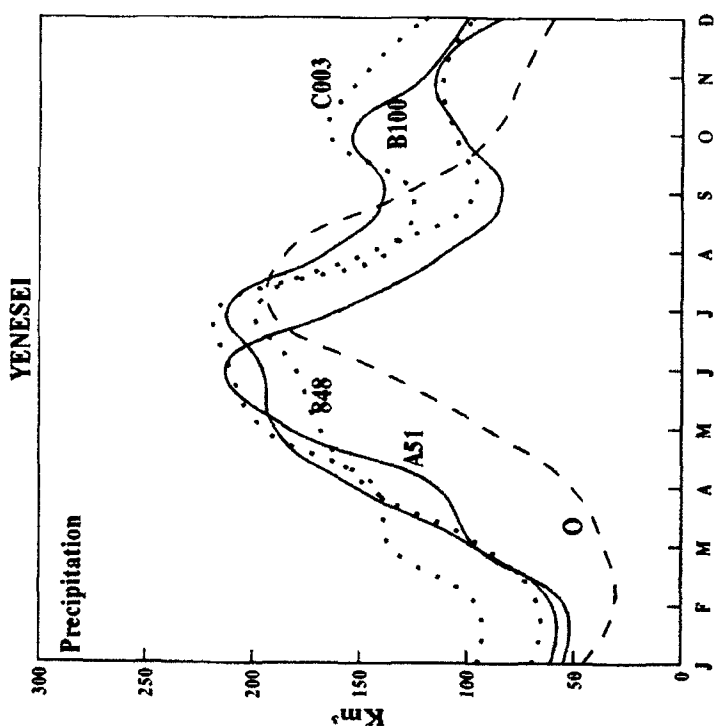
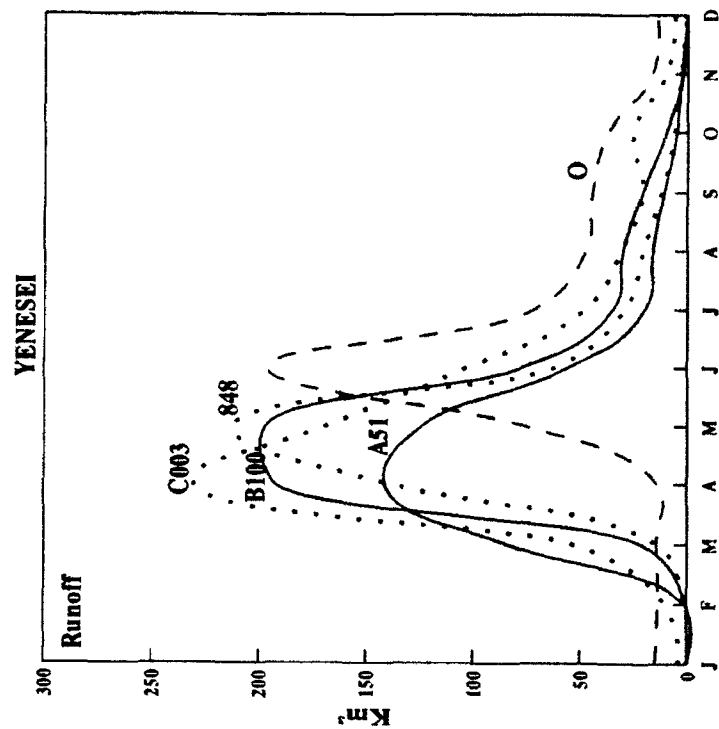


Figure 3.13. Model-generated (A51, B100, C003, 848) and observed (O) precipitation and river runoff for the Yenesei River. Observed precipitation is from *Legates and Willmott* [1990] and observed runoff is from *UNESCO* [1969, 1974, 1985]. A51, B100, C003, and 848 refer to the simulations shown in Table 3.1. River runoff, R_{tot} , is averaged over the entire river basin.

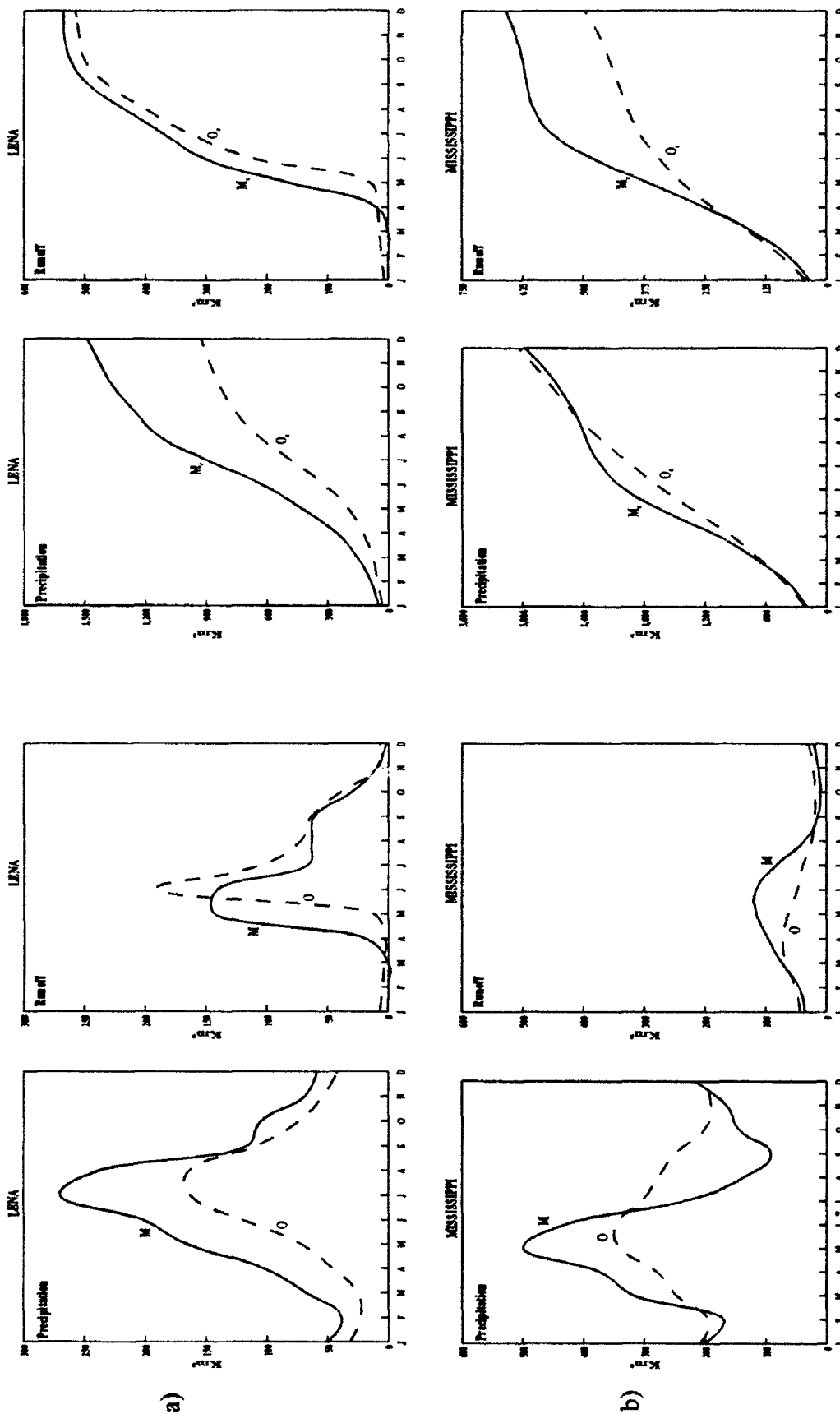


Figure 3.14. Monthly model-generated (M) and observed (O) precipitation and river runoff for the (a) Mississippi and (b) Lena rivers. Observed precipitation is from *Legates and Willmott* [1990] and observed runoff is from *UNESCO* [1969, 1974, 1985]. River runoff, R_m , is measured at the mouth.

Chapter 4. Mississippi River Basin

Hydrologists have generally focused on calculating river runoff at smaller scales (about 1 kilometer) than those considered by global atmospheric modelers. Global atmospheric modelers have used GCMs to calculate river runoff at much larger scales. *Vörösmarty et al.* [1989] have developed a continental drainage basin runoff scheme and applied it to the Amazon River basin using observed data as input. The model calculates water flow from one grid box to another, however, it is based on observed data and can not be used directly to calculate potential changes in river runoff due to global warming. The new routing scheme discussed in chapters 2 and 3 allows the calculation of runoff at any grid box in a river basin. The new routing scheme was used in the analysis of the Mississippi river and its tributaries.

Figure 4.1 shows a map of the Mississippi River basin divided into 2° X 2.5° grid boxes and the direction of the downstream flow for each grid box. The map is also divided into the major tributaries of the Mississippi River, the Missouri, Arkansas, Illinois, and Ohio rivers. For each river basin, runoff moves from grid box to grid box within the basin and is calculated at the grid box or sum of grid boxes which leave the basin and enter into the Mississippi River. Observed and model-generated precipitation and snow mass are interpolated from a 4° X 5° grid box into four 2° X 2.5° grid boxes. Precipitation and snow mass were assumed to be equal throughout the grid box. Hence, if the precipitation averaged 2 mm per day in a 4° X 5° grid box than it would average the same 2 mm per day in each 2° X 2.5° grid box.

The drainage area of each basin is the sum of the areas of all grid boxes within the river basin. The area of each grid box was calculated as follows:

$$Area = (2 \times 2.5) \times (110km)^2 \times \cos \theta \quad (4.1)$$

where θ is the latitude of the northern edge of a grid box. Table 4.1 shows model and observed areas of each river basin and three locations within the Mississippi River basin, Keokuk, Iowa, St Louis, Missouri, and Vicksburg, Mississippi. The model to observed ratio is near one for all except the three smallest basins, Arkansas, Illinois, and Upper Mississippi rivers.

Table 4.1. Model and observed drainage basin areas (Km²) for the Mississippi River and it's tributaries. The last column is the ratio of the model to the observed drainage area.

<i>River</i>	<i>Area</i>	<i>Area</i>	
<i>Location</i>	<i>Model</i>	<i>Observed</i>	<i>Ratio</i>
Missouri / Boonville, Missouri	1283025	1299403	0.99
Arkansas / Dardanelle, Arkansas	428955	398005	1.08
Ohio / Metropolis, Illinois	518818	525770	0.99
Illinois / Meredosia, Illinois	88480	67412	1.31
Upper Mississippi / Keokuk, Iowa	385552	308210	1.25
Central Mississippi / St Louis, Missouri	1803400	1805230	1.00
Lower Mississippi / Vicksburg, Mississippi	2991969	2953895	1.01

Observed runoff is from the US Geological Survey [1987]

The Illinois and Missouri rivers enter the Mississippi River before reaching St Louis and the Ohio and Arkansas rivers enter the Mississippi River between St Louis and Vicksburg. Figures 4.2-4.4 show observed and model-generated precipitation for the various river basins within the Mississippi. The figure for the lower Mississippi river at Vicksburg (Fig 4.4) is the same as Fig 3.7a. As discussed before, the overall annual model-generated precipitation is within 5% of the observed precipitation, however, there is too much precipitation in the spring and too little in the summer and fall. The reason to further divide the Mississippi River into it's tributaries is to find the origin of the precipitation and runoff and how it compares to observed values.

In general, the model is too dry in the eastern part and too wet in the western part of the Mississippi basin. The high precipitation in the spring is caused by too much precipitation being generated in the Missouri River basin, which encompasses 44% of the Mississippi River basin. The late summer and fall differences are caused by too little

precipitation being generated in the upper Mississippi, Arkansas and Ohio rivers, 42% of the Mississippi River basin. Therefore, although the annual precipitation is within 5% of the observed, the monthly precipitation generated by the model is occurring in the wrong regions of the basin. This also affects the monthly river runoff at the mouth. The observed river runoff peaks in March for the Ohio River and April for the Mississippi River at Vicksburg while the model shows river runoff peaks in May at Vicksburg, following an April peak for the Missouri River. Although the observed and model-generated river runoff peaks for Vicksburg are off by one month, the model is able to simulate the lag as water moves downstream to the mouth of the river basin.

The model generates too much annual river runoff (16%) for the entire river basin. Figures 4.2a, 4.3a, and 4.4 show the upper, central, and lower stations along the Mississippi River. The model generates 10%, 170%, and 16%, too much river runoff, respectively, for all three stations. The model-generated runoff is too high for the Missouri River and too low for the Ohio River. The problem with the Missouri River is that the model generates too much precipitation from October through July, some of which is in the form of snow. The model generates too little precipitation from July through February for the Ohio River causing the low model-generated runoff. The combination of too much runoff for the Missouri River and too little runoff for the Ohio River causes the annual runoff to be within 16% of the observed runoff near Vicksburg. A separate analysis of the Mississippi's tributaries can show why monthly and annual simulations differ in a particular river basin.

A useful tool in examining river runoff is comparing the annual runoff coefficient, which is defined as the ratio of annual runoff to annual precipitation, for observed and model-generated river runoff. The observed and model runoff coefficients for the Missouri River are .08 and .29, respectively. The observed and model coefficients for the Ohio River are .38 and .17, respectively. The significantly different observed runoff coefficients for the Missouri and Ohio rivers, which is not so prominent in the model,

indicates that the runoff generation for the two basins given by Eqn. 2.8 should be examined further. Possible differences between the two basins are that most of the Missouri basin is comprised of relatively flat plains while most of the Ohio basin is more mountainous. The vegetation types would also be different between the two basins. The model runoff coefficients suggest that the evaporation of water over the Missouri basin is too low and the evaporation over the Ohio River is too high. The difference in the observed and model runoff coefficients for the Missouri and Ohio rivers balance each other out closer to the mouth of the Mississippi basin where the observed and model runoff coefficients for the Mississippi River at Vicksburg are .22 and .23, respectively.

Table 4.2 shows the model-generated snow mass for the various basins averaged for the fall, winter, and spring seasons. Most snow falls in the Missouri basin, which produces a river runoff maximum in April and May. However, the observed river runoff is much lower and shows little monthly variation suggesting that the model generates too much snow and snow melt runoff for the Missouri River. The model generates very low snow amounts for the Ohio River suggesting model-generated river runoff there is dependent on precipitation only. Observed river runoff in the Ohio River shows a maximum in March despite uniform precipitation throughout the year. This suggests that snow melt is contributing to the observed runoff maximum. The model generates too little snow in the Ohio basin causing less runoff than observed and generates too much snow in the Missouri basin causing more runoff than observed.

Table 4.2. Seasonal model-generated snow mass (Km³) averaged over fall, winter, and spring for the Mississippi River and its tributaries for the present climate

<i>River Basin</i>	<i>Average Seasonal Snow Mass Present Climate</i>		
	<i>Fall</i>	<i>Winter</i>	<i>Spring</i>
Illinois	0.0	0.4	0.0
Missouri	1.4	39.0	8.6
Ohio	0.0	0.7	0.0
Arkansas	0.2	1.7	0.1
Upper Mississippi	0.4	6.6	0.6
Central Mississippi	1.8	46.2	9.3
Lower Mississippi	2.1	50.2	9.7

One problem can be the interpolation of precipitation and snow mass from a 4° X 5° grid box to four 2° X 2.5° grid boxes. It is assumed that precipitation occurs uniformly over the entire grid box. The problem with the Missouri River basin is with the northwest grid boxes bordering the mountains. The most western 2° X 2.5° grid boxes were interpolated from a 4° X 5° grid box that covered part of a mountainous region. Only half of the 4° X 5° grid box was within the Missouri River basin. Because precipitation and snow fall is assumed uniform over the entire 4° X 5° grid box it was the same for each 2° X 2.5° grid box.

Another related problem is that grid boxes may contain several rivers which belong to different basins. Water from the entire grid box is assumed to flow in one direction, thus, river runoff may enter the wrong river basin. This is also happening in the Missouri River basin in which the western most grid box contains precipitation and snow interpolated from a 4 X 5 grid box encompassing both the Missouri and Snake rivers. Since grid box runoff must be assigned to a particular basin, some runoff intended to flow into the Snake River is flowing into the Missouri River.

The goal of this chapter was to further analyze a large river basin by dividing it into its tributaries. This could be done for any of the rivers discussed in chapter 3. The Mississippi River was chosen because annual precipitation was simulated well while the

model-generated monthly precipitation differed in the spring and fall and good observed data was available. The model generates too much precipitation in the western Mississippi and too little in the eastern Mississippi causing differences in the simulations of monthly and annual river runoff. Care must be given to areas of the grid which border mountainous regions. Because precipitation and snow amounts are assumed uniform throughout a grid box, interpolation into smaller grid boxes can cause errors in precipitation amounts and eventually in the routing of the runoff. For the Missouri and Ohio rivers, model-generated snow seems to be reversed, with the model generating too much snow for the Missouri and too little snow for the Ohio River. However, this study did not utilize observed snow data for the Missouri and Ohio basins causing this conclusion. Finer spatial and temporal resolution should improve the model's ability to simulate river runoff and precipitation for the world's river basins.

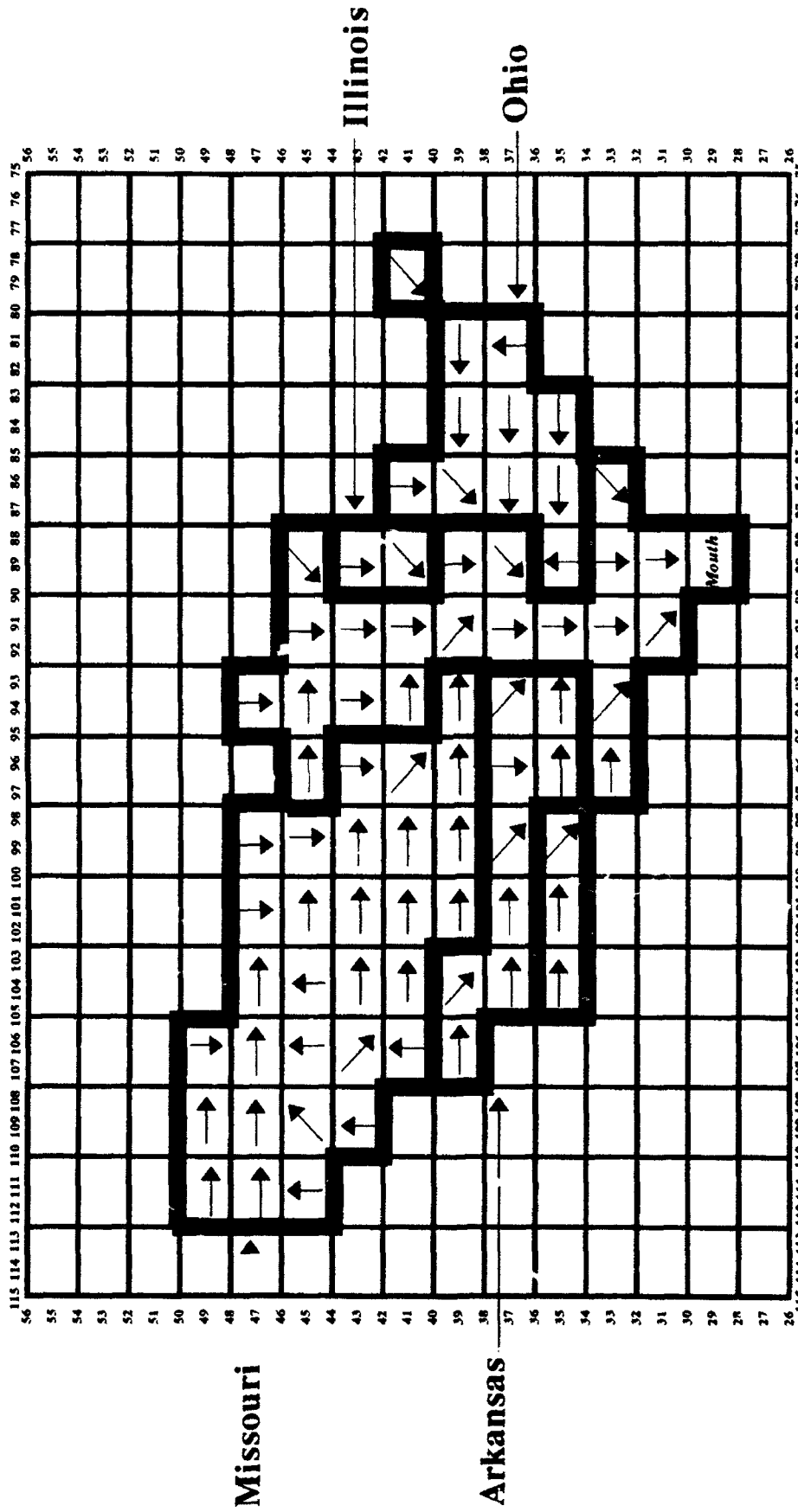


Figure 4.1. A 2° X 2.5° grid map of the Mississippi River basin and its tributaries, Missouri, Illinois, Ohio, and Arkansas rivers. The arrows indicate the downstream flow of the river runoff and the numbers are latitude and longitude.

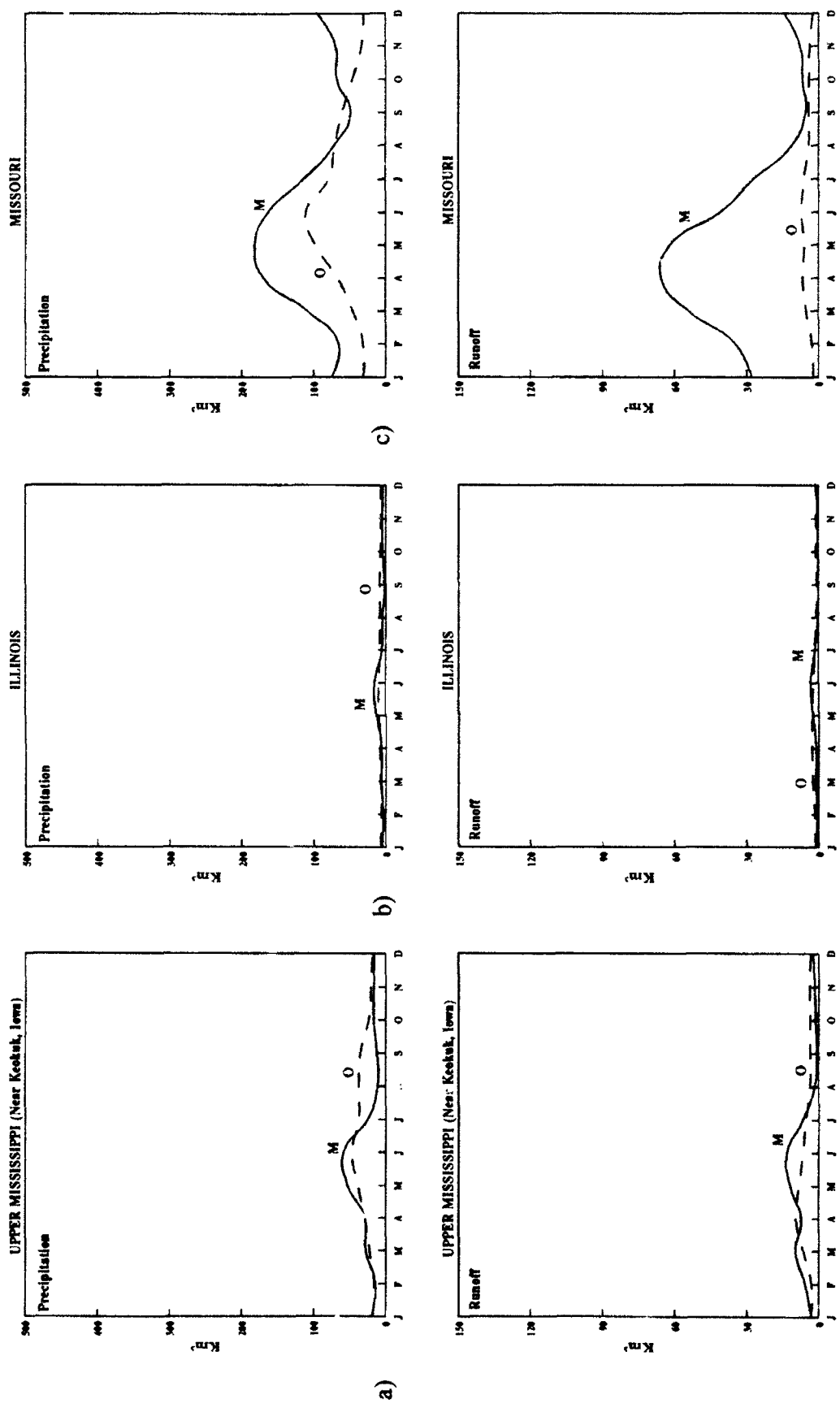


Figure 4.2. Observed and model-generated monthly precipitation and runoff for the (a) Mississippi River at Keokuk, Iowa, (b) Illinois River, and (c) Missouri River. Observed precipitation is from Legates and Willmott [1990] and observed river runoff is from the U.S. Geological Survey.

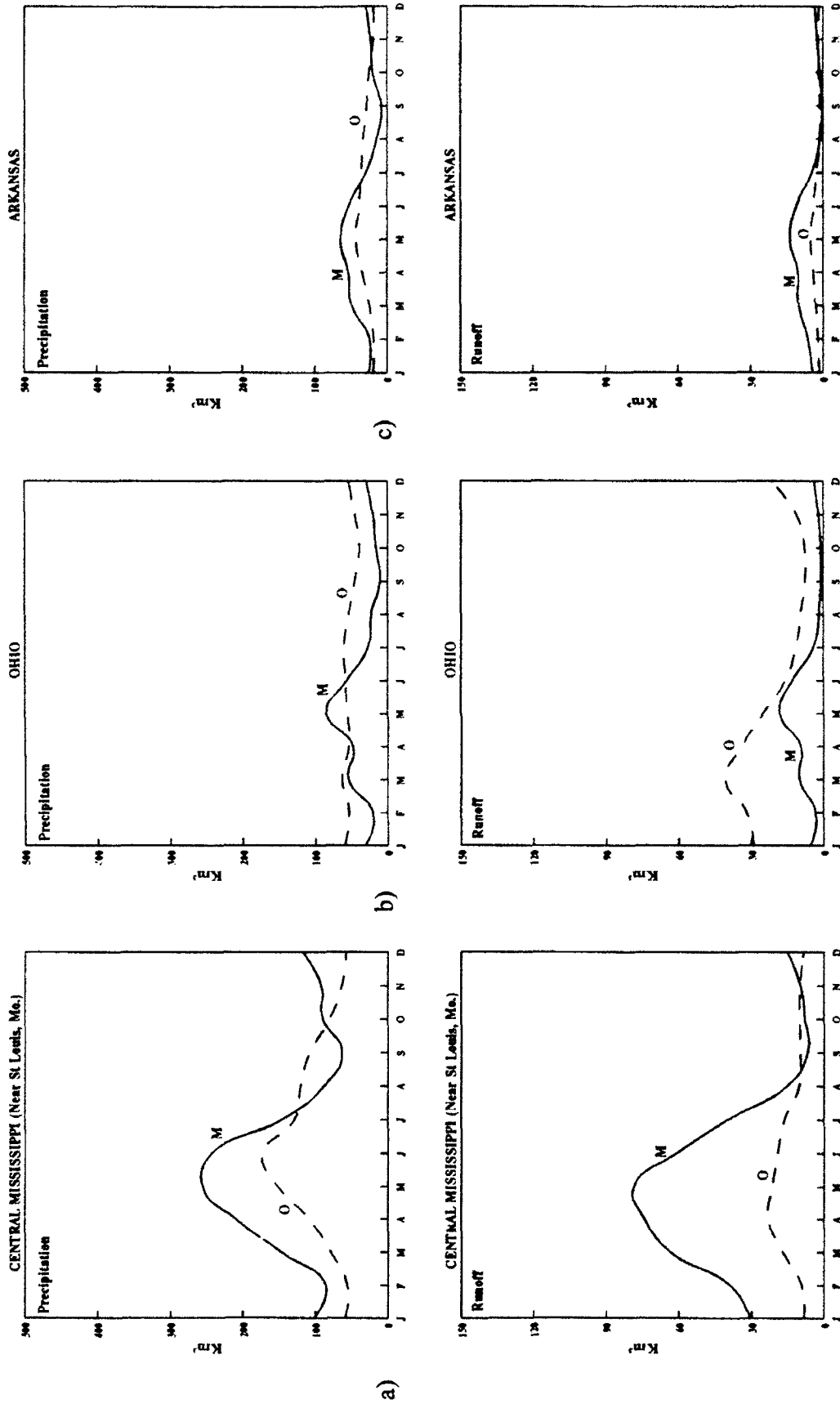


Figure 4.3. Observed and model-generated monthly precipitation and runoff for the (a) Mississippi River at St Louis, Missouri, (b) Ohio River, and (c) Illinois River. Observed precipitation is from *Legates and Willmott [1990]* and observed river runoff is from the *US Geological Survey*.

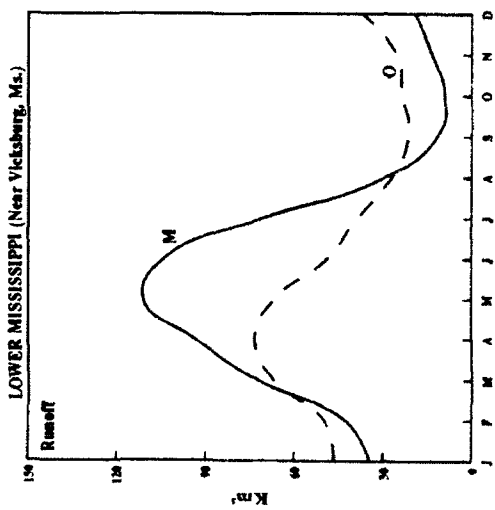
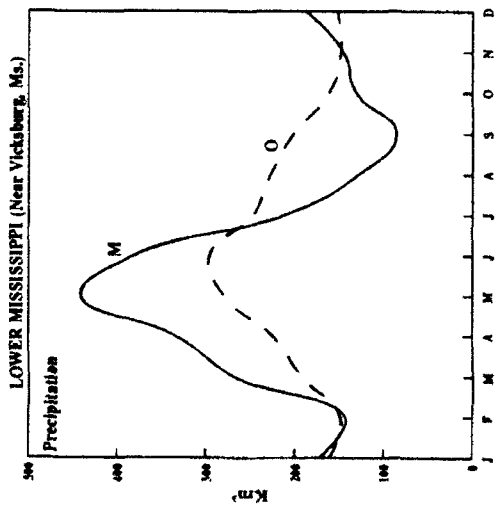


Figure 4.4. Observed and model-generated monthly precipitation and runoff for the Mississippi River at Vicksburg, Mississippi. Observed precipitation is from *Legates and Willmott [1990]* and observed river runoff is from the *US Geological Survey*.

Chapter 5. Changes in monthly runoff in a doubled CO₂ climate

Future changes in river runoff will impact many areas, including agriculture, water resources, and land use. In this chapter potential changes in river runoff are examined for a doubled CO₂ climate. *Miller and Russell* [1992] examined mean annual river runoff for the present climate and for a doubled CO₂ climate and found increased river runoff for 25 of the world's 33 major rivers. The largest increases were found in the higher latitudes, where substantial shifts in runoff patterns may occur because temperature changes can effect the ratio of rain to snow. Less snow during the winter could have a major impact on water resources during spring and summer. This chapter extends the work of *Miller and Russell* [1992] to examine seasonal changes in river runoff with emphasis on high latitudes where snow melt is an important component of river runoff. It is important to examine monthly runoff to determine whether changes are uniform throughout the year or are caused by seasonal variations in precipitation and river runoff.

The off-line method discussed in chapter 1 can be used with temperatures and precipitation from GCMs or other sources. *Gleick* [1987] and *Lettenmaier and Gan* [1990] have used precipitation and temperature from GCMs. *Gleick* [1987] examined the Sacramento River basin in California for 18 widely varying climate changes, ten from hypothetical temperature and precipitation changes and eight from precipitation and temperature changes generated by GCMs. He found that climate change caused increased runoff in the winter and decreased runoff in the summer. The principal physical mechanism concluded by *Gleick* [1987] was a decrease snow. *Lettenmaier and Gan* [1990] found similar results for several northern California river basins.

Flaschko et al. [1987] used the off-line method and examined changes of river runoff in the Great Basin Region of the western United States by applying water balance models to four watersheds in Nevada and Utah. They modeled the effects of four climatic change scenarios suggested by *Stockton and Boggess* [1979]: 1) a 2°C increase in

temperature and a 10% decrease in precipitation (warm/dry), 2) a 2°C increase in temperature and a 25% decrease in precipitation (warm/very dry), 3) a 2°C decrease in temperature and a 10% increase in precipitation (cool/wet), and 4) a 2°C decrease in temperature and a 25% increase in precipitation (cool/very wet), on the Carson, Martin, Bear, and Sevier basins, with emphasis on the warmer/dry case, the more likely scenario. They found that runoff decreased by 17% to 28% from the present mean for the four river basins. *Roos* [1989] and *Ayers et al.* [1990] used the same type of water balance model to examine changes in runoff for the Sacramento River, San Joaquin River, and rivers in the Tulare Lake system of California and the Delaware River, respectively, with emphasis on spring snow melt. In both instances, precipitation patterns were assumed to remain the same in the doubled CO₂ climate, however, because of the warmer temperatures, the majority of the winter precipitation was in the form of rain with much less snow in the mountain regions. Thus, spring runoff was reduced impacting both agriculture and water resources.

This chapter will focus on river runoff using grid box runoff produced directly from a GCM. Three-year simulations for the present climate and the doubled CO₂ climate were performed at 4° X 5° resolution using the GISS model. The same simulations were used in *Miller and Russell* [1992] for examining changes in mean annual runoff. As discussed in *Miller and Russell* [1992], this relatively short simulation introduces the potential for temporal sampling errors. Such errors will be greater in monthly computed runoff. The annual cycle of sea surface temperatures (SST) and ice distribution were specified by interpolating from equilibrium simulations at 8° X 10° resolution, in which SST and ice distribution were predicted [*Hansen et al.*, 1984]. The model simulations are A51 and 947 as shown in Table 3.1.

The model-generated annual river runoff and precipitation for the present climate and doubled CO₂ climate are shown in Table 5.1 and Figures 5.1-5.2 for 30 river basins. These results are not identical to those of *Miller and Russell* [1992] because the grid

boxes assigned to specific rivers have been modified somewhat and observed runoff for this study is from *UNESCO* [1969, 1974, 1985] and not from *Millman and Meade* [1983]. Drainage areas for the model are compared with the observed areas in Table 5.2. Observed river runoff and areas are from *UNESCO* [1969, 1974, 1985] while observed precipitation is from *Legates and Willmott* [1990]. Observed areas for runoff may differ from the model-generated areas because the observed stations are not always at the river mouth. Hence, in most cases the model-generated runoff is based on a larger drainage basin area than the observed.

The world's rivers were divided into three categories, those with less than 60 cm of annual precipitation, those with between 60 and 120 cm, and those with more than 120 cm yr⁻¹ which are referred to as dry, moderately wet, and wet [*Kuhl and Miller* 1992]. Dry basins are separated into dry and high latitude dry (north of 45°N) basins. When averaged over all 30 rivers, the model-generated annual precipitation and runoff are 25% and 13% too high, respectively, for the present climate. Model-generated annual precipitation is high for all four categories with the greatest discrepancy in the dry river basins where the model-generated precipitation is more than 50% too high. This is also true for the annual model-generated river runoff, where the model does poorest in the dry river basins. *Rind et al.* [1990] suggests that β in Eq. 2.7 is not calculated accurately in the GISS model. This could lead to incorrect evaporation and incorrect runoff. The model also does not allow for runoff to evaporate as it moves downstream. This effect would be most pronounced in the dry basins.

Figures 5.3a-5.3d show the seasonal changes (Km³) in the model-generated precipitation and runoff for the doubled CO₂ climate. The greatest changes in precipitation for the wet climates (Fig 5-3a) occurs between September and February. The Congo and to a lesser extent the Amazon are the only rivers in which the precipitation increases are fairly uniform for all seasons. The smallest changes occur between March

and May. The Magdalena is the only river to show decreases in both runoff and precipitation.

The Niger River (Fig 5-3c) is particularly interesting because an increase in precipitation from December through May is accompanied by a decrease in runoff for the same period. The decreased runoff is further enhanced in the latter part of the year when a decrease in precipitation also occurs. The decrease in runoff is due to increased evapotranspiration.

High latitude rivers (Fig 5-3d) show the greatest change in runoff to occur in the spring months (MAM), due to a combination of snow melt and increase precipitation. The confidence in these results is reduced somewhat because the model-generated river runoff and precipitation are generally too high in the present climate and also because the simulations are for only three years. The short simulations are likely to be more of a factor for the Magdalena and Sao Francisco rivers because the drainage areas are small. A more detailed examination of several river basins follows.

Figures 5.4-5.16 show monthly precipitation and river runoff for the present and doubled CO₂ climates. The world's two largest rivers, the Amazon and Congo, (Fig. 5.4) are classified as wet river basins. Results for these two rivers are not too reliable because river runoff is poorly simulated for the present climate. The Amazon has increased precipitation between November and February, the southern hemisphere summer, and increased runoff from November through April. As discussed in chapter 3, model-generated river runoff using the new routing scheme, will peak after the precipitation maximum by approximately 1 to 2 months. The routing scheme allows for movement of runoff from one grid box to another until it reaches the mouth of the river basin. The Congo river has increased precipitation and runoff throughout the entire year, with a slight maximum in the spring and summer months.

The Sao Francisco river (Fig. 5.5) is one of the rivers in which annual precipitation increases slightly (6%) while annual runoff decreases slightly (3%). Monthly precipitation

and runoff show little change throughout the year. The Mekong River is shown in Fig 5.6. Besides precipitation and runoff, average monthly snow mass is shown for the snow season. The snow decrease is primarily due to the warmer temperatures associated with the doubled CO₂ climate. Since we have not compared model-generated snow fall with observed snow fall, this result is tentative. Because snow decreases, one would expect a decrease in snow melt runoff during the late spring and summer months. However, the Mekong river runoff actually increases during these months because of the increased spring and summer rainfall.

Figures 5.7-5.9 show six of the basins classified as moderately wet. Figure 5.5 shows the Mississippi and Yangtze rivers. Changes in snow mass can significantly affect river runoff. Although snow mass decreases for both rivers during the winter months, spring runoff shows little change because of the increased rainfall during the spring and summer.

The Niger (Fig. 5.8) and the Nile (Fig. 5.9) rivers are two moderately wet rivers in which there is little change in annual precipitation. However, a decrease in precipitation occurs from June to October and an increase in precipitation occurs from November to February for the Nile River and November through April for the Niger River. The precipitation decrease between June and October is approximately equal for both the Nile and Niger rivers, however, the decrease in river runoff is much greater for the Niger River. The decreased river runoff must be due to increased evapotranspiration. Observed temperatures average 26° - 27°C while precipitation varies significantly over the Niger basin. Temperature increases in response to global warming may only enhance evaporation in the drier regions of the Niger River. Unfortunately the observed station for the Niger River is far away from the mouth of the river. Hence, one cannot be certain about the model's ability to simulate the runoff for the present climate.

The model-generated river runoff for the low and mid-latitude dry river basins is poorly simulated. Hence, the confidence in the runoff results for these basins is much

lower than for the other cases. The model-generated runoff for the Colorado River (Fig. 5.10b) is too high when compared to observed runoff and precipitation is poorly simulated. The major change in the precipitation for the Yellow River (Fig 5.10a) is an enhancement of the summer monsoon in the doubled CO₂ climate. River runoff is maximum in October, approximately one month after the monsoon season.

River runoff at the higher latitudes is more interesting to analyze because of the contribution of snow melt. Because observed snow data have not been obtained to compare with the model-generated snow, the ability of the model to simulate the actual snow mass is not known. However, changes in the total snow mass in a doubled CO₂ climate can be used to further analyze the effects of snow melt on river runoff in the higher latitude rivers. Table 5.3 shows the seasonal average snow mass for both the present climate and the doubled CO₂ climate. For all rivers, except the Amur, which shows little change, fall snow mass, in a doubled CO₂ climate, is reduced by an average of 30%.

There is an interesting difference between northeast Asia and other high latitude rivers. In northeast Asia the net snow mass actually increases for the Yenesei, Lena, Kolyma, Indigirka, and Amur rivers. For all other high latitude rivers, the average winter and spring snow mass decrease. The snow decrease is caused primarily by an increase in temperatures for a doubled CO₂ climate. However, because the average temperatures in the northeastern region of Asia are well below freezing, temperature changes of 2-7 degrees Celsius will not cause changes in the rain to snow ratio, thus, an increase in precipitation in a doubled CO₂ climate will generate more snow mass for the river basins in that region. Despite differences in amounts of snow mass, high latitude rivers all show one thing in common, a faster snow melt during spring in a doubled CO₂ climate. This faster snow melt causes the river runoff maximum to occur earlier for all high latitude river basins.

The two high latitude rivers in North America are the Yukon and the Mackenzie (Fig. 5.12). For both rivers there is a decrease in the monthly snow mass throughout the

snow season, and the melting season begins approximately one month earlier in the doubled CO₂ climate. This causes a shift in the timing of the spring river runoff peak. However, the magnitude of the maximum river runoff is the same for the Yukon and increases slightly for the Mackenzie due to increased spring precipitation in the doubled CO₂ climate. The shift in the runoff peak also occurs in the Severnaya Dvina and Ob rivers located in north central Asia (Fig. 5.13). The changes in timing of the maximum river runoff could be studied better if daily data were available.

Figures 5.14-5.16 show the Yenesei, Lena, Kolyma, Indigirka, and Amur rivers, all of which have an increase in average monthly snow mass during the winter and spring months. However, despite the increase in snow mass, the snow melt ends at about the same time for both the present and doubled CO₂ climates. The increase in snow mass is associated with increased winter precipitation, however, unlike the other high latitude rivers, temperature increases are not large enough to push the temperature over the freezing point. Climatology for the present climate from *Critchfield* [1974] shows high pressure is centered over the Tibetan Plateau, with the average surface flow to be southerly to southwesterly for all river basins west of the Yenesei for January. The Yenesei river basin and river basins to the east are under an average westerly to northwesterly surface flow for January. Observed January temperatures average between -50°C and -30°C for the regions east of the Yenesei river basin and between -25°C and -10°C for the region west of the Yenesei river basin. In the doubled CO₂ climate, the temperature is projected to rise between 2°C and 7°C for the high latitude rivers. The temperature increase is not affecting the snow to rain ratio in river basins in which the average temperatures are well below freezing. This can explain the differences in snowfall between the high latitude river basins.

The major change in the high latitude rivers is that the spring runoff peak occurs one month earlier in a doubled CO₂ climate. The shift is primarily due to the earlier melting of snow and ice. Despite an increase in precipitation for all high latitude rivers,

the magnitude of the runoff peak is greater in the doubled CO₂ climate for only the Yenesei, Lena, Kolyma, Indigirka, and Amur rivers. This is caused by the combination of increased precipitation and snow.

One advantage of the new routing scheme of *Miller et al.* [1992] is that larger river basins can be divided into smaller basins. The Mississippi River and its tributaries were examined for a doubled CO₂ climate. Figures 5.17 - 5-20 show present and doubled CO₂ climates for precipitation, runoff, and snow mass. Annual runoff and precipitation increase 16% and 21%, respectively, and snow mass decreased for the Mississippi River basin. The most significant changes occurred in the Missouri basin in which runoff maxima occur in March and May. The combination of decreases in snow mass and April precipitation cause this double maxima to occur. The confidence in these results is not too high because the major tributaries, the Missouri and Ohio, are poorly simulated by the model. For the present climate the model generates too much precipitation and runoff for the Missouri and too little for the Ohio.

Annual and monthly changes in precipitation and river runoff in a doubled CO₂ climate were examined for several river basins worldwide. It is important to examine monthly changes to determine whether any of the changes are uniform throughout the year. Most river basins have increased precipitation and river runoff in a doubled CO₂ climate. The one exception is the Niger river in which there is little change in precipitation and a reduction in river runoff of 36%, caused by increased evapotranspiration. The most interesting changes in runoff occur in the higher latitudes where snow melt is part of the total river runoff. The spring peak is earlier and the magnitude is higher for the northeastern rivers in Asia where snow mass increases in a doubled CO₂ climate. The increase in snow mass is unique to only the rivers in northeastern Asia.

Table 5.1. Annual observed and model-generated runoff (Km³/yr) and precipitation (Km³/yr) for the world's major rivers for the present climate (1XCO₂) and the doubled CO₂ climate (2XCO₂). Change from 1XCO₂ to 2XCO₂ is given by the % change column.

<i>Climate Type</i> <i>River</i>	<i>Precipitation</i>			<i>Runoff</i>			<i>% Change</i>	
	<i>OBS</i>	<i>1XCO2</i>	<i>2XCO2</i>	<i>OBS</i>	<i>1XCO2</i>	<i>2XCO2</i>	<i>Precip</i>	<i>Runoff</i>
<i>Wet</i>								
Amazon	13942	14224	15538	4886	3079	3341	9%	9%
Congo	5516	8470	9766	1398	2095	2632	15%	26%
Orinoco	2193	2005	2422	794	466	682	21%	46%
Mekong	1477	2138	2317	449	711	815	8%	15%
Magdalena	758	1056	924	213	303	217	-13%	-28%
Sao Francisco	799	1273	1344	83	274	265	6%	-3%
Average	4114	4861	5385	1304	1155	1325	11%	15%
<i>Moderately Wet</i>								
Yangtze	1985	3465	4126	792	1499	1947	19%	30%
Mississippi	3039	2981	3559	498	660	766	19%	16%
LaPlata (Parana)	3662	3164	4064	---	(475)	(723)	28%	52%
St Lawrence	1070	1102	1256	214	321	350	14%	9%
Danube	1192	1683	1984	---	(516)	(585)	18%	13%
Columbia	507	774	827	172	249	265	7%	6%
Zambesi	1218	1356	1475	105	197	213	9%	8%
Fraser	179	307	329	87	134	146	7%	9%
Nile	1960	3659	3690	---	(657)	(633)	1%	-4%
Niger	1618	2116	2141	---	(332)	(211)	1%	-36%
Average	1643	2061	2345	311	510	615	14%	16%
<i>Dry</i>								
Indus	392	592	489	76	204	124	-17%	-39%
Tigris-Euphrates	497	497	481	---	(76)	(77)	-3%	1%
Yellow	541	1454	1642	---	(563)	(710)	13%	26%
Colorado	205	339	385	12	69	91	14%	32%
Murray	528	585	702	8	97	122	20%	26%
Average	433	693	740	32	202	225	7%	11%
<i>High Latitude Dry</i>								
Yenesei	1126	1371	1770	558	462	651	29%	41%
Lena	926	1486	1712	516	535	681	15%	27%
Ob	1354	1066	1564	388	464	632	47%	36%
Amur	1120	1394	1438	309	273	298	3%	9%
Mackenzie	607	1242	1504	264	644	756	21%	17%
Yukon	333	715	824	197	511	630	15%	23%
Severnay Dvina	206	241	322	107	132	165	34%	25%
Kolyma	258	506	692	71	367	526	37%	43%
Indigirka	100	228	275	49	134	169	21%	26%
Average	670	917	1122	273	391	501	22%	28%
Total Average	1644	2050	2319	510	578	687	13%	18%

Observed precipitation is from Legates and Willmott [1990]. Observed runoff is from UNESCO [1969, 1974, 1985]. (---) Indicates river basins in which observed runoff station is not near the mouth of the river. Values in () are not included in climate type and total runoff averages.

Table 5.2. Model and observed drainage basin areas (Km²) for the world's major rivers. The ratio is defined as the model to observed ratio.

<i>Climate Type</i>	<i>Area</i>		
<i>River</i>	<i>Model</i>	<i>Observed</i>	<i>Ratio</i>
<i>Wet</i>			
Amazon	6500000	4640285	1.40
Congo	3510000	3475000	1.01
Orinoco	950000	850000	1.12
Mekong	860000	646000	1.33
Magdalena	360000	257438	1.40
Sao Francisco	650000	622600	1.04
Average	2138333	1748554	1.22
<i>Moderately Wet</i>			
Yangtze	1810000	1705383	1.06
Mississippi	3510000	2964300	1.18
LaPlata (Parana)	2910000	975375	2.98
St Lawrence	1140000	764600	1.49
Danube	1530000	807000	1.90
Columbia	710000	614000	1.16
Zambesi	1190000	940000	1.27
Fraser	230000	217000	1.06
Nile	2760000	---	---
Niger	1490000	---	---
Average	1728000	1123457	1.54
<i>Dry</i>			
Indus	830000	832418	1.00
Tigris-Euphrates	1150000	408100	2.82
Yellow	1060000	688421	1.54
Colorado	640000	629100	1.02
Murray	1040000	991000	1.05
Average	944000	709808	1.33
<i>High Latitude Dry</i>			
Yenesi	2700000	2440000	1.11
Lena	2400000	2430000	0.99
Ob	2630000	2430000	1.08
Amur	1870000	1730000	1.08
Mackenzie	1570000	1570000	1.00
Yukon	770000	767000	1.00
Severnay Dvina	340000	348000	0.98
Kolyma	710000	361000	1.97
Indigirka	350000	305000	1.15
Average	1482222	1375667	1.08
Total Average	1605667	1264608	1.27

Observed area from UNESCO [1969, 1974, 1985]

Table 5.3. Seasonal model-generated snow mass (Km^3) averaged over fall, winter, and spring for the world's major rivers for the present climate (1XCO₂) and the doubled CO₂ climate (2XCO₂). Change from 1XCO₂ to 2XCO₂ is given by the % change column.

<i>Climate Type</i>	<i>Average Seasonal Snow Mass</i>								
	<i>Fall</i>	<i>Fall</i>	<i>Fall</i>	<i>Winter</i>	<i>Winter</i>	<i>Winter</i>	<i>Spring</i>	<i>Spring</i>	<i>Spring</i>
<i>River</i>	<i>1XCO₂</i>	<i>2XCO₂</i>	<i>% Change</i>	<i>1XCO₂</i>	<i>2XCO₂</i>	<i>% Change</i>	<i>1XCO₂</i>	<i>2XCO₂</i>	<i>% Change</i>
<i>Wet</i>									
Mekong	6.7	1.7	-75%	21.3	18.3	-14%	17.3	11.0	-36%
Average	6.7	1.7	-75%	21.3	18.3	-14%	17.3	11.0	-36%
<i>Moderately Wet</i>									
Yangtze	12.0	3.3	-73%	54.3	28.3	-48%	31.7	16.7	-47%
Mississippi	2.0	0.7	-65%	49.7	19.7	-60%	9.7	1.3	-87%
St Lawrence	3.3	1.0	-70%	58.7	24.3	-59%	36.3	10.3	-72%
Danube	0.3	0.0	---	17.0	1.7	-90%	2.3	0.0	---
Columbia	0.3	0.0	---	8.3	4.3	-48%	1.0	0.0	---
Fraser	0.3	0.0	---	8.3	2.0	-76%	4.7	0.0	---
Average	3.0	0.8	-73%	32.7	13.4	-59%	14.3	4.7	-67%
<i>Dry</i>									
Indus	0.0	0.0	---	14.7	0.0	---	5.3	0.0	---
Yellow	1.7	0.0	---	7.0	3.7	-47%	2.3	0.3	-87%
Colorado	0.0	0.0	---	4.0	0.7	-83%	0.7	0.0	---
Average	0.6	0.0	---	8.6	1.5	-83%	2.8	0.1	-96%
<i>High Latitude Dry</i>									
Yenesei	34.0	25.3	-26%	221.0	237.0	7%	160.7	157.3	17%
Lena	44.3	35.3	-20%	203.0	225.0	11%	187.7	205.3	9%
Ob	22.0	14.0	-36%	205.0	171.3	-16%	118.7	88.0	-26%
Amur	6.0	6.3	5%	62.3	68.7	10%	35.7	39.0	9%
Mackenzie	31.3	21.0	-33%	216.0	179.3	-17%	212.0	134.0	-37%
Yukon	22.7	16.3	-28%	129.3	103.0	-20%	166.7	112.3	-33%
Severnay Dvina	5.3	1.7	-68%	45.3	29.3	-35%	30.0	12.0	-60%
Kolyma	26.3	20.3	-23%	108.0	125.3	16%	148.7	170.0	14%
Indigirka	14.0	10.7	-24%	43.7	46.7	7%	60.0	62.3	4%
Average	22.9	16.8	-27%	137.1	131.7	-4%	124.5	112.2	-10%
Total Average	12.2	8.3	-32%	77.7	67.8	-13%	64.8	55.3	-15%

Seasons are defined as the following: Fall (September, October, and November), Winter (December, January, and February), and Spring (March, April, and May). The amounts represent the average snow mass over the three month period.

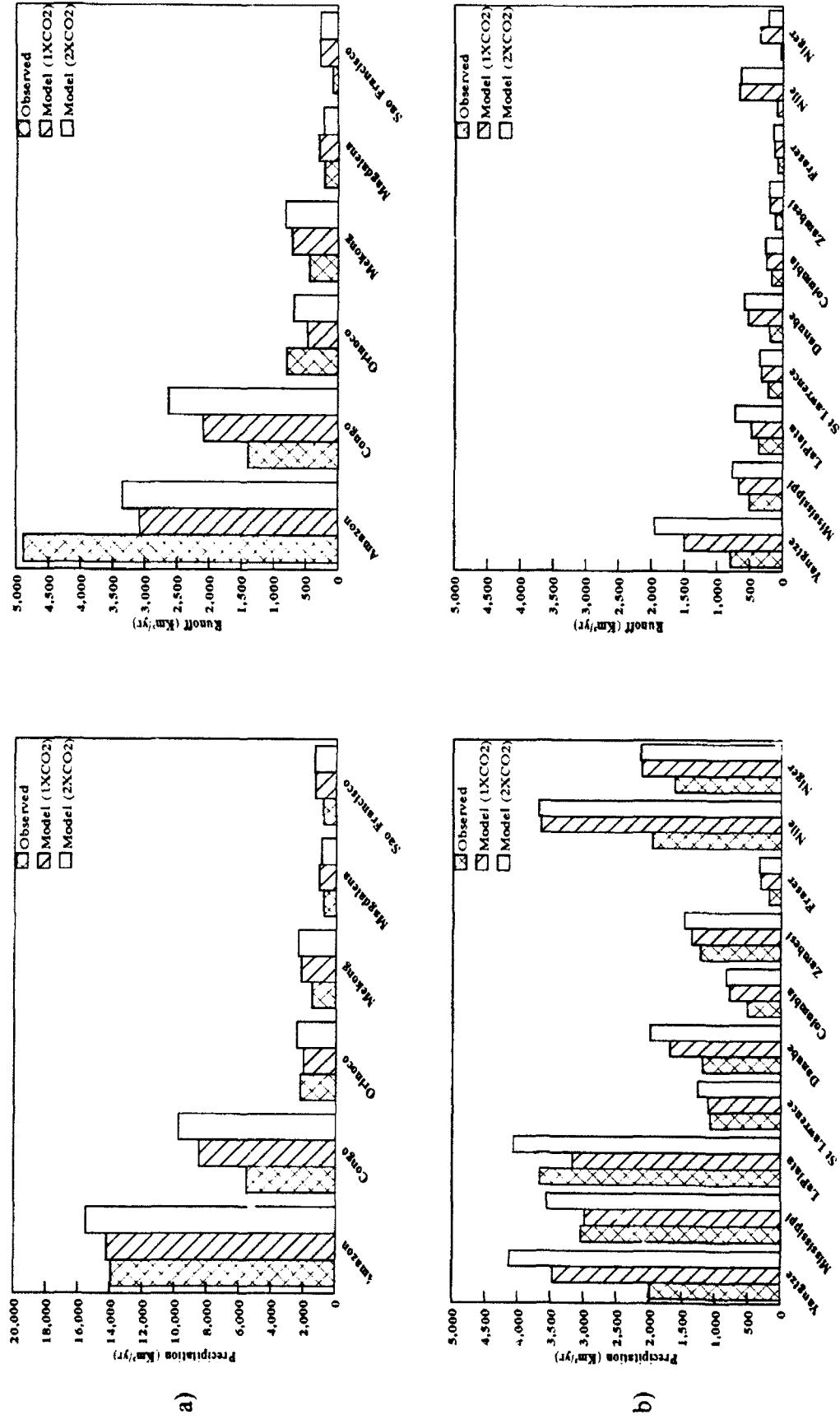


Figure 5.1. Comparison between model-generated mean annual precipitation and runoff for the present and doubled CO₂ climates and the observed precipitation from Legates and Willmott [1990] and runoff from UNE/SCO [1969, 1974, 1985] for (a) wet river basins and (b) moderately wet river basins.

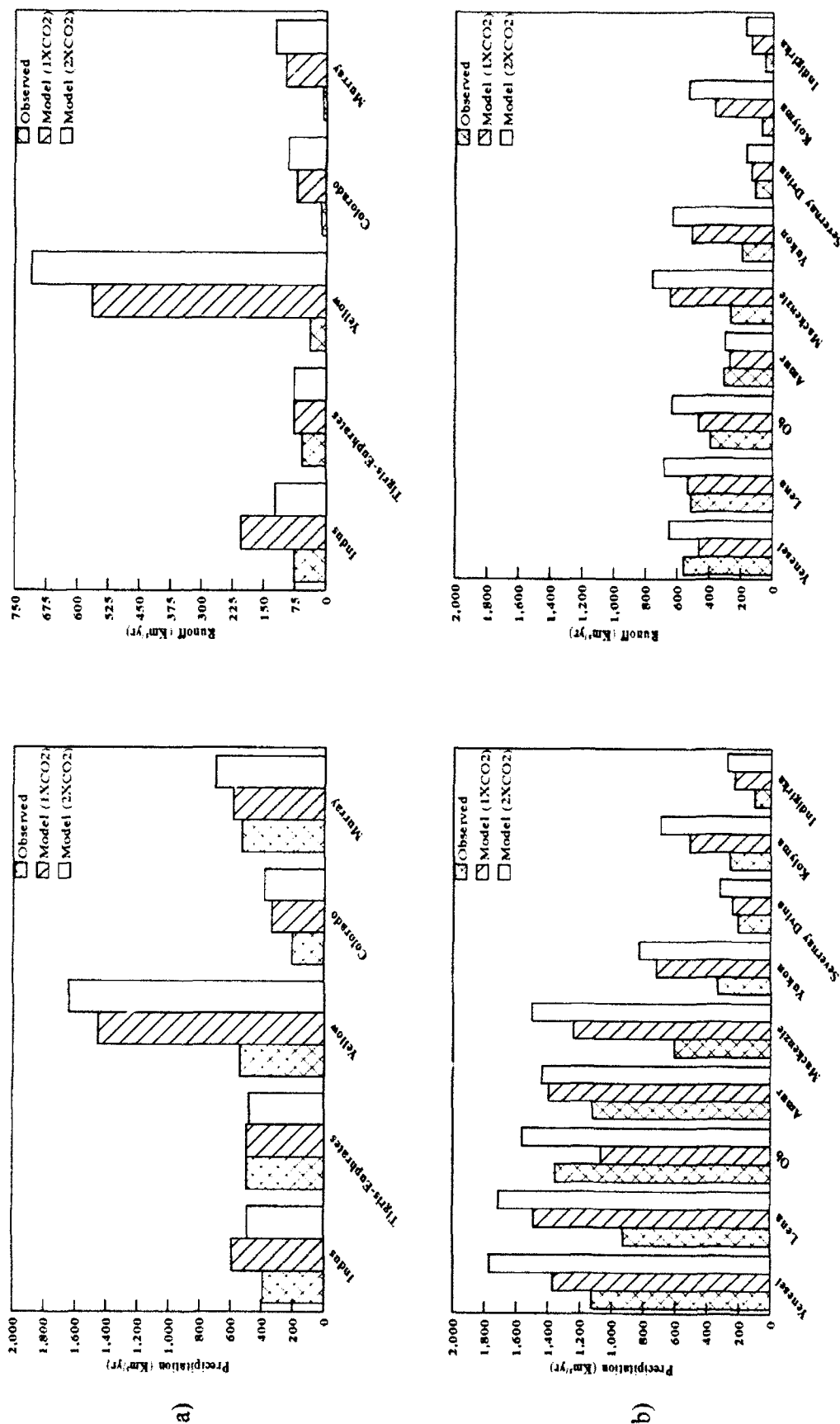


Figure 5.2. Comparison between model-generated mean annual precipitation and runoff for the present and doubled CO₂ climates and the observed precipitation from *Legates and Willmott* [1969, 1974, 1985] for (a) dry river basins and (b) high latitude dry river basins.

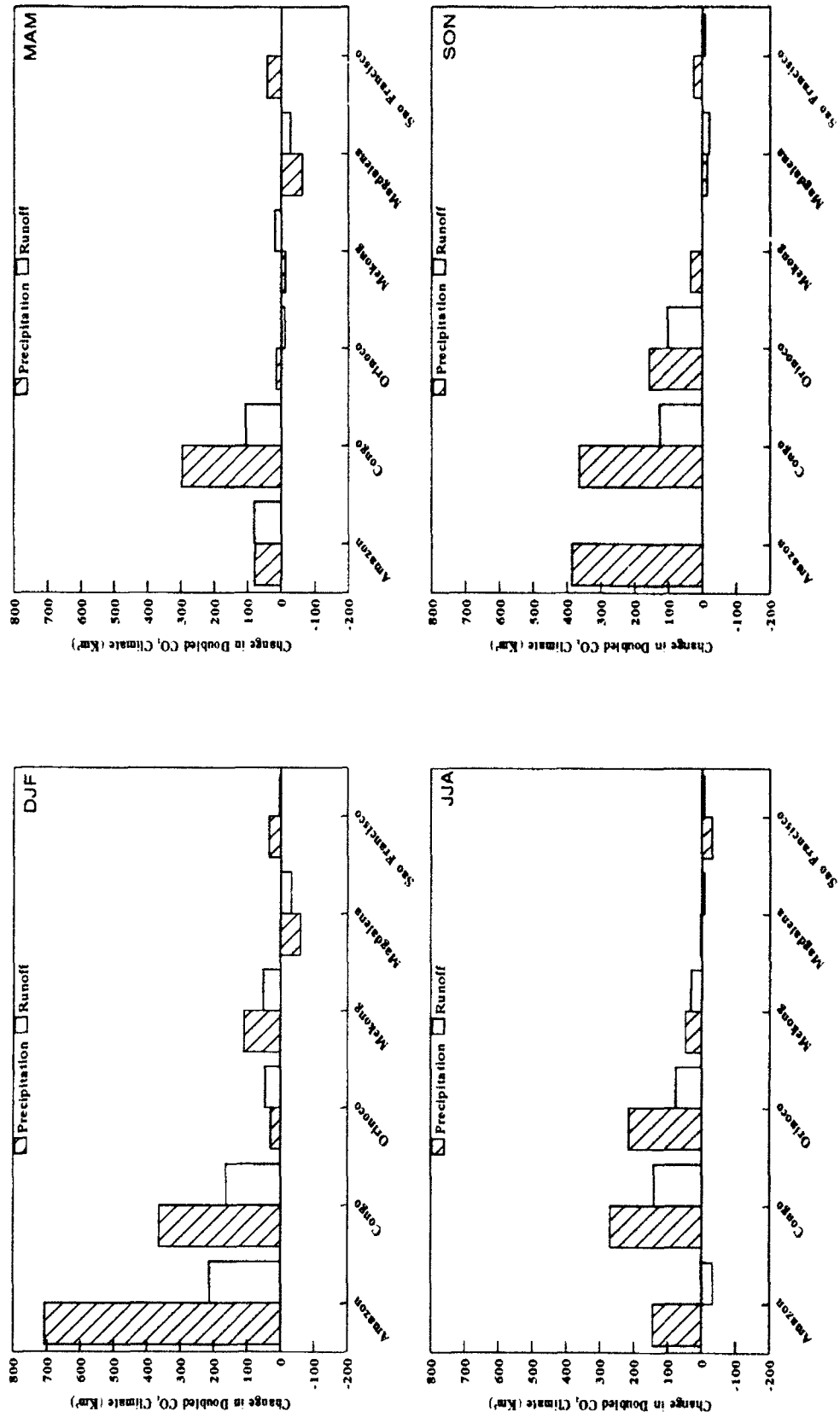


Figure 5.3a. Model-generated precipitation and runoff seasonal changes for the wet river basins in the doubled CO₂ climate for Dec, Jan, Feb (DJF), Mar, Apr, May (MAM), Jun, Jul, Aug (JJA), and Sep, Oct, Nov (SON).

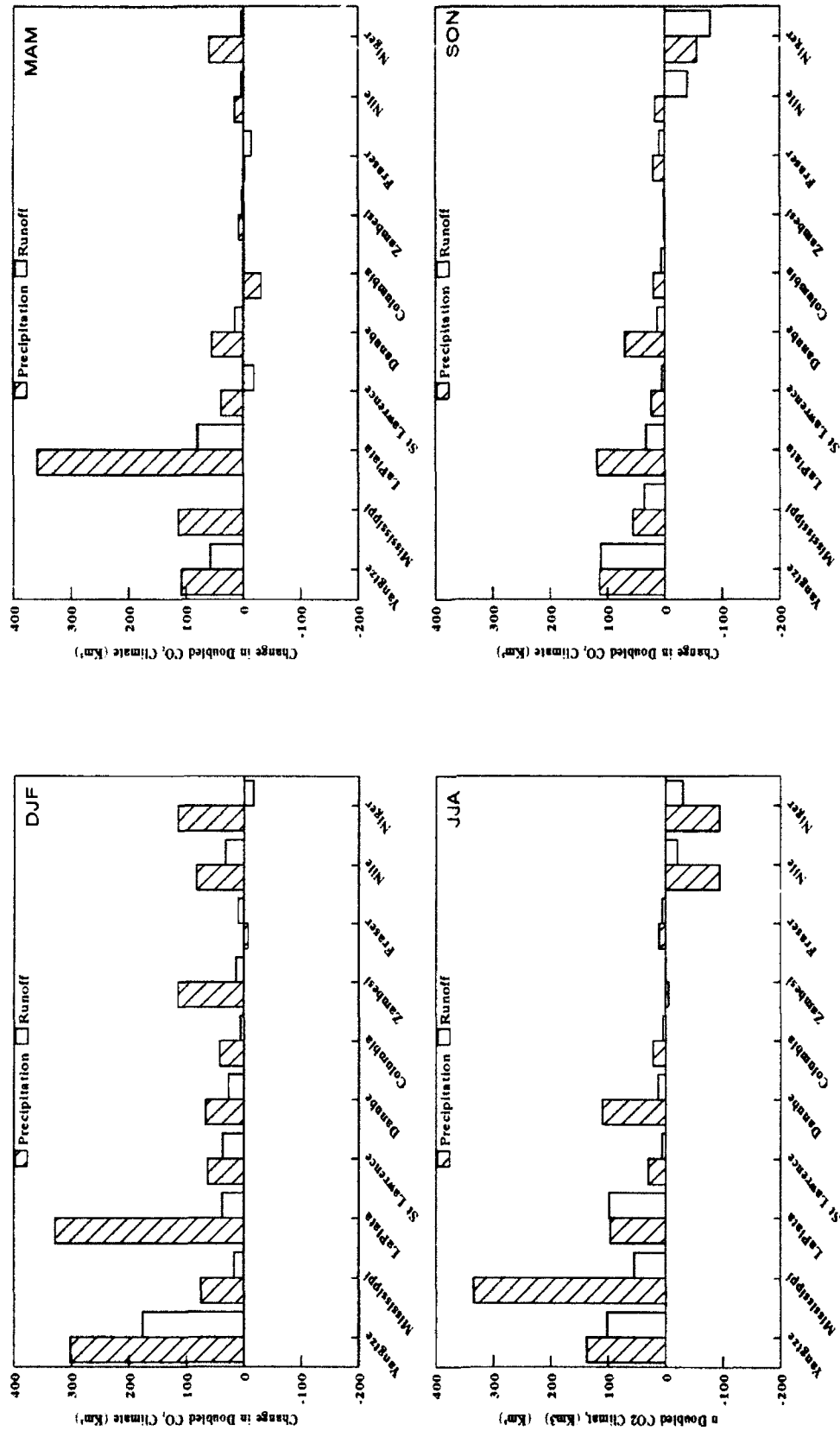


Figure 5.3b. Model-generated precipitation and runoff seasonal changes for the moderately wet river basins in the doubled CO₂ climate for Dec, Jan, Feb (DJF), Mar, Apr, May (MAM), Jun, Jul, Aug (JJA), and Sep, Oct, Nov (SON).

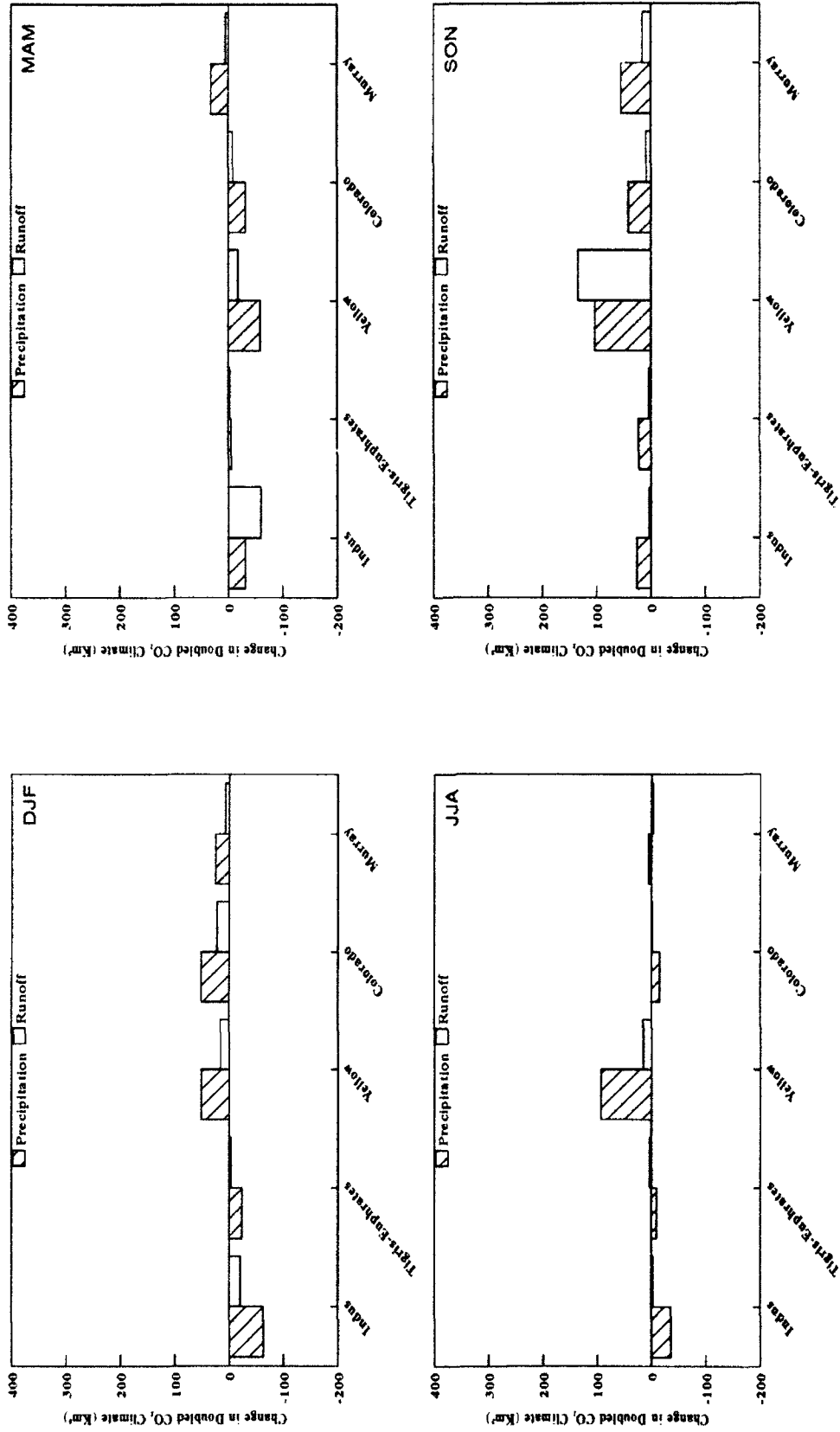


Figure 5.3c. Model-generated precipitation and runoff seasonal changes for the dry river basins in the doubled CO₂ climate for Dec, Jan, Feb (DJF), Mar, Apr, May (MAM), Jun, Jul, Aug (JJA), ar ' sep, Oct, Nov (SON).

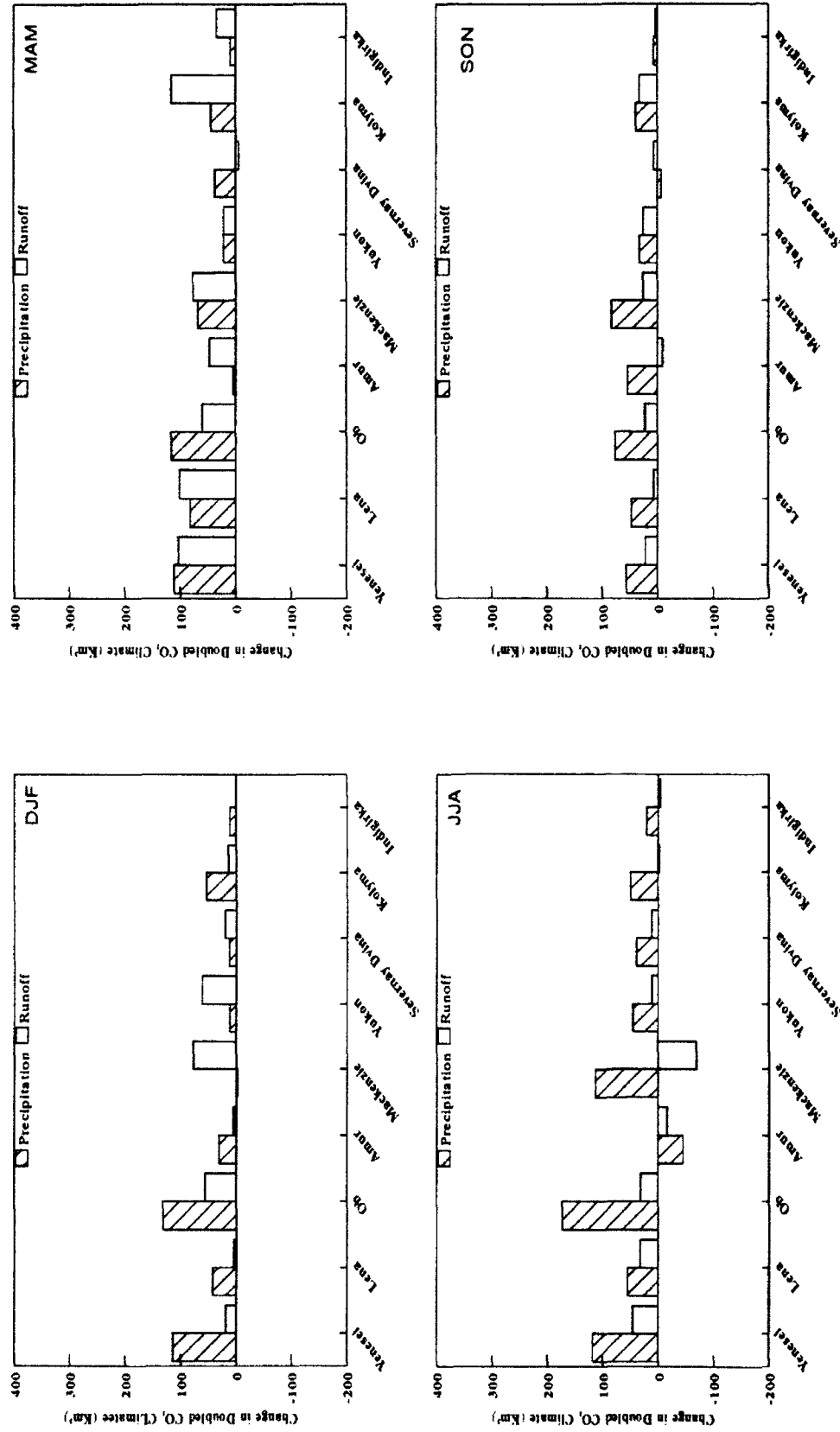


Figure 5.3.d. Model-generated precipitation and runoff seasonal changes for the high-latitude dry river basins in the doubled CO₂ climate for Dec, Jan, Feb (DJF), Mar, Apr, May (MAM), Jun, Jul, Aug (JJA), and Sep, Oct, Nov (SON).

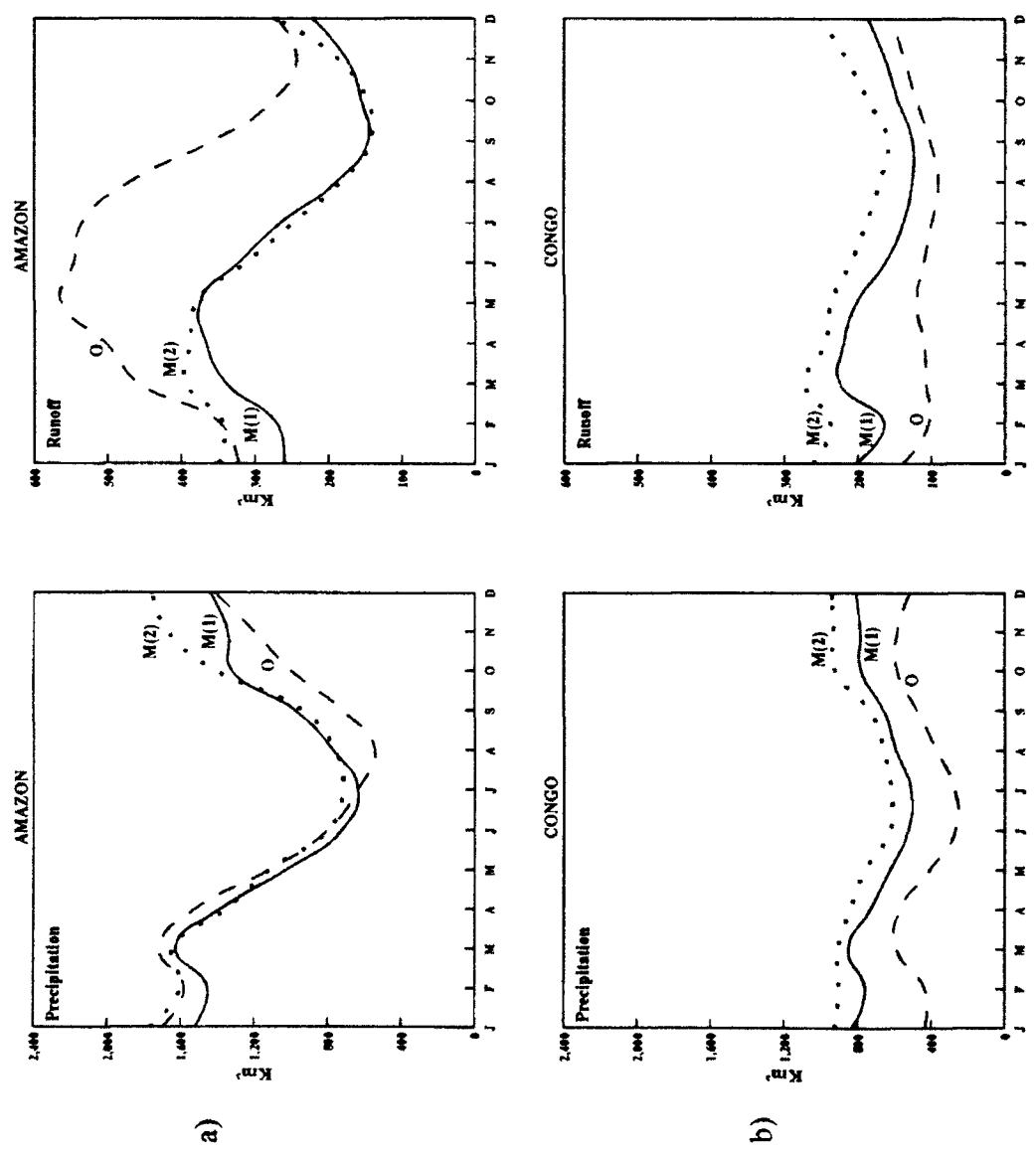


Figure 5.4. Model-generated monthly precipitation and runoff for the present climate [M(1)] and the doubled CO₂ climate [M(2)] and observed [O] precipitation from *Legates and Willmott* [1969, 1974, 1985] for the (a) Amazon and (b) Congo rivers.

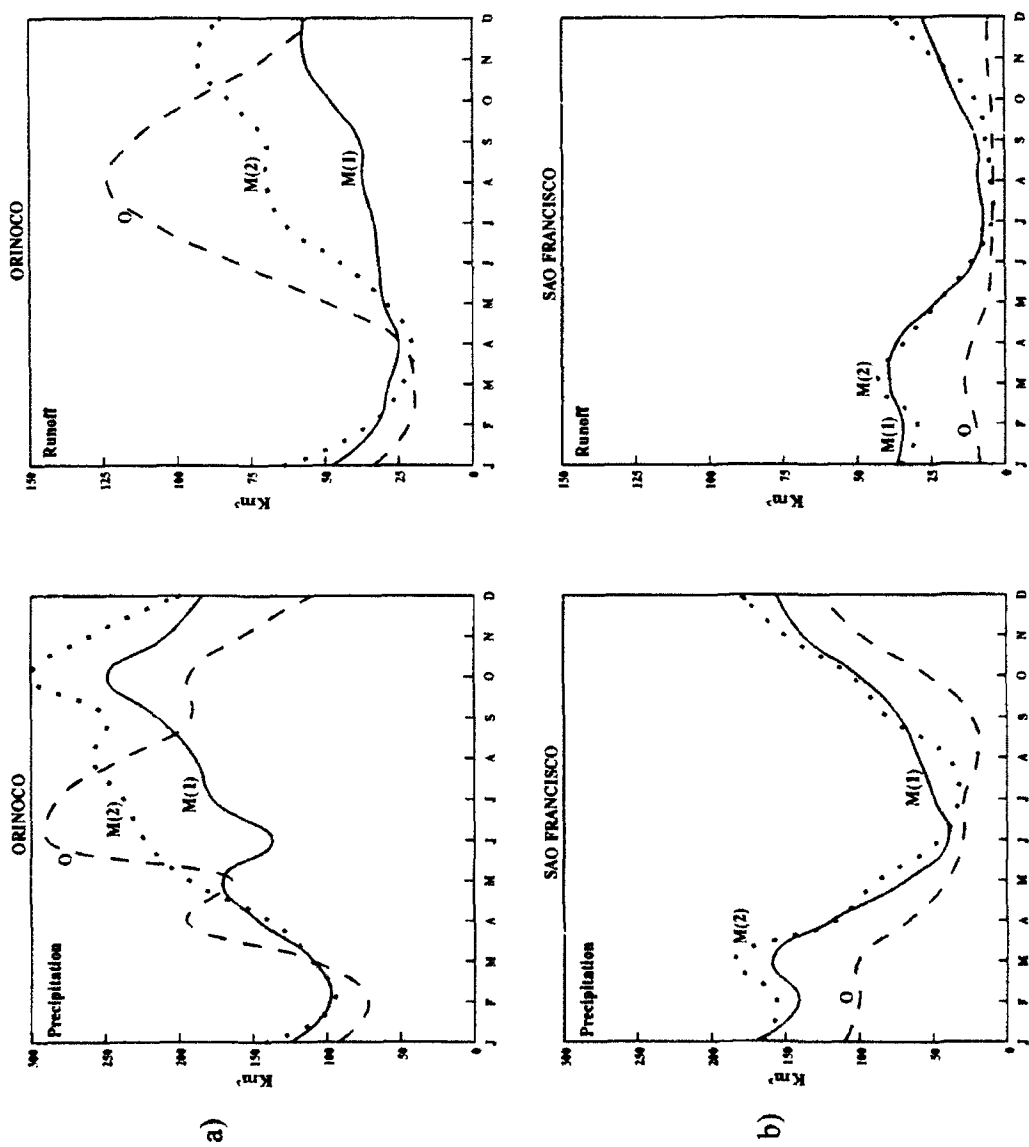


Figure 5.5. Model-generated monthly precipitation and runoff for the present climate [M(1)] and the doubled CO₂ climate [M(2)] and observed [O] precipitation from Legates and Willmott [1990] and runoff from UNESCO [1969, 1974, 1985] for the (a) Orinoco and (b) Sao Francisco rivers.

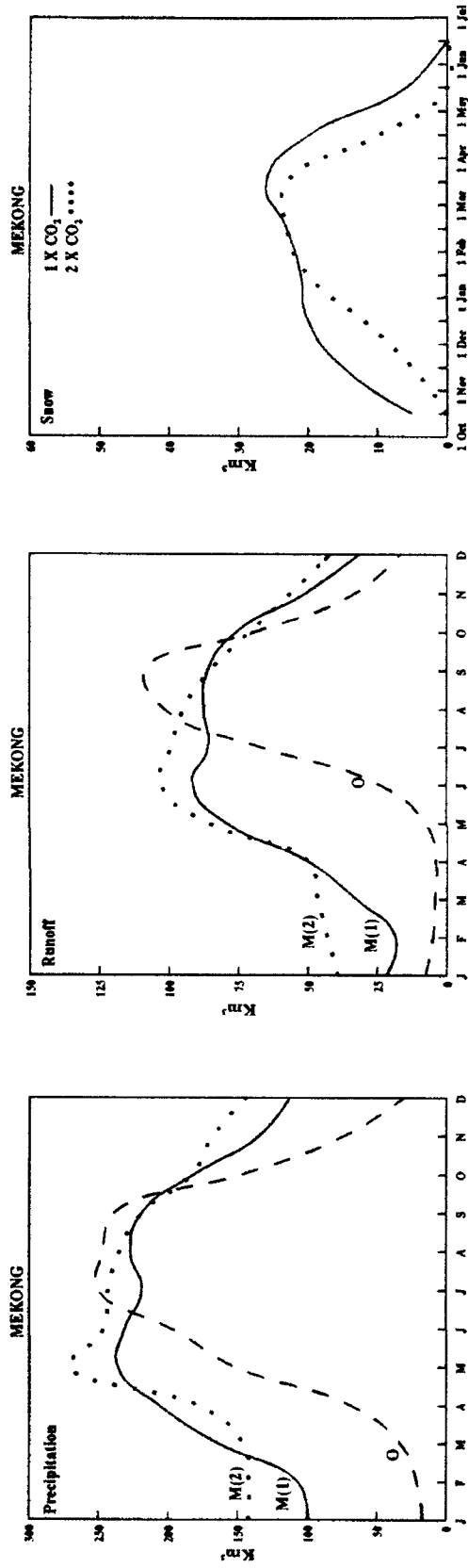


Figure 5.6. Model-generated monthly precipitation, runoff, and averaged snow mass during the snow season for the present climate [M(1)] and the doubled CO₂ climate [M(2)] and observed [O] precipitation from *Legates and Willmott* [1990] and runoff from *UNESCO* [1969, 1974, 1985] for the Mekong River.

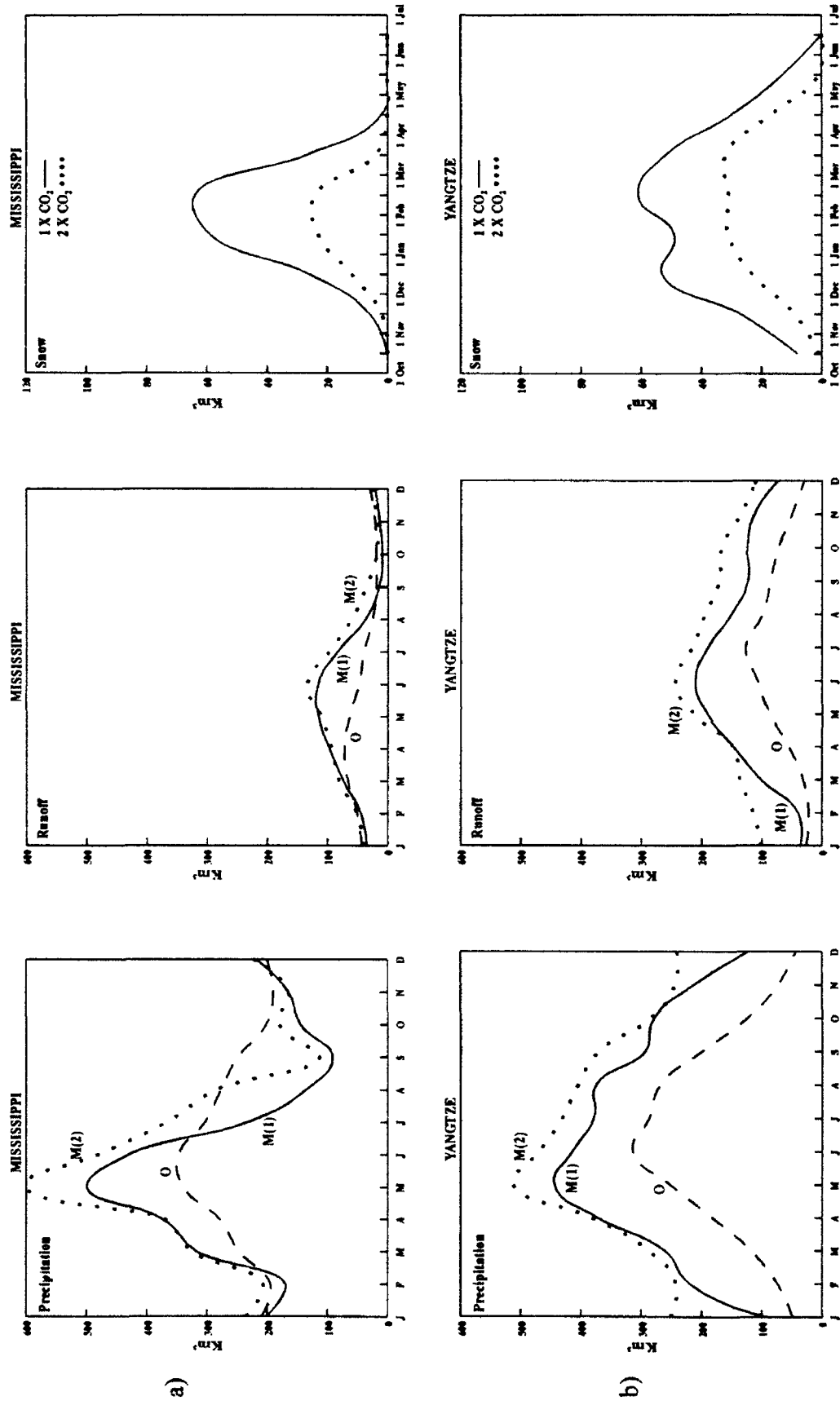


Figure 5.7. Model-generated monthly precipitation, runoff, and averaged snow mass during the snow season for the present climate [M(1)] and the doubled CO₂ climate [M(2)] and observed [O] precipitation from *Legates and Willmott [1990]* and runoff from *UNESCO [1969, 1974, 1985]* for the (a) Mississippi and (b) Yangtze rivers.

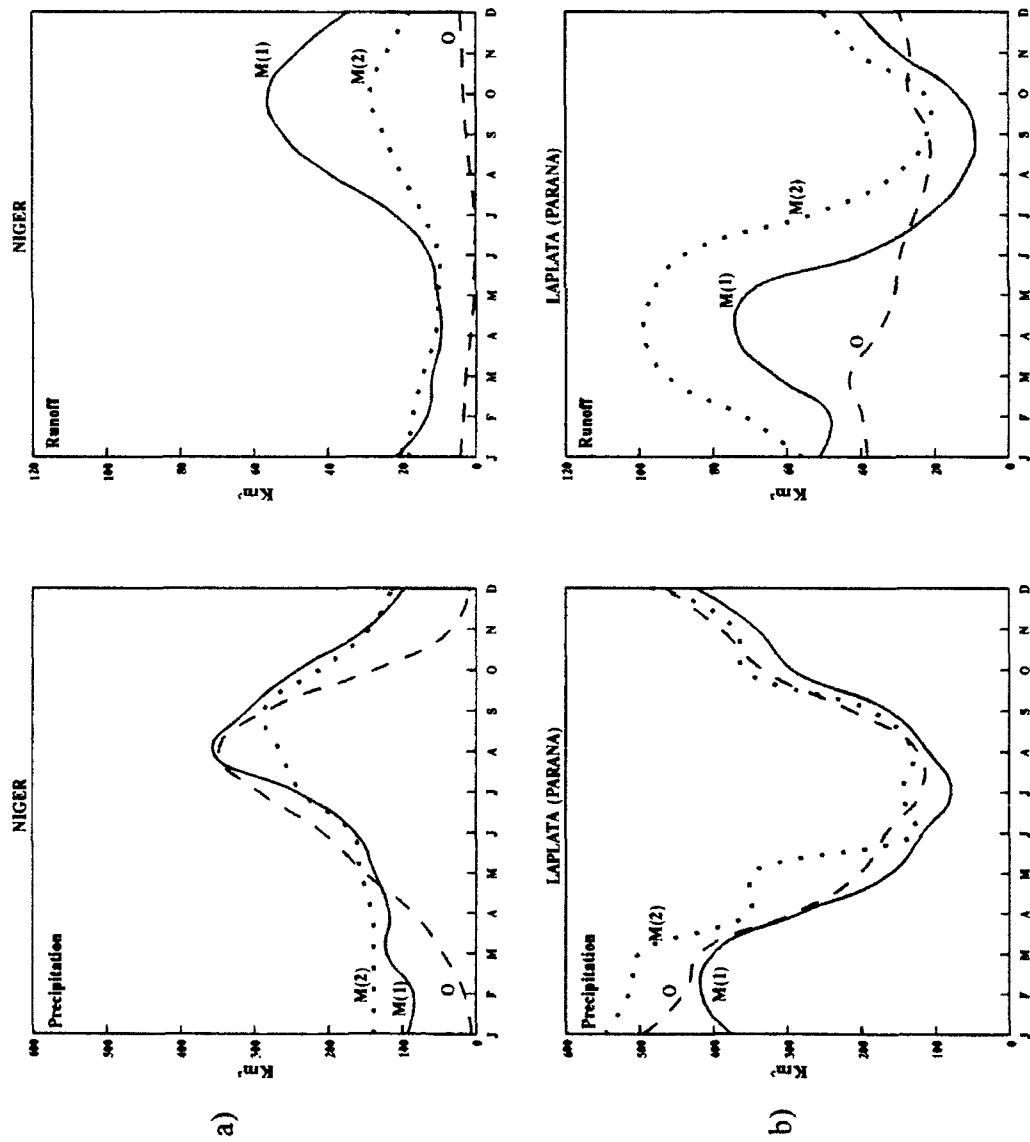


Figure 5.8. Model-generated monthly precipitation and runoff for the present climate [M(1)] and the doubled CO₂ climate [M(2)] and observed [O] precipitation from *Legates and Willmott* [1990] and runoff from *UNESCO* [1969, 1974, 1985] for the (a) Niger and (b) LaPlata (Parana) rivers. Observed runoff stations for Niger and LaPlata are not near the mouth of the river.

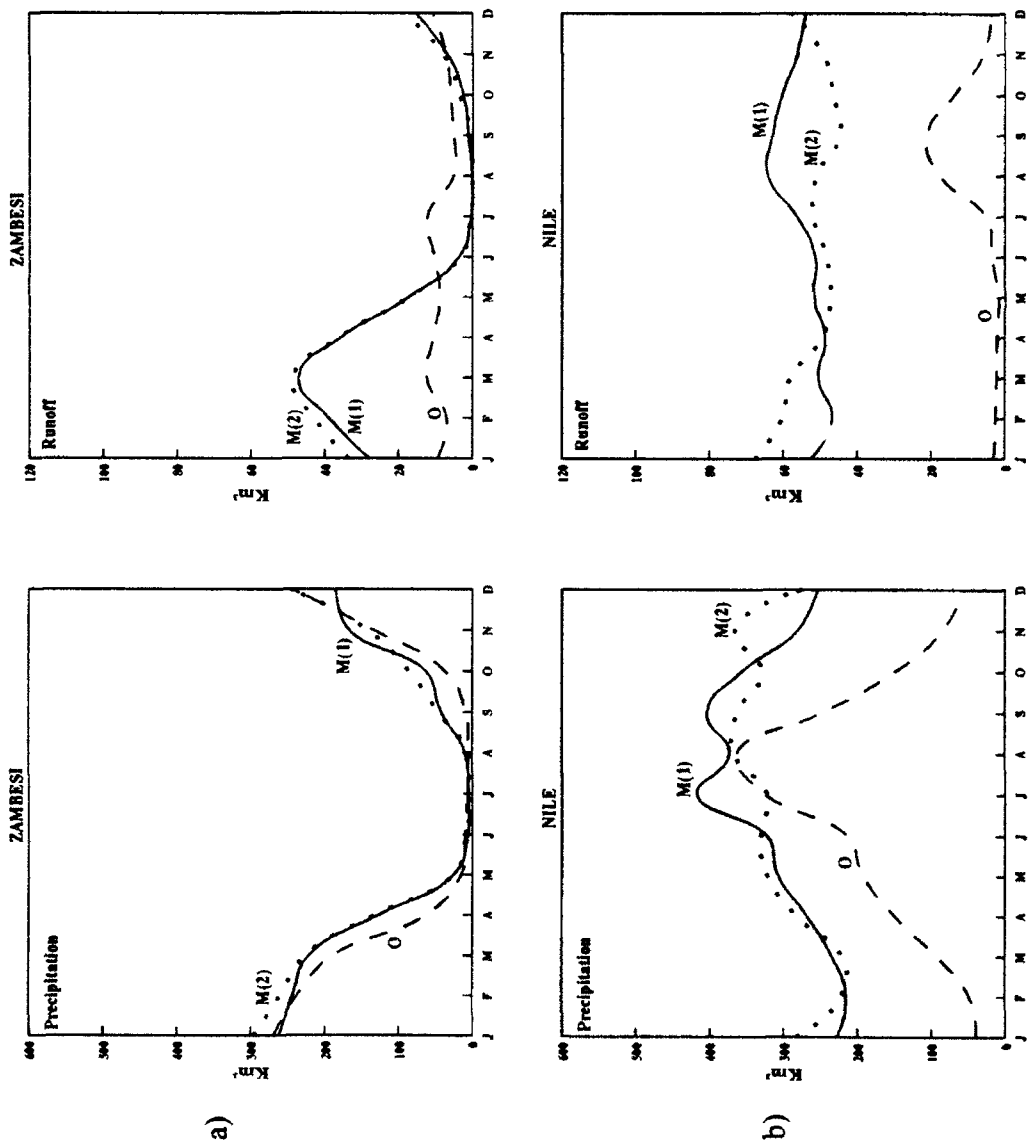


Figure 5.9. Model-generated monthly precipitation and runoff for the present climate [M(1)] and the doubled CO₂ climate [M(2)] and observed [O] precipitation from *Legates and Willmott* [1990] and runoff from *UNESCO* [1969, 1974, 1985] for the (a) Zambezi and (b) Nile rivers. Observed runoff station for the Nile is not near the mouth of the river.

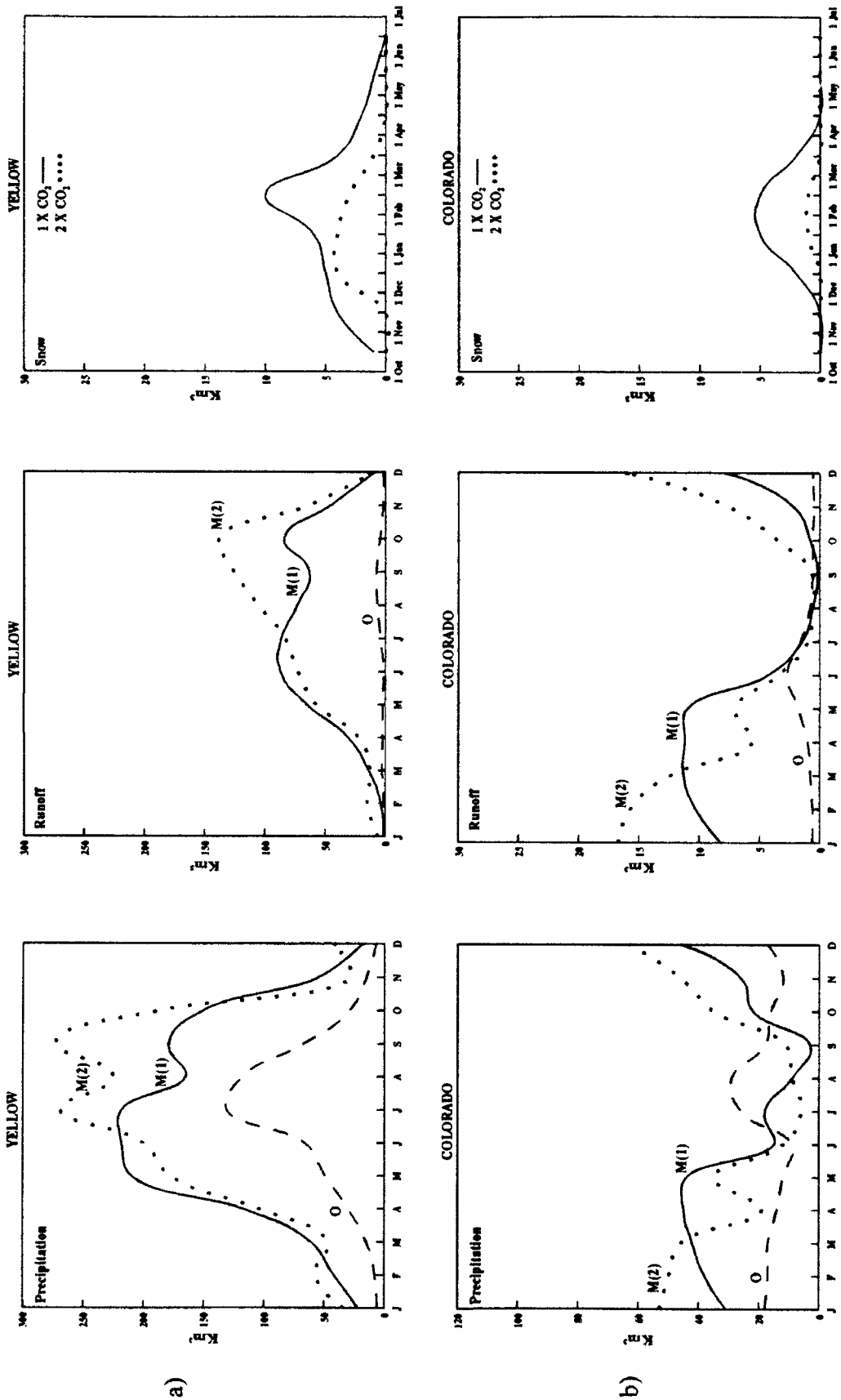


Figure 5.10. Model-generated monthly precipitation, runoff, and averaged snow mass during the snow season for the present climate [M(1)] and the doubled CO₂ climate [M(2)] and observed [O] precipitation from *Legates and Willmott [1990]* and runoff from *UNESCO [1969, 1974, 1985]* for the (a) Yellow and (b) Colorado rivers.

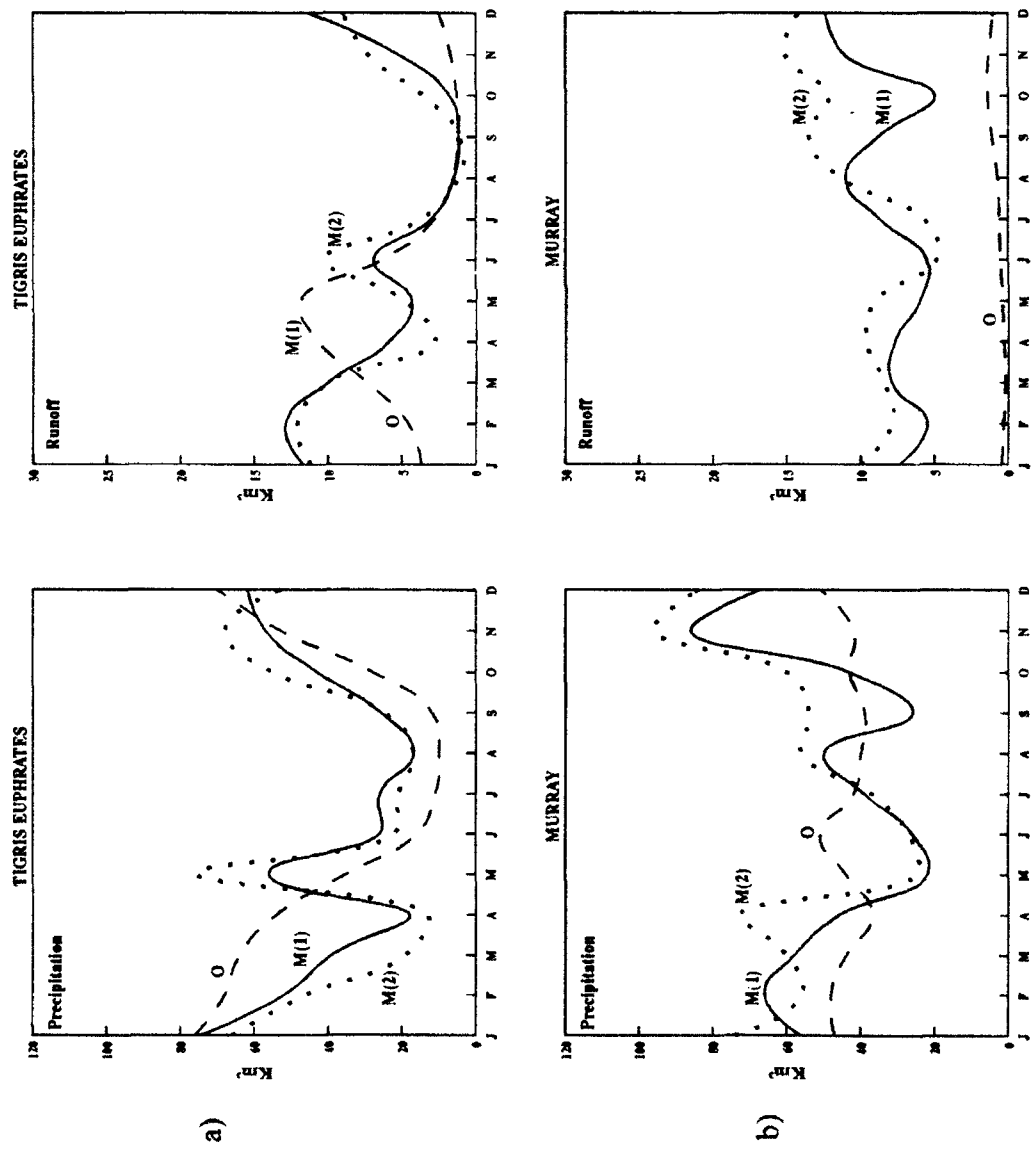


Figure 5.11. Model-generated monthly precipitation and runoff for the present climate [M(1)] and the doubled CO₂ climate [M(2)] and observed [O] precipitation from Legates and Willmott [1990] and runoff from UNESCO [1969, 1974, 1985] for the (a) Tigris-Euphrates and (b) Murray rivers. Observed runoff station for the Tigris-Euphrates is not near the mouth of the river.

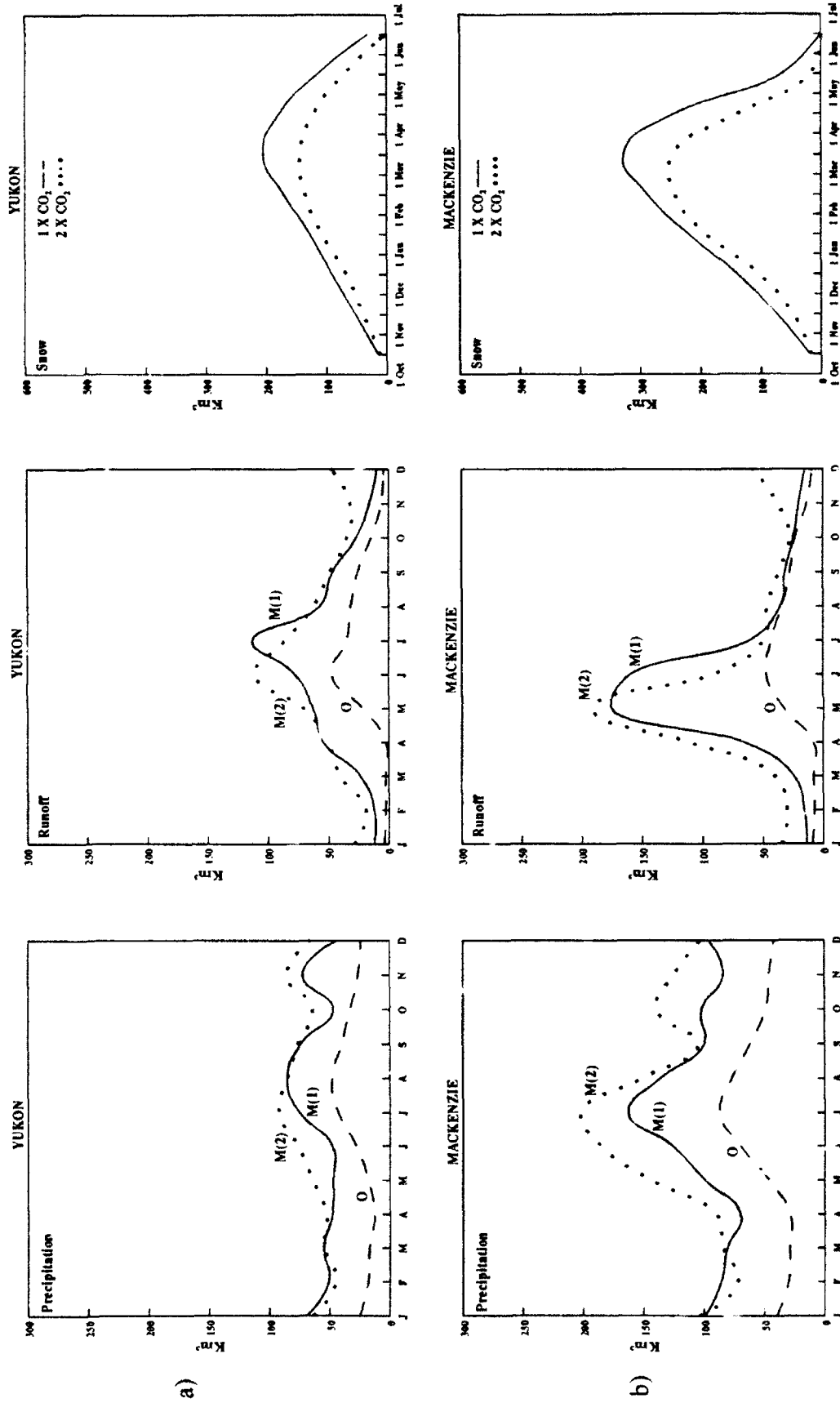


Figure 5.12. Model-generated monthly precipitation, runoff, and averaged snow mass during the snow season for the present climate [M(1)] and the doubled CO₂ climate [M(2)] and observed [O] precipitation from Legates and Willmott [1990] and runoff from UNESCO [1969, 1974, 1985] for the (a) Yukon and (b) Mackenzie rivers.

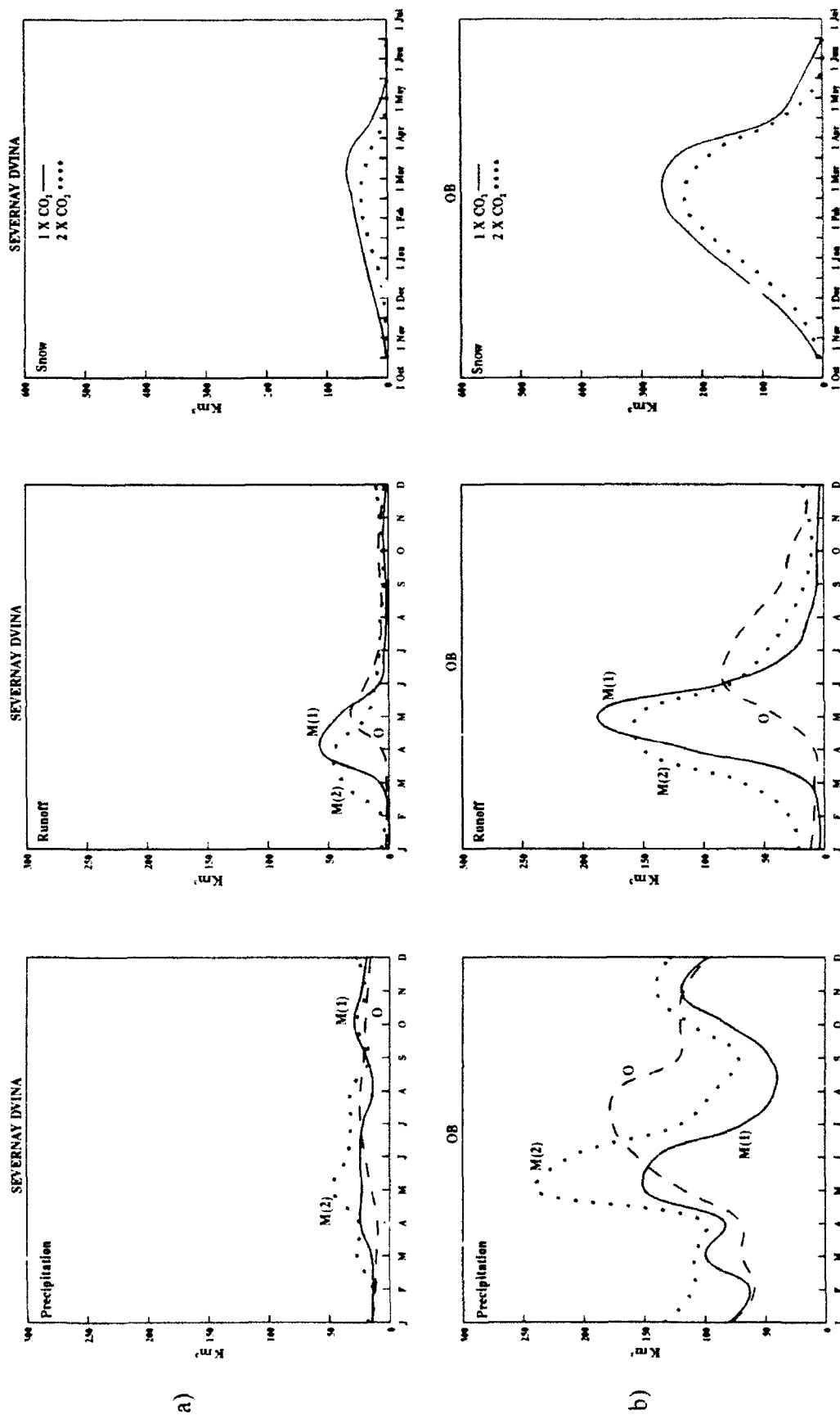


Figure 5.13. Model-generated monthly precipitation, runoff, and averaged snow mass during the snow season for the present climate [M(1)] and the doubled CO₂ climate [M(2)] and observed [O] precipitation from *Legates and Willmott [1990]* and runoff from *UNESCO [1969, 1974, 1985]* for the (a) Severnaya Dvina and (b) Ob rivers.

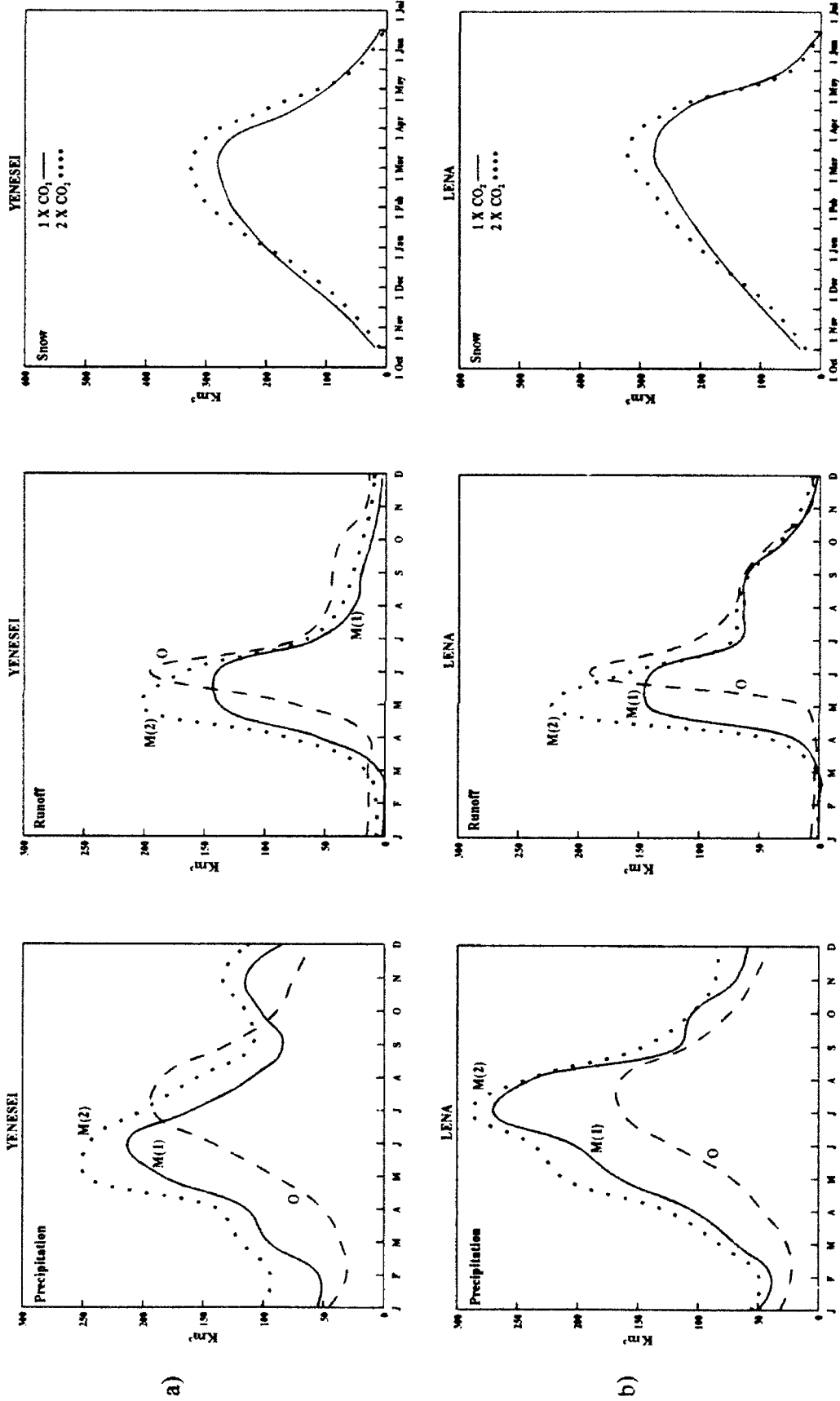


Figure 5.14. Model-generated monthly precipitation, runoff, and averaged snow mass during the snow season for the present climate [M(1)] and the doubled CO₂ climate [M(2)] and observed [O] precipitation from *Legates and Willmott* [1990] and runoff from *UNESCO* [1969, 1974, 1985] for the (a) Yenesei and (b) Lena rivers.

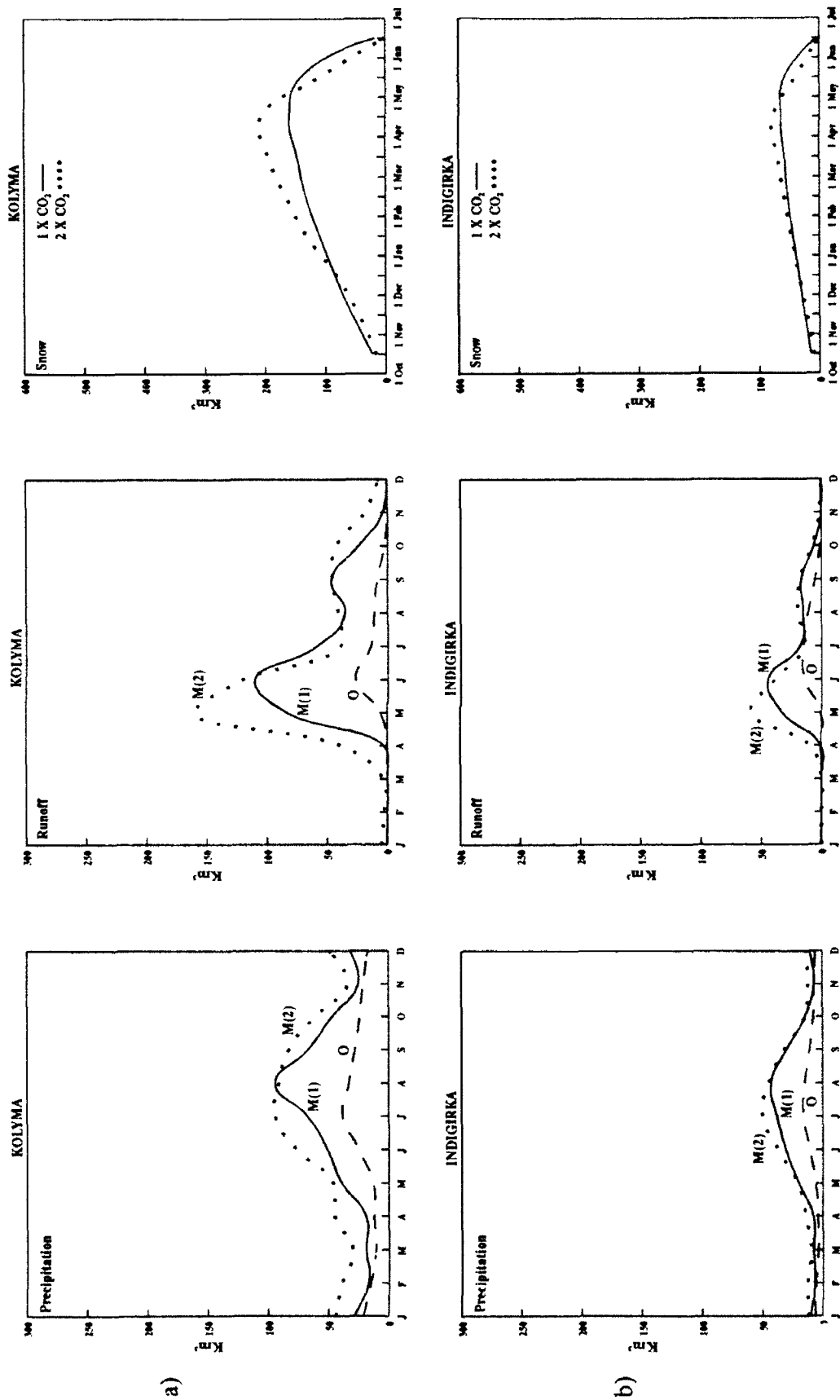


Figure 5.15. Model-generated monthly precipitation, runoff, and averaged snow mass during the snow season for the present climate [M(1)] and the doubled CO₂ climate [M(2)] and observed [O] precipitation from *Legates and Willmott* [1990] and runoff from *UNESCO* [1969, 1974, 1985] for the (a) Kolyma and (b) Indigirka rivers.

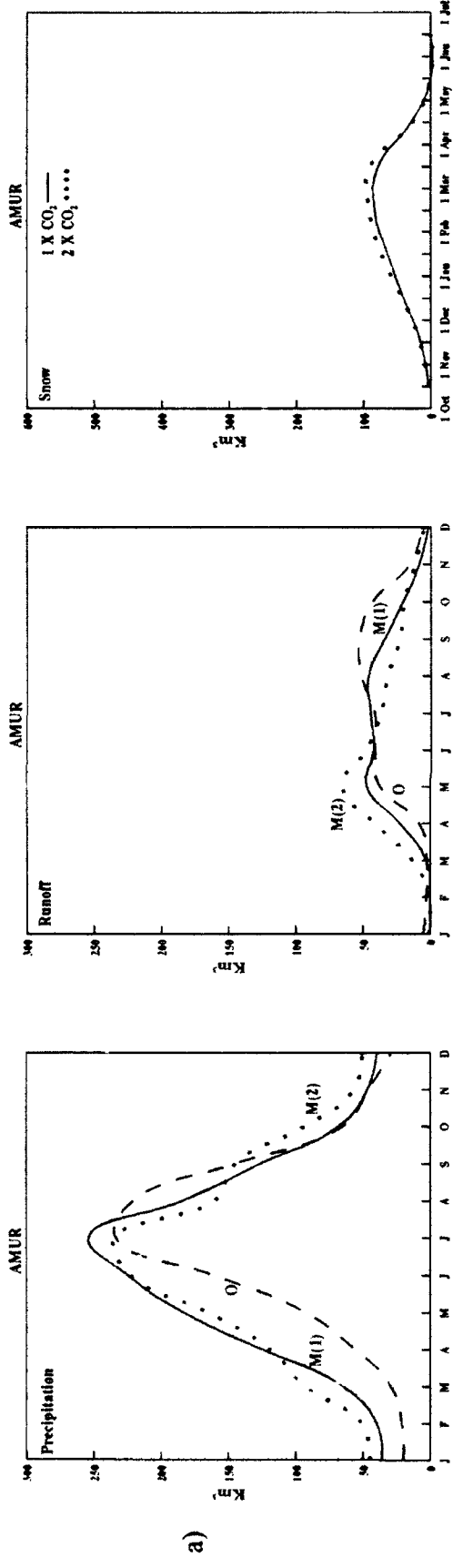


Figure 5.16. Model-generated monthly precipitation, runoff, and averaged snow mass during the snow season for the present climate [M(1)] and the doubled CO₂ climate [M(2)] and observed [O] precipitation from *Legates and Willmott [1990]* and runoff from *UNESCO [1969]* for the Amur River.

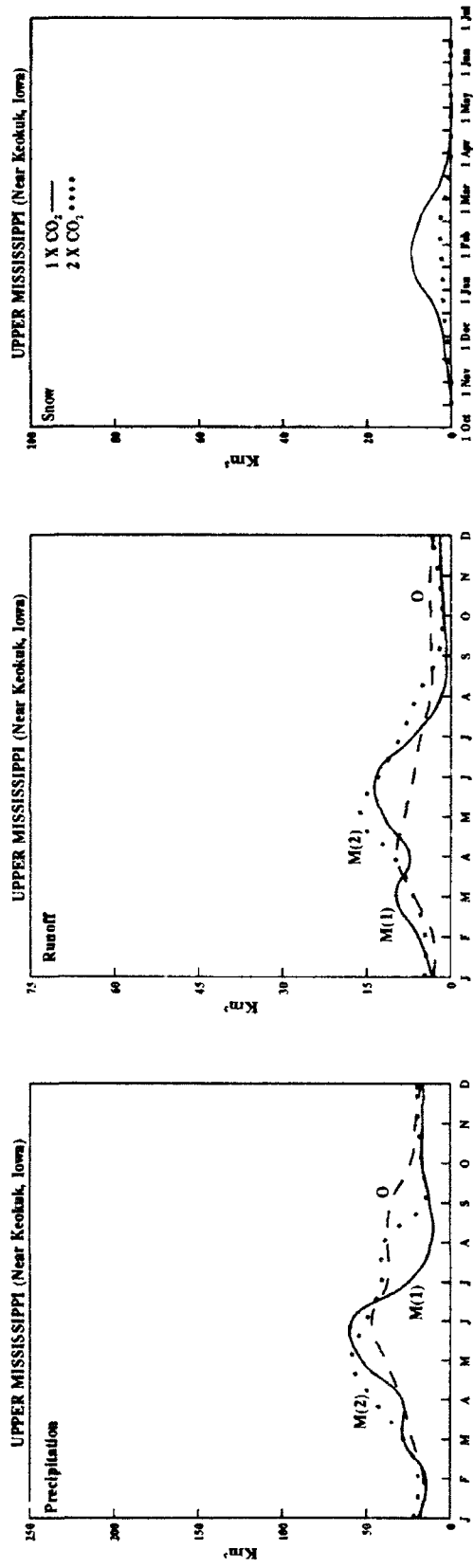


Figure 5.17. Model-generated monthly precipitation, runoff, and averaged snow mass during the snow season for the present climate [M(1)] and the doubled CO_2 climate [M(2)] and observed [O] precipitation from *Legates and Willmott [1990]* and runoff from the *US Geological Survey [1987]* for the Mississippi River at Keokuk, Iowa.

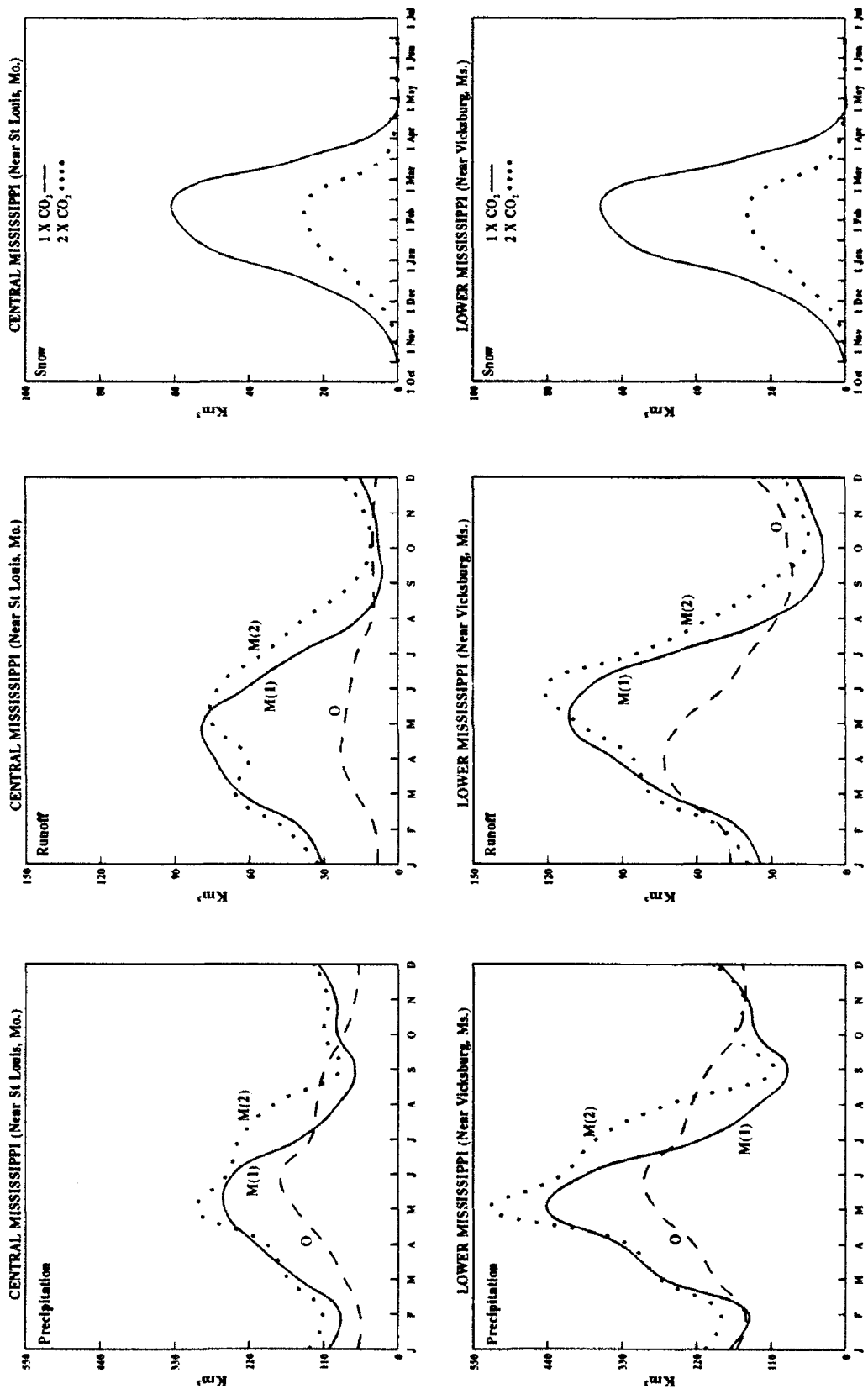


Figure 5.18 Model-generated monthly precipitation, runoff, and averaged snow mass during the snow season for the present climate [M(1)] and the doubled CO₂ climate [M(2)] and observed [O] precipitation from *Legates and Willmott [1990]* and runoff from the *US Geological Survey [1987]* for the Mississippi River at St. Louis, Missouri and Vicksburg, Mississippi.

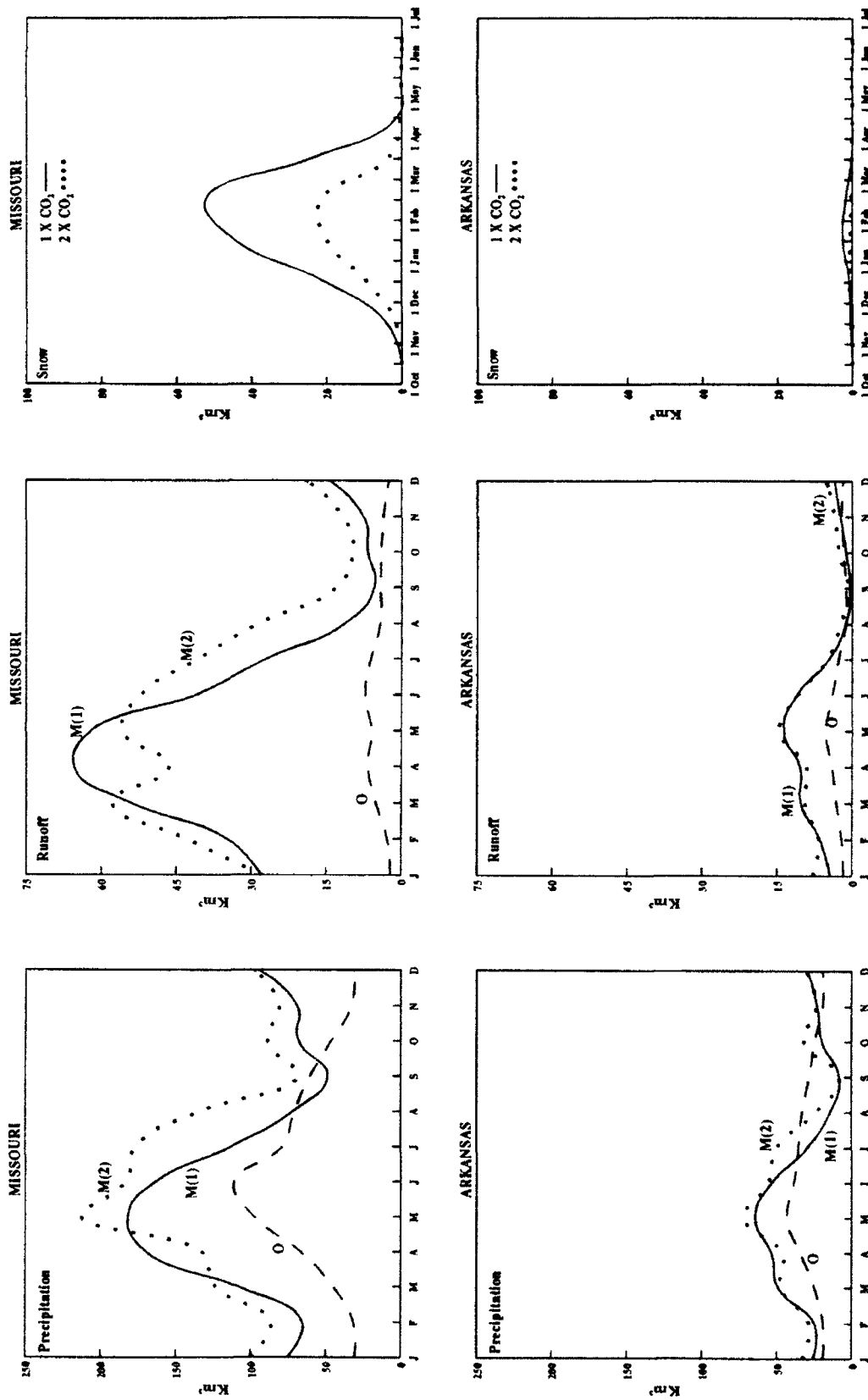


Figure 5.19. Model-generated monthly precipitation, runoff, and averaged snow mass during the snow season for the present climate [M(1)] and the doubled CO₂ climate [M(2)] and observed [O] precipitation from *Legates and Willmott* [1990] and runoff from the *US Geological Survey* [1987] for the Missouri and Arkansas rivers.

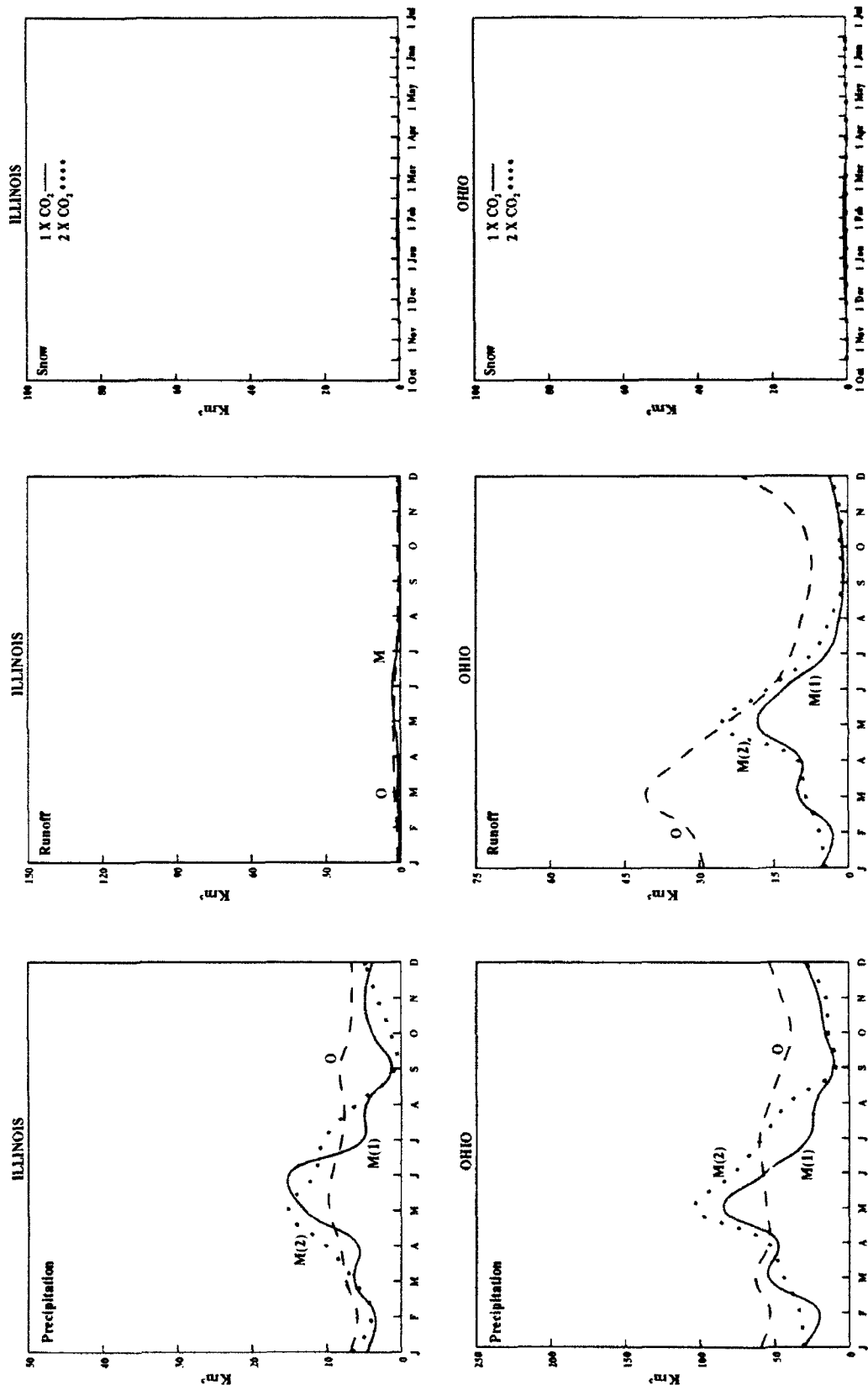


Figure 5.20. Model-generated monthly precipitation, runoff, and averaged snow mass during the snow season for the present climate [M(1)] and the doubled CO₂ climate [M(2)] and observed [O] precipitation from *Legates and Willmott [1990]* and runoff from the *US Geological Survey [1987]* for the Illinois and Ohio rivers.

Chapter 6. Summary and Conclusions

The purpose of this thesis was to obtain a better understanding of annual and monthly precipitation and river runoff as it is modeled in several simulations for the present and doubled CO₂ climates using the GISS GCM of *Hansen et al.* [1983]. The river basins are divided into categories depending on precipitation rates [*Kuhl and Miller*, 1992]. Observed precipitation was compared using two studies, *Shea* [1986] and *Legates and Willmott* [1990]. For the majority of the river basins, annual precipitation was higher (10%) in *Legates and Willmott* [1990], however, the monthly variation was very similar between the two studies. Therefore, observed precipitation was taken from *Legates and Willmott* [1990], which contained more observations and was the more recent of the two studies.

The mean annual and total basinwide monthly runoff studies of *Russell and Miller* [1990], *Miller and Russell* [1992], and *Kuhl and Miller* [1992] were extended by allowing river runoff to be routed between grid boxes within a river's basin using the routing scheme of *Miller et al.* [1992]. The timing of the model-generated total river runoff, R_{tot} , without the routing scheme is primarily based on the model's precipitation. This was clearly illustrated in the Congo River in which precipitation and runoff maxima occurred in the same month. However, with the routing scheme model-generated runoff at the river mouth, R_m , was lower in the maximum precipitation month and higher in the following months, indicating that water that contributed to the peak in R_{tot} reached the mouth in the following months similar to observed river runoff.

A common characteristic of the observed runoff in rivers at high latitudes in the northern hemisphere is a peak occurring in spring and early summer. This peak is due to the melting of snow and ice. The new routing scheme allows water to move downstream and simulate the magnitude and timing of the runoff peak at the river mouth. In this

particular formulation of the routing scheme, Ω and Δy of Eqn 2.10 are constants. The flow rate does depend on topography and the distance across the grid box, Δs .

As noted in *Miller et al.* [1992], Ω is a function of grid resolution. It is also likely to be dependent on other characteristics of the grid box. An alternative formulation for Eqn. 2.10 given by *Miller et al.* [1992] can eliminate or reduce the dependence on grid resolution. However, the effects of the physical characteristics of a particular grid box could serve as a basis for parameterizing Ω within each grid box so that it would no longer be a globally uniform constant. Ultimately the objective is to accurately route river runoff through the basin with routing coefficients based on the simplest possible parameterizations of Ω .

The model-generated runoff in the dry regions is too large. The combination of too little evaporation or percolation into the soil and too much model-generated precipitation contribute to the excess computed runoff in the dry regions. Also as discussed in *Miller and Russell* [1992], the model does not allow runoff to evaporate or percolate into the soil as it moves downstream from one grid box to another.

River runoff within the Mississippi river basin was examined. Although the model-generated annual precipitation was within 5% of the observed precipitation, monthly precipitation was not as close. This affected the model-generated monthly river runoff. Model-generated precipitation was too high for the Missouri River and too low for the Ohio River. There also seemed to be too much model-generated snow in the Missouri River basin and not enough for the Ohio River basin. This problem can be caused, in part, by the resolution of the grid box. Precipitation and snow were interpolated from a $4^\circ \times 5^\circ$ grid box in which precipitation, snow, and runoff were assumed equal for the entire grid box. In the case of the Missouri River, the western edge of the basin borders the rocky mountains with only half of the $4^\circ \times 5^\circ$ grid box covering the Missouri River basin. It is possible that most of the precipitation and snow accumulates in the western part of the $4^\circ \times 5^\circ$ grid causing higher amounts of precipitation and snow to occur in the Missouri river

basin after interpolation. Problems in resolutions near mountainous regions can cause erroneous amounts of precipitation and runoff to occur in a river basin. Other problems which occur in mountainous regions are grid boxes that contain more than one basin. Water from the entire grid box is assumed to flow in one direction, thus, some portion of the river runoff may enter the wrong river basin. Finer resolution models could be used to avoid this problem.

This study extended the study of *Miller and Russell* [1992] to examine seasonal variations in river runoff in a doubled CO₂ climate. They found that for the doubled CO₂ climate, mean annual runoff increases for 27 of the 30 rivers examined. The annual runoff increased in all the high latitudes, with increases averaging approximately 28%. This is consistent with other studies which show increasing runoff at high latitudes for a doubled CO₂ climate [*Manabe and Stouffer*, 1980; *Rind*, 1988; *Mitchell*, 1989; *Stouffer et al.*, 1989].

Precipitation and temperatures from GCMs have been used in hydrologic models (off-line method) to predict regional runoff changes that would accompany global warming [*Gleick*, 1987; *Flaschko, et al.*, 1987; *Roos*, 1989; *Lettenmaier and Gan*, 1990, and *Ayers et al.*, 1990]. *Gleick* [1987] and *Lettenmaier and Gan* [1990] found that the principal physical mechanism affecting increased winter runoff and decreased summer runoff was a decrease in snow as a proportion of the winter precipitation, similar to the results found in this study.

The most interesting changes in seasonal runoff occurred in the higher latitudes where snow melt is an important component of river runoff. The timing of the snow melt depends on temperature. Hence, the delays for the present climate could be related to temperature as well as the routing scheme. This will affect the timing in a doubled CO₂ climate as well. Precipitation increases and the spring runoff peak occurs earlier for all high latitude rivers. Of the nine high latitude basins examined, five river basins in northeastern Asia (the Yenesei, Lena, Kolyma, Indigirka, and Amur) also show an

increase in the magnitude of the runoff peak. This region is the only region to show an increase in snow mass in a doubled CO₂ climate. The geographical location and climatology of this region indicate that winter temperatures do not increase there sufficiently to reduce the winter snowfall.

The model-generated river runoff decreases 36% in a doubled CO₂ climate for the Niger River, despite little change in the annual precipitation between the present and doubled CO₂ climates. This must be due to increased evapotranspiration which would increase more in regions of high temperatures because of the non linearity of the Clausius Clapeyron equation.

Although changes in river runoff were obtained for a doubled CO₂ climate, further improvements in the model are needed to increase the confidence in the results. The limited three-year and five-year simulations should be extended to reduce the chance of temporal errors. Finer resolutions in defining river basins are needed, especially in areas which border mountainous regions. Also, grid boxes need to be divided so that the river's drainage area is equal to the appropriate percentage of a grid box's runoff.

The conclusions about river runoff in the present and doubled CO₂ climates depend on the model's ability to simulate the hydrologic cycle, which depends on the model's parameterizations of land-atmosphere interactions. It is essential for hydrologists and climate modelers to develop the best possible parameterizations of land-atmosphere interactions within GCMs. The confidence in the model's ability to generate snow for the present climate is hard to evaluate because observed snow was not obtained for comparison with model snow. *Rind et al.*, [1990] conclude that drought intensification is understated in a doubled CO₂ climate for several GCMs, including the GISS model used for this study, because of their failure to show extensive soil moisture reductions. This is due to unrealistic simulations of the land surface. A new soil-moisture storage scheme has been developed by *Abramopoulos et al.*, [1988] to replace the simplified two-layer storage scheme used here, but the new scheme has not been implemented fully into the GCM.

This scheme also includes groundwater. A primary concern of climatic modelers must be to obtain accurate precipitation, evapotranspiration, and soil moisture storage. River runoff provides a useful diagnostic for examining parameterizations of these processes. The ability to predict changes in river runoff are essential for forecasting future water resource needs.

APPENDIX: Tables of monthly statistics for each river basin

River runoff (Km³) and precipitation (Km³) for the following rivers:

<u>Wet</u>	<u>Moderately Wet</u>	<u>Dry</u>	<u>High Latitude Dry</u>
Amazon	Yangtze	Indus	Yenesei
Congo	Mississippi	Tigris-Euphrates	Lena
Orinoco	LaPlata (Parana)	Yellow	Ob
Mekong	St Lawrence	Colorado	Amur
Magdalena	Danube	Murray	Mackenzie
Sao Francisco	Columbia		Yukon
	Zambesi		Severnay Dvina
	Fraser		Kolyma
	Nile		Indigirka
	Niger		

Obs - Observed

R(tot) - Model-generated runoff averaged over the entire river basin

R(m) - Model-generated runoff at the mouth of the river basin

1XCO2 - Present climate

2XCO2 - Doubled CO₂ climate

848F - Model simulation

C003 - Model simulation

B100 - Model simulation

A51M - Model simulation

947B - Model simulation

Observed runoff is from *UNESCO* [1969, 1974, 1985], observed precipitation is from *Legates and Willmott* [1990] and *Shea* [1986], and areas are from *Millman and Meade* [1983] and *UNESCO* [1969, 1974, 1985].

AMAZON (Wet)

	Runoff Obs	UNESCO	848F 1XCO2	R(tot) C003 1XCO2	R(m) C003 1XCO2	R(tot) B100 1XCO2	R(m) B100 1XCO2	R(tot) A51M 1XCO2	R(m) A51M 1XCO2	R(tot) 947B 2XCO2	R(m) 947B 2XCO2	Precip Obs	Precip 848F 1XCO2	Precip C003 1XCO2	Precip B100 1XCO2	Precip A51M 1XCO2	Precip 947B 2XCO2
Jan	322.1		213.3	413.0	370.7	248.0	206.1	305.0	260.2	349.0	349.0	1576.0	1289.7	1413.0	1410.0	1524.0	1766.0
Feb	346.6		266.0	433.0	359.1	280.0	212.4	323.0	270.7	383.0	341.0	1560.0	1418.0	1377.0	1416.0	1454.0	1603.0
Mar	458.6		301.1	491.0	435.6	338.0	277.6	405.0	339.0	408.0	394.0	1662.0	1399.9	1441.0	1521.0	1626.0	1644.0
Apr	503.0		303.5	416.0	446.1	306.0	306.0	381.0	366.6	327.0	387.8	1408.0	1233.2	1187.0	1250.0	1380.0	1348.0
May	563.2		244.0	319.0	447.6	228.0	317.6	288.0	374.3	264.0	378.7	1045.0	909.0	937.0	914.0	1020.0	1113.0
Jun	545.7		171.0	236.0	368.7	162.0	262.4	199.0	320.8	184.0	310.7	631.0	641.5	725.0	656.0	720.0	795.0
Jul	534.1		129.5	225.0	295.3	130.0	198.8	161.0	263.2	152.0	246.6	507.0	591.9	688.0	592.0	636.0	718.0
Aug	468.6		108.7	226.0	236.4	104.0	140.6	149.0	187.9	150.0	182.3	423.0	588.9	734.0	559.0	774.0	761.0
Sep	356.6		112.4	263.0	207.6	118.0	102.6	136.0	145.8	170.0	142.7	597.0	780.5	928.0	774.0	978.0	942.0
Oct	274.5		153.8	327.0	239.1	166.0	102.3	219.0	154.6	230.0	146.9	945.0	1110.6	1242.0	1204.0	1324.0	1416.0
Nov	242.8		156.9	335.0	295.4	188.0	125.7	230.0	174.7	306.0	185.6	1123.0	1143.9	1266.0	1258.0	1345.0	1674.0
Dec	270.3		177.8	371.0	352.9	211.0	172.2	263.0	221.5	390.0	273.8	1362.0	1189.0	1303.0	1288.0	1443.0	1758.0
Winter	939.0		657.1	1217.0	1082.7	739.0	590.7	891.0	752.4	1150.0	965.7	4498.0	3896.7	4093.0	4114.0	4421.0	5127.0
Spring	1524.8		848.6	1226.0	1329.2	872.0	901.1	1074.0	1079.9	999.0	1160.5	4105.0	3542.1	3565.0	3685.0	4026.0	4105.0
Summer	1548.5		409.2	687.0	900.4	396.0	601.7	509.0	771.8	486.0	739.6	1561.0	1822.3	2147.0	1807.0	2130.0	2274.0
Fall	873.9		423.1	925.0	742.1	472.0	330.6	605.0	475.1	706.0	475.1	2665.0	3035.0	3436.0	3236.0	3647.0	4032.0
Annual	4886.3		2338.0	4055.0	4054.4	2479.0	2424.2	3079.0	3079.2	3341.0	3340.9	12829.0	12296.1	13241.0	12842.0	14224.0	15538.0

UNESCO Runoff Location

Obidos, Brazil

Lat 1.55° S

Long 53.28° W

Area Model	Area Model	Area Model	Area Model	Area Model	Area Model	Area Model	Area Model
848F (km**2)	A51M (km**2)	C003 (km**2)	Milliman Merade (km**2)	UNESCO (km**2)	Obidos, Brazil	Lat	Long
6500000	6500000	6500000	6150000	4640285			

CONGO (Wet)

Area Model	Area Model	Area Model	Area Model	R(tot) C003 1XC02	R(m) C003 1XC02	R(tot) B100 1XC02	R(m) B100 1XC02	R(tot) AS1M 1XC02	R(m) AS1M 1XC02	R(tot) 947B 2XC02	R(m) 947B 2XC02	Precip Obs Legats	Precip Obs Sheb	Precip B48F 1XC02	Precip C003 1XC02	Precip B100 1XC02	Precip AS1M 1XC02	Precip 947B 2XC02
3820000	3510000	3510000	3475000	174.0	168.6	160.0	154.6	223.0	203.2	250.0	261.0	435.0	428.0	826.5	605.0	699.0	833.0	925.0
Jan	139.5	221.8	174.0	163.0	156.3	155.0	144.6	205.0	194.5	257.0	237.6	434.0	413.0	868.9	599.0	687.0	759.0	900.0
Feb	103.8	236.4	163.0	176.5	172.0	168.6	161.1	228.0	224.6	254.0	272.1	588.0	571.0	860.5	630.0	754.0	850.0	907.0
Mar	107.3	232.2	178.0	174.4	146.0	161.1	192.0	192.0	219.9	277.0	245.2	573.0	538.0	764.1	602.0	668.0	733.0	839.0
Apr	110.7	195.6	172.0	166.4	113.0	142.8	162.0	162.0	202.6	21.0	236.5	411.0	373.0	615.0	484.0	561.0	626.0	761.0
May	120.7	148.5	134.0	122.6	90.0	111.3	132.0	162.9	162.9	171.0	209.7	268.0	249.0	525.7	335.0	466.0	528.0	624.0
Jun	110.5	123.1	83.0	92.2	78.0	92.4	119.0	138.7	138.7	172.0	188.7	272.0	260.0	482.9	298.0	446.0	511.0	619.0
Jul	99.8	107.7	64.0	75.3	87.0	84.9	89.9	133.0	126.7	173.0	170.6	369.0	351.0	581.4	382.0	526.0	592.0	658.0
Aug	90.8	125.1	68.0	81.6	114.0	97.4	97.4	142.0	126.4	178.0	159.9	475.0	447.0	741.0	559.0	640.0	659.0	735.0
Sep	102.4	157.5	104.0	114.6	146.0	126.0	126.0	172.0	145.7	230.0	185.5	586.0	563.0	854.7	707.0	749.0	782.0	924.0
Oct	120.7	189.8	162.0	140.1	154.0	135.4	135.4	183.0	162.8	244.0	215.0	586.0	574.0	884.5	637.0	736.0	786.0	932.0
Nov	136.5	215.6	163.0	162.4	159.0	149.6	149.6	203.0	186.9	266.0	250.1	519.0	498.0	835.8	648.0	703.0	811.0	942.0
Dec	154.7	216.5	178.0	487.3	474.0	474.0	448.8	631.0	584.6	773.0	748.7	1388.0	1339.0	2531.2	1812.0	2089.0	2403.0	2767.0
Winter	398.0	674.7	515.0	517.3	484.0	472.5	472.5	582.0	647.1	692.0	753.8	1572.0	1482.0	2239.6	1716.0	1983.0	2209.0	2507.0
Spring	338.8	576.3	484.0	290.1	255.0	288.6	288.6	384.0	428.3	516.0	569.0	909.0	860.0	1590.0	1015.0	1438.0	1631.0	1901.0
Summer	301.1	355.9	215.0	336.3	414.0	358.9	358.9	497.0	434.8	652.0	560.4	1647.0	1584.0	2480.2	1903.0	2125.0	2227.0	2591.0
Fall	359.6	562.9	429.0	1631.0	1631.0	1574.0	1568.8	2094.0	2094.7	2633.0	2632.0	5516.0	5265.0	8841.0	6446.0	7635.0	8470.0	9766.0
Annual	1397.5	2169.8	1643.0															

UNESCO Runoff Location
Brazzaville, Congo

Lat 4.16°S
Long 15.19°E

| Area Model |
|------------|------------|------------|------------|------------|------------|
| 3820000 | 3510000 | 3510000 | 3820000 | 3475000 | 3475000 |
| UNESCO | Milliman | UNESCO | Milliman | UNESCO | Milliman |
| B48F | AS1M | C003 | Mende | C003 | Mende |
| (km**2) | (km**2) | (km**2) | (km**2) | (km**2) | (km**2) |

MEKONG (West)

	Runoff Obs	R(tot) 848F 1XCO2	R(tot) C003 1XCO2	R(m) C003 1XCO2	R(tot) B100 1XCO2	R(m) B100 1XCO2	R(tot) AS1M 1XCO2	R(m) AS1M 1XCO2	R(tot) 947B 2XCO2	R(m) 947B 2XCO2	Precip Obs Legates	Precip Obs Siles	Precip 848F 1XCO2	Precip C003 1XCO2	Precip B100 1XCO2	Precip AS1M 1XCO2	Precip 947B 2XCO2
Jan	7.7	42.8	23.0	22.2	30.0	35.6	18.0	21.9	47.0	39.2	17.0	19.0	112.8	112.0	120.0	99.0	142.0
Feb	5.1	53.9	17.0	17.5	43.0	37.9	26.0	18.5	45.0	42.9	21.0	14.0	132.7	85.0	132.0	107.0	142.0
Mar	4.3	57.7	21.0	18.3	72.0	61.5	44.0	32.6	44.0	46.5	33.0	25.0	126.3	96.0	182.0	164.0	146.0
Apr	4.1	61.8	22.0	21.1	75.0	72.2	71.0	50.0	74.0	49.8	68.0	52.0	177.4	121.0	197.0	206.0	178.0
May	7.8	79.1	27.0	24.9	89.0	83.1	98.0	79.2	112.0	85.6	152.0	125.0	227.5	167.0	223.0	236.0	271.0
Jun	23.7	84.6	43.0	34.0	69.0	74.7	84.0	91.4	95.0	102.7	197.0	163.0	221.2	195.0	196.0	211.0	246.0
Jul	67.0	56.7	63.0	53.5	68.0	67.7	89.0	85.8	96.0	99.1	250.0	169.0	175.4	207.0	195.0	219.0	243.0
Aug	101.5	48.9	71.0	69.1	63.0	63.8	87.0	87.4	88.0	94.7	247.0	84.0	184.5	226.0	201.0	227.0	235.0
Sep	108.6	69.6	47.0	58.6	67.0	62.7	80.0	86.1	76.0	85.3	239.0	92.0	207.8	179.0	199.0	219.0	219.0
Oct	69.4	72.1	33.0	41.2	55.0	61.7	57.0	75.9	60.0	71.0	148.0	53.0	179.8	153.0	179.0	182.0	183.0
Nov	33.2	47.3	23.0	27.5	38.0	46.5	33.0	50.9	43.0	56.2	74.0	71.0	133.0	121.0	146.0	135.0	168.0
Dec	16.8	37.8	20.0	21.8	40.0	41.5	23.0	31.8	36.0	42.1	31.0	41.0	117.7	96.0	142.0	113.0	144.0
Winter	29.6	134.5	60.0	61.5	113.0	115.1	67.0	72.2	128.0	124.1	69.0	74.0	363.2	293.0	394.0	319.0	428.0
Spring	16.3	198.6	70.0	64.3	236.0	216.8	213.0	161.9	230.0	181.8	253.0	202.0	531.2	384.0	602.0	606.0	595.0
Summer	192.2	190.2	177.0	156.6	200.0	206.2	260.0	264.6	279.0	296.5	694.0	516.0	581.1	628.0	592.0	677.0	724.0
Fall	211.2	189.0	103.0	127.3	160.0	171.0	170.0	212.8	179.0	212.6	461.0	416.0	526.6	453.0	524.0	536.0	570.0
Annual	449.2	712.3	410.0	409.6	709.0	709.0	710.0	711.4	816.0	815.0	1477.0	1208.0	1996.1	1758.0	2112.0	2138.0	2317.0

UNESCO Runoff Location

Kratie, Cambodia

Lat 12.28° N

Long 106.00° E

Area	Area	Area	Area	Area
Model	Model	Model	Model	Model
848F	AS1M	C003	Milliman	UNESCO
(km**2)	(km**2)	(km**2)	(km**2)	(km**2)
820000	860000	860000	790000	640000

MAGDALENA (Wet)

Runoff	R(848F)		R(1060)		R(1100)		R(A51M)		R(947B)		Precip	
	Obs	1XCO2	848F	1XCO2								
Jan	15.5	28.8	35.0	36.5	45.0	30.7	24.0	25.4	12.0	14.5	68.6	70.0
Feb	8.2	25.4	35.0	33.8	42.0	28.5	18.0	19.4	6.0	7.6	62.7	75.0
Mar	8.9	21.6	42.0	40.6	46.0	32.1	15.0	16.0	5.0	5.2	59.7	91.0
Apr	12.9	18.7	50.0	47.5	39.0	28.2	17.0	16.1	9.0	7.6	62.2	107.0
May	18.7	21.0	61.0	58.9	37.0	26.0	22.0	20.9	15.0	13.4	72.6	117.0
Jun	21.3	23.2	51.0	52.7	36.0	24.0	21.0	21.2	21.0	19.1	76.0	90.0
Jul	20.9	25.4	55.0	52.4	42.0	26.4	27.0	25.2	22.0	22.5	77.8	98.0
Aug	17.4	28.3	54.0	51.7	45.0	28.7	31.0	28.7	28.0	26.3	80.5	93.0
Sep	16.2	32.5	56.0	52.3	52.0	32.7	31.0	30.7	22.0	22.8	85.7	96.0
Oct	21.8	32.0	55.0	55.0	52.0	36.1	38.0	36.2	29.0	27.8	79.8	104.0
Nov	25.7	29.4	47.0	47.7	43.0	31.0	32.0	33.0	28.0	28.6	71.0	84.0
Dec	25.7	27.9	40.0	41.7	41.0	29.7	28.0	30.0	20.0	21.6	65.9	70.0
Winter	49.4	82.1	110.0	112.0	128.0	88.9	70.0	74.8	38.0	43.7	197.2	215.0
Spring	40.5	61.3	153.0	146.9	122.0	86.3	54.0	53.1	29.0	26.2	194.5	315.0
Summer	59.7	76.9	160.0	156.8	123.0	79.1	79.0	75.2	71.0	68.0	234.3	281.0
Fall	63.8	93.9	158.0	154.9	147.0	99.7	101.0	99.9	79.0	79.2	236.5	284.0
Annual	213.4	314.2	581.0	570.7	520.0	354.0	304.0	302.9	217.0	217.0	862.5	1095.0

UNESCO Runoff Location
Calamar, Columbia

Lat 10.16°N
Long -74.55°W

Area Model	Area Model	Area Model	Area UNESCO
848F (km**2)	A51M (km**2)	C003 (km**2)	(km**2)
240000	360000	360000	257438

SAO FRANCISCO (Wet)

Area Model	Area (km**2)	Runoff Obs	R(848F)		R(C003)		R(B100)		R(A51M)		R(947B)		R(C003)		R(848F)		R(Precip Obs Shear)		R(Precip 1XC02)		R(Precip 1XC02)		R(Precip 1XC02)		R(Precip 1XC02)			
			1XC02	1XC02	1XC02	1XC02	1XC02	1XC02	1XC02	1XC02	1XC02	1XC02	1XC02	1XC02	1XC02	1XC02												
Jan	8.7	31.7	34.0	31.2	25.0	22.7	41.0	36.8	33.0	35.5	110.0	106.0	163.5	139.0	143.0	170.0	165.0											
Feb	10.0	37.0	33.0	32.5	27.0	26.1	34.0	34.8	33.0	29.8	100.0	103.0	167.3	116.0	132.0	141.0	156.0											
Mar	13.8	38.7	36.0	36.1	33.0	32.1	40.0	39.2	46.0	43.1	101.0	104.0	159.2	117.0	144.0	159.0	185.0											
Apr	11.2	26.5	29.0	30.9	23.0	25.6	32.0	36.7	27.0	34.3	67.0	84.0	117.0	91.0	94.0	119.0	116.0											
May	6.2	10.3	15.0	19.2	16.0	18.0	16.0	23.1	17.0	22.6	40.0	66.0	57.5	56.0	57.0	68.0	87.0											
Jun	4.7	4.5	2.0	5.0	10.0	11.3	7.0	10.4	7.0	11.2	30.0	41.0	31.2	17.0	43.0	40.0	46.0											
Jul	4.2	3.8	0.0	0.8	4.0	4.7	8.0	7.4	3.0	4.3	29.0	39.0	27.2	9.0	29.0	49.0	33.0											
Aug	4.0	4.3	0.0	0.4	3.0	2.5	9.0	9.1	5.0	4.9	20.0	25.0	35.8	12.0	27.0	60.0	40.0											
Sep	4.1	4.5	0.0	0.4	2.0	1.8	10.0	9.6	9.0	6.4	24.0	29.0	40.6	12.0	36.0	73.0	81.0											
Oct	4.7	8.9	4.0	2.6	6.0	4.7	18.0	16.4	12.0	10.1	53.0	67.0	88.0	43.0	63.0	100.0	105.0											
Nov	5.7	17.9	12.0	9.5	10.0	9.1	26.0	22.0	30.0	23.8	99.0	99.0	128.0	87.0	88.0	138.0	150.0											
Dec	5.8	22.9	24.0	21.2	19.0	16.0	31.0	28.1	44.0	38.8	126.0	111.0	144.8	122.0	131.0	156.0	180.0											
Winter	24.5	91.6	91.0	84.9	71.0	64.8	106.0	99.7	110.0	104.1	336.0	320.0	475.6	377.0	406.0	467.0	501.0											
Spring	31.2	75.5	80.0	86.2	72.0	75.6	88.0	99.0	89.0	100.0	208.0	254.0	333.7	264.0	295.0	346.0	388.0											
Summer	12.9	12.6	2.0	6.1	17.0	18.5	24.0	27.0	15.0	20.4	79.0	105.0	94.2	38.0	99.0	149.0	119.0											
Fall	14.5	31.3	16.0	12.5	18.0	15.6	54.0	48.0	51.0	40.2	176.0	195.0	256.6	142.0	187.0	311.0	336.0											
Annual	83.1	211.0	189.0	189.8	178.0	174.6	272.0	273.7	265.0	264.6	799.0	874.0	1160.1	821.0	987.0	1273.0	1344.0											

UNESCO Runoff Location
Trelpu, Brazil

Area Model	Area (km**2)						
UNESCO	622600	Milliman	640000	C003	650000	A51M	650000
Mede	640000	Mede	640000	Mede	640000	Mede	640000

Lat 9.59° S
Long 36.59° W

YANGTZE (Moderately Wet)

	Runoff		R(tot)		R(m)		R(tot)		R(m)		R(tot)		R(m)		Precip		Precip		Precip				
	Obs	UNESCO	848F	C003	B100	A51M	947B	2XCO2	B100	A51M	947B	2XCO2	Obs	Legates	Obs	Shen	848F	C003	B100	A51M	947B	2XCO2	
Jan	25.8	31.0	55.5	24.9	18.0	29.8	35.9	130.0	100.6	48.0	42.0	168.4	102.0	105.0	91.0	251.0							
Feb	22.4	32.0	91.8	27.8	67.0	29.7	39.8	124.0	114.1	74.0	63.0	209.9	99.0	142.0	219.0	243.0							
Mar	31.2	52.0	126.8	-1.2	163.0	95.7	101.5	141.0	136.1	118.0	104.0	274.9	186.0	299.0	261.0	288.0							
Apr	54.8	52.0	148.4	50.8	124.0	145.7	147.2	213.0	148.0	182.0	172.0	374.8	203.0	299.0	373.0	385.0							
May	86.9	110.0	205.0	72.2	182.0	147.5	191.0	263.0	213.1	252.0	248.0	471.8	353.0	396.0	444.0	513.0							
Jun	107.4	133.0	189.8	110.3	130.0	157.7	210.1	211.0	243.2	314.0	290.0	440.0	392.0	348.0	414.0	469.0							
Jul	126.7	174.0	130.6	150.4	136.0	137.0	189.4	202.0	214.8	287.0	306.0	391.9	483.0	409.0	379.0	431.0							
Aug	98.9	152.0	104.3	162.1	125.0	131.7	150.5	172.0	194.1	268.0	268.0	349.7	418.0	378.0	375.0	405.0							
Sep	85.6	82.0	103.3	127.2	98.0	110.5	123.6	168.0	170.6	200.0	196.0	278.9	243.0	257.0	294.0	371.0							
Oct	72.3	34.0	86.0	71.9	107.0	104.7	124.4	137.0	166.8	125.0	116.0	216.4	118.0	235.0	279.0	285.0							
Nov	50.2	24.0	35.8	33.3	58.0	92.3	112.7	95.0	135.2	73.0	66.0	111.4	98.0	163.0	213.0	244.0							
Dec	30.0	22.0	26.5	25.7	31.0	56.2	73.2	91.0	110.1	44.0	40.0	148.2	92.0	136.0	123.0	241.0							
Winter	78.3	85.0	173.8	78.5	116.0	115.7	149.0	345.0	324.8	166.0	145.0	526.5	293.0	383.0	433.0	735.0							
Spring	172.9	214.0	480.2	164.2	469.0	388.9	439.7	617.0	497.3	552.0	524.0	1121.5	742.0	994.0	1078.0	1186.0							
Summer	333.0	459.0	424.7	422.7	391.0	426.3	550.0	585.0	652.2	869.0	864.0	1181.6	1293.0	1135.0	1168.0	1305.0							
Fall	208.1	140.0	225.1	232.4	263.0	307.5	360.7	400.0	472.6	398.0	378.0	606.7	459.0	655.0	786.0	900.0							
Annual	792.2	898.0	1303.8	897.7	1239.0	1238.4	1499.3	1947.0	1946.8	1985.0	1911.0	3436.3	2787.0	3167.0	3465.0	4126.0							

UNESCO Runoff Location

Datong, China
36.46° N
117.37° E

Area	Area	Area	Area	Area
Model	Model	Model	Milliman	UNESCO
848F	A51M	C003	Meade	
(km**2)	(km**2)	(km**2)	(km**2)	(km**2)
1970000	1810000	1810000	1940000	1705383

MISSISSIPPI (Moderately Wet)

	Runoff	R(tot)	R(m)	R(tot)	R(m)	Precip	Precip	Precip	Precip	Precip	Precip									
	Obs	848F	C003	B100	B100	B100	B100	947B	947B	947B	947B	947B	947B	Obs	848F	C003	B100	AS1M	947B	
	UNESCO	1XCO2	1XCO2	1XCO2	1XCO2	1XCO2	1XCO2	2XCO2	2XCO2	2XCO2	2XCO2	2XCO2	2XCO2	Shea	1XCO2	1XCO2	1XCO2	1XCO2	1XCO2	2XCO2
Jan	43.4	21.4	25.0	27.0	27.5	27.5	52.0	35.0	68.0	40.8	209.0	157.0	122.1	141.0	162.0	201.0	235.0			
Feb	51.0	36.0	27.0	41.0	28.5	28.5	71.0	44.3	77.0	50.7	195.0	154.0	173.8	142.0	169.0	170.0	207.0			
Mar	66.4	55.9	57.0	107.0	51.6	51.6	112.0	73.6	88.0	80.7	247.0	209.0	239.0	241.0	265.0	317.0	325.0			
Apr	72.3	94.1	70.0	118.0	95.8	95.8	95.0	96.5	81.0	92.7	279.0	251.0	355.4	303.0	349.0	373.0	369.0			
May	63.2	122.4	84.0	134.0	127.6	127.6	121.0	114.7	173.0	110.9	339.0	304.0	487.9	402.0	506.0	499.0	608.0			
Jun	48.0	87.1	61.0	86.0	121.9	88.0	88.0	115.6	94.0	133.3	347.0	307.0	415.9	350.0	428.0	431.0	482.0			
Jul	39.1	37.3	27.0	43.0	80.8	25.0	25.0	83.3	52.0	97.2	304.0	283.0	251.1	196.0	320.0	234.0	368.0			
Aug	25.0	14.4	11.0	26.4	43.7	10.0	10.0	37.5	31.0	60.4	277.0	250.0	150.2	93.0	236.0	136.0	285.0			
Sep	19.0	8.2	2.0	10.0	23.1	7.0	7.0	14.7	9.0	36.2	249.0	233.0	112.6	23.0	102.0	92.0	113.0			
Oct	19.0	10.2	3.0	13.0	13.1	14.0	14.0	9.5	23.0	18.7	202.0	169.0	113.1	33.0	130.0	145.0	180.0			
Nov	21.3	15.1	8.0	13.0	13.4	13.4	19.0	13.8	25.0	19.0	190.0	162.0	128.2	69.0	127.0	165.0	165.0			
Dec	29.7	15.1	20.0	28.0	17.2	17.2	46.0	20.8	44.0	25.7	201.0	163.0	95.3	134.0	171.0	218.0	222.0			
Winter	124.2	72.5	72.0	96.0	73.1	73.1	169.0	100.6	189.0	117.1	605.0	474.0	391.2	417.0	502.0	589.0	664.0			
Spring	202.0	272.4	211.0	359.0	275.0	275.0	328.0	284.8	342.0	284.3	865.0	764.0	1082.3	946.0	1120.0	1189.0	1302.0			
Summer	112.1	138.8	99.0	155.0	246.4	246.4	123.0	236.4	177.0	290.9	928.0	840.0	817.2	639.0	984.0	801.0	1135.0			
Fall	59.3	33.5	13.0	36.0	49.5	49.5	40.0	38.0	57.0	73.9	641.0	564.0	353.9	125.0	359.0	402.0	458.0			
Annual	497.5	517.2	395.0	646.0	644.0	644.0	660.0	659.7	765.0	766.2	3039.0	2642.0	2644.6	2127.0	2965.0	2981.0	3559.0			

UNESCO Runoff Location
Vicksburg, Mississippi

Lat 32.19° N
Long 90.34° W

Area	Area	Area	Area
Model	Model	Model	Model
848F	AS1M	MIHiman	UNESCO
(km**2)	(km**2)	(km**2)	(km**2)
3270000	3510000	3270000	2964300

ST. LAWRENCE (Moderately Wet)

	Runoff Obs UNESCO	R(tot) 848F 1XC02	R(tot) C003 1XC02	R(m) B100 1XC02	R(tot) A51M 1XC02	R(m) B100 1XC02	R(m) A51M 1XC02	R(tot) 947B 2XC02	R(m) 947B 2XC02	Precip Obs Legates	Precip Obs Shea	Precip 848F 1XC02	Precip C003 1XC02	Precip B100 1XC02	Precip A51M 1XC02	Precip 947B 2XC02
Jan	16.7	13.0	23.3	17.3	14.0	17.3	9.9	38.0	26.2	82.0	65.0	70.9	79.0	81.0	69.0	98.0
Feb	14.9	40.4	31.2	17.4	31.0	17.4	18.5	30.0	30.0	67.0	57.0	77.3	77.0	79.0	64.0	85.0
Mar	17.2	81.6	59.7	45.1	48.0	45.1	36.0	58.0	56.5	74.0	67.0	98.6	109.0	99.0	85.0	96.0
Apr	18.1	75.7	100.7	86.0	78.0	86.0	76.1	47.0	48.5	74.0	71.0	115.4	101.0	96.0	105.0	119.0
May	19.4	62.4	81.6	61.2	40.0	61.2	51.3	43.0	39.9	90.0	82.0	134.7	133.0	126.0	132.0	145.0
Jun	19.0	40.1	50.0	37.6	32.0	37.6	37.0	33.0	38.7	105.0	98.0	144.0	127.0	143.0	143.0	151.0
Jul	19.5	39.5	45.0	29.9	18.0	29.9	28.4	21.0	31.3	109.0	105.0	143.5	122.0	119.0	108.0	132.0
Aug	19.0	36.8	34.0	22.2	19.0	22.2	21.6	17.0	23.0	101.0	104.0	129.9	92.0	104.0	111.0	109.0
Sep	17.8	19.0	11.0	15.5	8.0	15.5	13.4	12.0	16.2	104.0	99.0	78.4	38.0	74.0	60.0	72.0
Oct	17.8	12.3	13.4	10.2	13.0	10.2	11.2	12.0	10.7	93.0	82.0	65.8	40.0	62.0	79.0	75.0
Nov	16.9	15.7	11.5	10.0	9.0	10.0	8.8	15.0	11.5	89.0	84.0	70.9	58.0	73.0	70.0	85.0
Dec	17.3	25.8	17.1	13.6	12.0	13.6	8.7	24.0	17.8	82.0	75.0	74.2	77.0	88.0	76.0	89.0
Winter	48.8	79.2	93.0	48.3	57.0	48.3	37.1	92.0	73.9	231.0	197.0	222.4	233.0	248.0	209.0	272.0
Spring	54.7	219.7	243.0	192.3	166.0	192.3	163.3	148.0	144.9	238.0	220.0	348.7	343.0	321.0	322.0	360.0
Summer	57.6	116.4	129.0	89.7	69.0	89.7	87.0	71.0	92.9	315.0	307.0	417.4	341.0	366.0	362.0	392.0
Fall	52.4	47.0	40.0	35.7	30.0	35.7	33.3	39.0	38.3	286.0	265.0	215.1	136.0	209.0	209.0	232.0
Annual	213.5	462.3	505.0	365.9	322.0	365.9	320.8	350.0	350.1	1070.0	989.0	1203.6	1053.0	1144.0	1102.0	1256.0

Area Model	Area Model	Area Model	Area UNESCO	UNESCO Runoff Location
848F (km**2)	A51M (km**2)	C003 (km**2)	Milliman Meade (km**2)	Ogdensburg, New York
1140000	1140000	1140000	1030000	44.42° N
			764600	75.30° W

DANUBE (Moderately Wet)

	Runoff Obs	UNESCO	R(tot) 848F	R(tot) C003	R(m) C003	R(tot) B100	R(m) B100	R(tot) A51M	R(m) A51M	R(tot) 947B	R(m) 947B	R(m) 947B	Precip Obs	Precip Legates	Precip Shea	Precip 848F	Precip C003	Precip 100	Precip A51M	Precip 947B	
	(mm**2)	(km**2)	(km**2)	(km**2)	(km**2)	(km**2)	(km**2)	(km**2)	(km**2)	(km**2)	(km**2)	(km**2)	(mm)	(mm)	(mm)	(mm)	(mm)	(mm)	(mm)	(mm)	(mm)
Jan	15.3		21.1	22.0	20.2	38.0	31.7	55.0	44.0	52.0	51.3	51.3	68.0	89.0	89.0	51.8	95.0	103.0	119.0	129.0	
Feb	14.0		28.0	31.0	25.4	33.0	31.8	51.0	47.8	59.0	51.0	51.0	64.0	80.0	80.0	69.0	97.0	94.0	112.0	139.0	
Mar	16.7		27.1	42.0	37.8	50.0	43.2	69.0	61.9	72.0	66.6	66.6	61.0	80.0	80.0	85.3	136.0	142.0	138.0	183.0	
Apr	21.9		29.9	30.0	34.2	30.0	37.3	37.0	53.3	45.0	59.2	59.2	70.0	87.0	87.0	99.5	126.0	116.0	140.0	157.0	
May	23.6		46.8	56.0	46.5	58.0	46.2	77.0	58.2	79.0	62.4	62.4	96.0	112.0	112.0	131.2	199.0	193.0	229.0	222.0	
Jun	21.6		32.5	48.0	48.0	39.0	43.6	63.0	68.8	72.0	73.2	73.2	114.0	130.0	130.0	116.1	193.0	164.0	221.0	250.0	
Jul	18.8		24.4	30.0	38.9	23.0	29.6	40.0	52.3	41.0	60.7	60.7	110.0	125.0	125.0	95.2	137.0	124.0	161.0	200.0	
Aug	14.3		14.0	12.0	21.4	13.0	17.1	27.0	35.4	34.0	35.9	35.9	97.0	108.0	108.0	62.5	60.0	73.0	131.0	173.0	
Sep	11.4		8.5	7.0	10.5	11.0	11.4	16.0	23.1	15.0	25.8	25.8	78.0	90.0	90.0	52.8	49.0	72.0	90.0	96.0	
Oct	11.1		12.7	6.0	7.0	17.0	14.8	17.0	17.8	24.0	20.8	20.8	71.0	98.0	98.0	63.8	55.0	103.0	104.0	133.0	
Nov	13.0		25.0	9.0	7.5	15.0	14.7	28.0	21.1	37.0	28.8	28.8	83.0	96.0	96.0	87.9	61.0	76.0	107.0	142.0	
Dec	15.4		28.3	16.0	13.3	25.0	19.9	36.0	32.9	55.0	47.2	47.2	78.0	97.0	97.0	79.8	81.0	89.0	131.0	160.0	
Winter	44.7		77.4	69.0	58.9	96.0	83.4	142.0	124.8	166.0	151.5	151.5	210.0	266.0	266.0	200.6	273.0	286.0	362.0	428.0	
Spring	62.2		103.8	128.0	118.5	138.0	126.7	183.0	173.4	196.0	188.1	188.1	227.0	279.0	279.0	316.0	461.0	451.0	507.0	562.0	
Summer	54.8		70.9	90.0	108.3	75.0	90.3	130.0	156.4	147.0	169.8	169.8	321.0	363.0	363.0	273.8	390.0	361.0	513.0	623.0	
Fall	35.5		46.2	22.0	25.0	43.0	40.8	61.0	61.9	76.0	75.3	75.3	232.0	284.0	284.0	204.5	165.0	251.0	301.0	371.0	
Annual	197.1		298.3	309.0	310.7	352.0	341.2	516.0	516.4	585.0	584.8	584.8	990.0	1192.0	1192.0	994.9	1289.0	1349.0	1683.0	1984.0	

UNESCO Runoff Location
Central Iznic, Romania

Lat 45.11'N
Long 28.48'E

Area Model	Area Model	Area Model	Area Model
(km**2)	(km**2)	(km**2)	(km**2)
850000	1530000	810000	807000

COLUMBIA (Moderately Wet)

	Runoff Obs	R(tot) 848F 1XCO2	R(tot) C903 1XCO2	R(m) C003 1XCO2	R(tot) B100 1XCO2	R(m) B100 1XCO2	R(tot) A51M 1XCO2	R(m) A51M 1XCO2	R(tot) 947B 2XCO2	R(m) 947B 2XCO2	Precip Obs Shes	Precip 848F 1XCO2	Precip C903 1XCO2	Precip B100 1XCO2	Precip A51M 1XCO2	Precip 947B 2XCO2
Jan	8.5	54.0	17.0	16.0	22.0	24.0	42.0	43.8	47.0	39.5	55.0	99.1	65.0	67.0	84.0	100.0
Feb	8.3	44.5	35.0	28.0	20.0	18.1	30.0	33.8	52.0	46.8	38.0	71.4	84.0	43.0	61.0	88.0
Mar	10.7	40.8	45.0	41.0	44.0	33.5	28.0	30.8	29.0	42.0	38.0	57.8	73.0	64.0	67.0	79.0
Apr	14.9	40.4	72.0	60.2	51.0	47.4	25.0	25.8	12.0	20.7	31.0	56.6	78.0	54.0	83.0	49.0
May	26.4	26.3	35.0	50.4	19.0	32.0	29.0	27.3	28.0	20.2	32.0	88.7	85.0	84.0	91.0	82.0
Jun	33.4	16.9	15.0	21.9	15.0	15.0	20.0	24.0	22.0	24.3	31.0	70.9	64.0	80.0	80.0	83.0
Jul	23.6	8.2	7.0	10.0	5.0	8.2	8.0	14.8	11.0	17.0	16.0	50.2	38.0	38.0	46.0	57.0
Aug	13.3	1.6	4.0	4.9	1.0	2.2	2.0	5.0	3.0	7.2	20.0	19.4	20.0	15.0	22.0	30.0
Sep	8.9	0.6	0.0	1.7	1.0	0.6	0.0	1.3	1.0	2.2	24.0	12.3	5.0	12.0	18.0	18.0
Oct	7.8	5.1	2.0	1.5	3.0	2.0	8.0	5.2	13.0	7.8	35.0	41.4	19.0	36.0	64.0	78.0
Nov	7.7	15.8	13.0	8.9	14.0	9.2	12.0	9.9	14.0	12.6	47.0	62.4	69.0	64.0	63.0	63.0
Dec	8.3	49.9	13.0	13.1	32.0	25.1	44.0	27.4	33.0	24.3	56.0	123.0	69.0	102.0	101.0	100.0
Winter	25.1	148.4	65.0	57.1	74.0	67.2	116.0	105.0	132.0	110.6	149.0	293.5	218.0	212.0	246.0	288.0
Spring	52.0	107.5	152.0	151.7	114.0	112.9	82.0	83.9	69.0	82.9	101.0	203.1	236.0	202.0	241.0	210.0
Summer	70.3	26.7	26.0	36.8	21.0	25.4	30.0	43.9	36.0	48.5	67.0	140.5	122.0	133.0	148.0	170.0
Fall	24.3	21.5	15.0	12.0	18.0	11.9	20.0	16.4	28.0	22.5	106.0	116.1	93.0	113.0	139.0	159.0
Annual	171.7	304.1	258.0	257.6	227.0	217.3	348.0	249.1	265.0	264.6	423.0	753.2	669.0	660.0	774.0	827.0

UNESCO Runoff Location
Dalles, Oregon

Lat 45 36' N
Long 121 11' W

Area Model	Area Model	Area Model	Area Milliman Meade	Area UNESCO
848F (km**2)	A51M (km**2)	C003 (km**2)	(km**2)	(km**2)
690000	710000	710000	670000	614000

ZAMBESI (Moderately Wet)

	Runoff Obs	R(tot) 848F 1XCO2	R(tot) C003 1XCO2	R(m) C003 1XCO2	R(tot) B100 1XCO2	R(m) B100 1XCO2	R(tot) AS1M 1XCO2	R(m) AS1M 1XCO2	R(tot) 947B 2XCO2	R(m) 947B 2XCO2	Precip Obs Legates	Precip Obs Shes	Precip 848F 1XCO2	Precip C003 1XCO2	Precip B100 1XCO2	Precip AS1M 1XCO2	Precip 947B 2XCO2
Jan	9.4	45.3	45.0	40.8	38.0	31.5	40.0	27.9	45.0	33.4	270.0	260.0	266.9	222.0	249.0	262.0	296.0
Feb	7.0	60.5	47.0	44.7	41.0	38.3	45.0	38.9	48.0	43.0	237.0	229.0	299.5	194.0	227.0	243.0	260.0
Mar	12.4	56.9	39.0	46.1	35.0	39.1	44.0	4.1	44.0	48.6	189.0	172.0	249.2	151.0	192.0	221.0	225.0
Apr	10.6	23.8	15.0	25.7	13.0	21.6	24.0	35.6	23.0	36.1	62.0	62.0	113.8	60.0	78.0	126.0	130.0
May	8.9	6.1	3.0	9.4	3.0	8.8	3.0	17.2	3.0	17.0	15.0	11.0	42.6	19.0	23.0	25.0	25.0
Jun	10.4	3.4	1.0	2.5	0.0	2.5	0.0	3.6	0.0	3.4	9.0	6.0	32.9	9.0	13.0	6.0	8.0
Jul	12.2	1.1	0.0	0.7	0.0	0.8	0.0	0.5	0.0	0.5	6.0	5.0	17.1	6.0	14.0	6.0	3.0
Aug	5.2	1.1	0.0	0.3	0.0	0.5	0.0	0.2	0.0	0.1	6.0	5.0	24.1	7.0	18.0	10.0	6.0
Sep	5.2	1.3	2.0	1.2	2.0	1.1	3.0	1.2	3.0	0.5	9.0	9.0	29.4	29.0	45.0	42.0	46.0
Oct	6.1	3.4	7.0	4.8	7.0	5.3	4.0	2.6	6.0	3.6	37.0	34.0	68.9	75.0	94.0	63.0	86.0
Nov	7.1	15.6	13.0	10.7	14.0	10.5	14.0	7.0	12.0	8.0	134.0	129.0	185.8	102.0	157.0	167.0	142.0
Dec	10.8	37.1	32.0	25.1	24.0	19.8	21.0	15.4	28.0	19.1	244.0	238.0	269.7	184.0	209.0	185.0	248.0
Winter	27.2	142.9	124.0	110.6	103.0	89.6	106.0	82.1	121.0	95.5	751.0	727.0	836.1	600.0	685.0	690.0	804.0
Spring	31.9	86.8	57.0	81.2	51.0	69.6	71.0	99.9	70.0	101.7	266.0	245.0	405.6	230.0	293.0	372.0	380.0
Summer	27.9	5.6	1.0	3.6	0.0	3.8	0.0	4.2	0.0	3.9	21.0	16.0	74.1	22.0	45.0	22.0	17.0
Fall	18.4	20.3	22.0	16.7	23.0	16.9	21.0	10.8	21.0	12.0	180.0	172.0	284.1	206.0	296.0	272.0	274.0
Annual	105.4	255.6	204.0	212.0	177.0	179.9	198.0	197.0	212.0	213.1	1218.0	1160.0	1599.9	1038.0	1319.0	1356.0	1475.0

UNESCO Runoff Location
Matundo-Cala, Mozambique

Area Model 848F (km**2)	Area Model AS1M (km**2)	Area Model C003 (km**2)	Area Milliman Metade (km**2)	Area UNESCO (km**2)	Lat 16.09°S	Long 33.35°E
1260000	1190000	1190000	1200000	940000		

FRASER (Moderately Wet)

	Runoff Obs	UNESCO	R(tot) 848F 1XCO2	R(tot) C903 1XCO2	R(m) C903 1XCO2	R(tot) B100 1XCO2	R(m) B100 1XCO2	R(tot) A51M 1XCO2	R(m) A51M 1XCO2	R(tot) 947B 2XCO2	R(m) 947B 2XCO2	Precip Obs Legates	Precip Obs Shea	Precip 848F 1XCO2	Precip C903 1XCO2	Precip B100 1XCO2	Precip A51M 1XCO2	Precip 947B 2XCO2
Jan	2.7		28.2	20.0	19.3	25.0	21.9	22.0	21.1	28.0	26.1	22.0	25.0	33.5	35.0	34.0	38.0	37.0
Feb	2.3		25.9	11.0	11.8	14.0	13.2	18.0	18.3	20.0	21.1	16.0	19.0	28.0	41.0	16.0	28.0	24.0
Mar	2.7		19.6	35.0	33.2	15.0	12.7	18.0	18.2	13.0	15.2	15.0	19.0	17.9	30.0	25.0	25.0	25.0
Apr	5.1		15.5	65.0	60.0	19.0	16.5	16.0	15.4	6.0	7.1	10.0	11.0	19.0	27.0	18.0	23.0	20.0
May	13.8		14.8	18.0	23.5	8.0	11.1	10.0	12.9	12.0	10.4	10.0	12.0	29.0	35.0	28.0	27.0	28.0
Jun	16.2		5.7	11.0	12.0	7.0	6.1	8.0	7.9	9.0	9.7	11.0	13.0	22.0	33.0	28.0	26.0	29.0
Jul	14.7		3.3	8.0	7.9	4.0	3.7	4.0	5.1	7.0	7.6	9.0	11.0	17.3	29.0	22.0	21.0	28.0
Aug	10.5		1.8	4.0	4.6	2.0	1.7	3.0	3.1	4.0	4.4	9.0	13.0	11.4	19.0	12.0	17.0	18.0
Sep	7.3		2.4	2.0	1.8	1.0	1.1	1.0	1.3	3.0	3.1	12.0	14.0	12.7	11.0	10.0	8.0	16.0
Oct	5.1		6.4	7.0	6.3	4.0	3.2	6.0	5.3	10.0	8.7	18.0	21.0	24.6	24.0	22.0	29.0	35.0
Nov	3.6		10.1	18.0	17.5	9.0	7.6	9.0	8.7	15.0	13.3	22.0	25.0	26.2	39.0	31.0	28.0	34.0
Dec	3.0		25.5	16.0	16.2	19.0	17.1	19.0	17.2	19.0	19.3	25.0	28.0	45.9	39.0	32.0	37.0	35.0
Winter	8.0		79.6	47.0	47.2	58.0	52.2	59.0	56.6	67.0	66.5	63.0	72.0	107.4	115.0	82.0	103.0	96.0
Spring	21.6		49.9	118.0	116.6	42.0	40.3	44.0	46.5	31.0	32.8	35.0	42.0	65.9	92.0	71.0	75.0	73.0
Summer	41.3		10.8	23.0	24.5	13.0	11.4	15.0	16.0	20.0	21.7	29.0	37.0	50.7	81.0	62.0	64.0	75.0
Fall	16.0		18.9	27.0	25.6	14.0	11.9	16.0	15.3	28.0	25.0	52.0	60.0	63.5	74.0	63.0	65.0	85.0
Annual	87.0		159.2	215.0	213.9	127.0	115.8	134.0	134.3	146.0	146.0	179.0	211.0	287.5	362.0	278.0	307.0	329.0

UNESCO Runoff Location
Hope, British Columbia

Lat 49°23' N
Long 121°22' W

Area Model	Area Model	Area Model	Area Model	Area UNESCO
848F (km**2)	A51M (km**2)	C903 (km**2)	Milliman Mende (km**2)	(km**2)
240000	230000	240000	220000	217000

NIGER (Moderately Wet)

	Runoff Obs	UNESCO	R(848F)	R(C903)	R(B100)	R(A51M)	R(947B)	R(947B)	R(947B)	R(947B)	Precip Obs	Precip Sheb	Precip 848F	Precip C903	Precip B100	Precip A51M	Precip 947B	Precip 947B
			1XC02	1XC02	1XC02	1XC02	2XC02	2XC02	2XC02	2XC02	Obs	Shea	1XC02	1XC02	1XC02	1XC02	1XC02	947B
Jan	4.2		21.9	22.0	22.0	15.0	21.7	19.0	18.1	7.0	7.0	91.3	83.0	101.0	94.0	139.0		
Feb	3.4		19.8	19.0	18.0	11.0	13.3	18.0	17.2	15.0	15.0	95.7	86.0	110.0	85.0	138.0		
Mar	2.8		16.9	26.0	24.8	12.0	11.9	13.0	14.5	44.0	44.0	121.6	136.0	120.0	121.0	139.0		
Apr	1.5		14.4	24.0	23.4	9.0	9.5	9.0	11.1	83.0	83.0	124.7	151.0	139.0	118.0	141.0		
May	0.6		12.8	29.0	25.6	12.0	10.5	10.0	10.1	144.0	144.0	129.0	191.0	154.0	138.0	157.0		
Jun	0.2		18.2	25.0	24.4	14.0	12.6	10.0	9.9	200.0	200.0	159.2	169.0	194.0	164.0	168.0		
Jul	0.3		33.1	34.0	28.8	31.0	22.0	20.0	14.3	278.0	278.0	227.5	222.0	306.0	244.0	237.0		
Aug	1.4		50.4	47.0	37.5	61.0	39.4	25.0	20.1	319.0	319.0	269.2	262.0	329.0	356.0	265.0		
Sep	2.7		55.7	59.0	48.4	63.0	52.3	33.0	25.0	273.0	273.0	254.2	292.0	307.0	310.0	287.0		
Oct	3.3		46.0	59.0	59.1	53.0	56.1	25.0	28.5	131.0	131.0	199.2	259.0	258.0	241.0	212.0		
Nov	3.7		35.6	41.0	53.9	32.0	48.3	17.0	24.1	31.0	31.0	141.1	163.0	175.0	148.0	144.0		
Dec	4.2		25.4	33.0	43.4	18.0	34.5	13.0	17.8	9.0	9.0	104.2	122.0	113.0	97.0	114.0		
Winter	11.9		67.1	74.0	93.5	44.0	69.5	50.0	53.1	31.0	31.0	291.2	291.0	324.0	276.0	391.0		
Spring	4.9		44.1	79.0	73.8	33.0	31.9	32.0	35.7	271.0	271.0	375.3	478.0	413.0	377.0	437.0		
Summer	1.9		101.7	106.0	90.7	106.0	74.1	55.0	44.3	849.0	797.0	655.9	653.0	829.0	764.0	670.0		
Fall	9.8		137.3	159.0	161.3	148.0	156.7	75.0	77.6	454.0	435.0	594.5	714.0	740.0	699.0	643.0		
Annual	28.4		350.2	418.0	419.4	331.0	332.2	212.0	210.7	1618.0	1534.0	1916.9	2136.0	2306.0	2116.0	2141.0		

UNESCO Runoff Location
Niamey, Niger

13.31°N
2.07°E

Area Model	Area Model	Area Model	Area UNESCO
(km**2)	A51M (km**2)	C903 (km**2)	(km**2)
1210000	1490000	1490000	257438

INDUS (Dry)

	Runoff Obs	R(m) 848F 1XCO2	R(tot) C003 1XCO2	R(m) C003 1XCO2	R(tot) B100 1XCO2	R(m) B100 1XCO2	R(tot) A51M 1XCO2	R(m) A51M 1XCO2	R(tot) 947B 2XCO2	R(m) 947B 2XCO2	R(m) A51M 1XCO2	R(tot) 947B 2XCO2	R(m) 947B 2XCO2	Precip Obs Shea	Precip Obs Legates	Precip 848F 1XCO2	Precip C003 1XCO2	Precip B100 1XCO2	Precip A51M 1XCO2	Precip 947B 2XCO2
Jan	0.8	23.1	3.0	2.1	12.0	7.5	40.0	26.3	21.0	18.8	29.0	28.0	28.0	90.3	36.0	37.0	82.0	56.0		
Feb	0.6	47.1	3.0	2.9	31.0	19.1	39.0	35.3	11.0	16.5	30.0	25.0	25.0	124.1	48.0	82.0	71.0	36.0		
Mar	1.4	79.5	2.0	2.6	13.0	23.7	45.0	43.2	24.0	16.0	35.0	35.0	35.0	90.8	39.0	41.0	73.0	67.0		
Apr	1.6	41.2	21.0	9.4	25.0	17.8	23.0	38.5	9.0	18.5	26.0	24.0	24.0	73.7	44.0	23.0	55.0	41.0		
May	3.1	25.8	73.0	42.6	25.0	25.3	16.0	24.9	16.0	12.2	17.0	19.0	19.0	55.8	38.0	26.0	64.0	53.0		
Jun	5.1	52.8	52.0	62.6	3.0	15.8	4.0	13.2	4.0	12.6	24.0	28.0	28.0	34.4	82.0	24.0	40.0	36.0		
Jul	13.6	8.3	21.0	39.9	0.0	2.3	3.0	4.6	1.0	4.0	84.0	94.0	94.0	24.0	85.0	10.0	38.0	15.0		
Aug	31.2	2.1	7.0	15.3	0.0	0.5	2.0	2.2	1.0	1.0	79.0	87.0	87.0	26.4	39.0	9.0	31.0	23.0		
Sep	14.1	0.6	9.0	7.7	1.0	0.6	2.0	1.9	1.0	1.0	36.0	44.0	44.0	12.1	40.0	9.0	22.0	10.0		
Oct	2.7	1.3	5.0	7.5	0.0	0.6	2.0	1.4	4.0	1.6	10.0	13.0	13.0	21.3	38.0	7.0	22.0	33.0		
Nov	1.0	7.6	1.0	3.7	2.0	1.1	5.0	2.7	14.0	6.3	6.0	6.0	6.0	49.6	28.0	23.0	34.0	61.0		
Dec	0.9	12.9	1.0	1.5	4.0	3.0	23.0	9.7	19.0	15.5	16.0	13.0	13.0	57.1	26.0	23.0	60.0	58.0		
Winter	2.4	83.1	7.0	6.4	47.0	29.6	102.0	71.3	51.0	50.8	75.0	66.0	66.0	271.5	110.0	142.0	213.0	150.0		
Spring	6.1	146.5	96.0	54.5	63.0	66.8	84.0	106.5	49.0	46.6	78.0	78.0	78.0	220.3	121.0	90.0	192.0	161.0		
Summer	49.8	63.2	80.0	117.8	3.0	18.5	9.0	20.0	6.0	17.5	187.0	209.0	209.0	84.8	206.0	43.0	109.0	74.0		
Fall	17.9	9.5	15.0	18.8	3.0	2.3	9.0	6.0	19.0	8.8	52.0	63.0	63.0	83.0	106.0	39.0	78.0	104.0		
Annual	76.2	302.3	198.0	197.6	116.0	117.2	204.0	203.8	125.0	123.8	392.0	416.0	416.0	659.6	543.0	314.0	592.0	489.0		

UNESCO Runoff Location
Coord, Pakistan

Lat	Long
25.22' N	
68.22' E	

Area Model	Area Model	Area Model	Area Model	Area UNESCO
848F (km**2)	A51M (km**2)	C003 (km**2)	Milliman Meade (km**2)	832418
830000	830000	830000	970000	832418

TIGRIS-EUPHRATES (Dry)

Area Model	Area (km**2)	Runoff Obs	R(tot) 848F 1XCO2	R(tot) C903 1XCO2	R(m) C903 1XCO2	R(tot) B100 1XCO2	R(m) B100 1XCO2	R(tot) AS1M 1XCO2	R(m) AS1M 1XCO2	R(m) 947B 2XCO2	R(tot) 947B 2XCO2	R(m) 947B 2XCO2	Precip Obs Legates	Precip Obs Shea	Precip 848F 1XCO2	Precip C903 1XCO2	Precip B100 1XCO2	Precip AS1M 1XCO2	Precip 947B 2XCO2
Jan	3.7	14.9	18.0	12.2	14.0	12.5	17.0	11.7	15.0	11.2	15.0	11.2	76.0	58.0	65.1	71.0	69.0	75.0	66.0
Feb	4.6	7.4	21.0	16.2	14.0	11.6	31.0	12.9	11.0	12.1	11.0	12.1	68.0	51.0	45.5	56.0	66.0	52.0	46.0
Mar	7.4	7.3	31.0	23.6	6.0	10.7	6.0	10.0	2.0	10.0	2.0	10.0	64.0	51.0	40.5	42.0	37.0	39.0	19.0
Apr	10.7	5.8	6.0	23.5	7.0	6.4	2.0	5.9	1.0	2.8	1.0	2.8	54.0	45.0	43.8	31.0	38.0	18.0	13.0
May	11.9	13.4	18.0	12.2	16.0	9.4	10.0	4.4	15.0	4.9	15.0	4.9	35.0	31.0	61.8	68.0	67.0	56.0	76.0
Jun	6.3	3.9	7.0	13.5	4.0	10.5	2.0	6.9	2.0	10.2	2.0	10.2	16.0	17.0	36.6	24.0	32.0	26.0	22.0
Jul	2.8	0.7	1.0	6.1	1.0	3.9	1.0	3.0	1.0	3.7	1.0	3.7	11.0	12.0	11.9	5.0	11.0	26.0	21.0
Aug	1.6	1.0	0.0	1.1	0.0	0.7	1.0	1.5	1.0	1.2	1.0	1.2	10.0	13.0	19.1	3.0	7.0	17.0	17.0
Sep	1.2	1.3	1.0	0.4	1.0	0.5	1.0	1.2	1.0	1.1	1.0	1.1	12.0	18.0	20.5	14.0	16.0	26.0	25.0
Oct	1.3	6.0	6.0	2.4	3.0	1.7	4.0	1.8	6.0	3.6	6.0	3.6	28.0	26.0	47.5	45.0	34.0	43.0	55.0
Nov	1.7	9.3	7.0	6.1	7.0	3.9	8.0	5.3	11.0	7.3	11.0	7.3	53.0	44.0	59.9	41.0	53.0	57.0	68.0
Dec	2.5	8.3	10.0	8.7	13.0	9.6	12.0	11.4	10.0	9.0	10.0	9.0	70.0	55.0	47.4	42.0	73.0	62.0	53.0
Winter	10.8	30.6	49.0	37.1	41.0	33.8	40.0	36.0	36.0	32.2	36.0	32.2	214.0	164.0	158.0	169.0	208.0	189.0	165.0
Spring	30.0	26.5	55.0	59.2	29.0	26.5	18.0	20.4	18.0	17.7	18.0	17.7	153.0	127.0	146.1	141.0	142.0	112.9	108.0
Summer	10.7	5.6	8.0	20.7	5.0	15.1	4.0	11.3	4.0	15.1	4.0	15.1	37.0	42.0	67.6	32.0	50.0	69.0	60.0
Fall	4.1	16.6	14.0	8.9	11.0	6.0	13.0	8.3	18.0	12.0	18.0	12.0	93.0	88.0	127.9	100.0	103.0	126.0	148.0
Annual	55.5	79.3	126.0	125.9	86.0	81.5	75.0	76.0	76.0	77.0	76.0	77.0	497.0	421.0	499.6	442.0	503.0	497.0	481.0

UNESCO Runoff Location
 Baghdad (Tigris), Hindiya (Euphrates), Iraq
 Lat 33.18' N 33.43' N
 Long 44.21' E 44.16' E

Area Model AS1M (km**2) 1150000
 Area Model C903 (km**2) 1150000
 Area Milliman Meade (km**2) 1050000
 Area UNESCO (km**2) 408100

YELLOW (Dry)

	Runoff Obs UNESCO	R(104) 848F 1XC02	R(104) C003 1XC02	R(m) C003 1XC02	R(104) B100 1XC02	R(m) B100 1XC02	R(104) A51M 1XC02	R(m) A51M 1XC02	R(104) 947B 2XC02	R(m) 947B 2XC02	R(104) 947B 2XC02	R(m) 947B 2XC02	Precip Obs Legates	Precip Obs Sites	Precip 848F 1XC02	Precip C003 1XC02	Precip B100 1XC02	Precip A51M 1XC02	Precip 947B 2XC02
Jan	1.5	1.4	14.0	13.2	0.0	1.2	0.0	1.2	8.0	6.0	6.0	6.0	5.0	5.0	29.5	38.0	17.0	22.0	34.0
Feb	1.3	5.1	21.0	16.4	4.0	3.7	9.0	3.7	19.0	14.8	14.8	14.8	9.0	9.0	46.2	55.0	30.0	42.0	57.0
Mar	2.7	18.9	18.0	19.8	16.0	11.4	18.0	14.0	10.0	12.7	15.0	15.0	15.0	15.0	68.6	71.0	63.0	61.0	47.0
Apr	2.4	20.1	12.0	13.6	27.0	22.5	44.0	30.8	36.0	22.2	30.0	30.0	32.0	32.0	91.6	58.0	91.0	117.0	104.0
May	2.3	67.1	51.0	34.5	108.0	71.4	92.0	65.1	80.0	57.2	49.0	48.0	48.0	48.0	172.8	155.0	232.0	210.0	178.0
Jun	1.6	111.3	35.0	41.1	108.0	101.5	98.0	87.2	72.0	72.8	66.0	66.0	62.0	62.0	259.8	147.0	248.0	218.0	200.0
Jul	4.1	70.7	39.0	37.8	71.0	82.7	88.0	86.3	117.0	83.4	131.0	125.0	125.0	115.0	189.5	167.0	197.0	218.0	269.0
Aug	6.8	58.9	34.0	35.6	48.0	57.2	55.0	73.0	101.0	105.5	118.0	115.0	115.0	115.0	163.8	158.0	147.0	165.0	225.0
Sep	7.4	94.7	16.0	22.8	50.0	46.5	76.0	63.3	145.0	125.6	67.0	71.0	71.0	71.0	204.7	77.0	136.0	179.0	273.0
Oct	4.5	58.8	9.0	13.7	51.0	54.6	67.0	83.9	111.0	137.9	29.0	34.0	34.0	34.0	133.1	50.0	122.0	150.0	185.0
Nov	2.0	6.0	14.0	13.5	12.0	30.8	14.0	45.3	6.0	63.0	15.0	16.0	16.0	16.0	23.3	67.0	41.0	54.0	28.0
Dec	1.8	0.5	12.0	14.0	2.0	7.6	2.0	9.1	4.0	9.3	7.0	7.0	6.0	6.0	20.5	45.0	23.0	18.0	42.0
Winter	4.5	7.0	47.0	43.6	6.0	10.7	11.0	14.0	31.0	30.1	21.0	20.0	20.0	20.0	96.2	138.0	70.0	82.0	133.0
Spring	7.4	106.1	81.0	67.9	151.0	105.3	154.0	109.9	126.0	92.0	94.0	95.0	95.0	95.0	333.0	284.0	386.0	388.0	329.0
Summer	12.5	240.9	108.0	114.4	227.0	241.3	241.0	246.5	290.0	261.6	315.0	302.0	302.0	302.0	613.1	472.0	592.0	601.0	694.0
Fall	13.8	159.5	39.0	50.0	113.0	131.9	157.0	192.5	262.0	326.5	111.0	121.0	121.0	121.0	361.1	194.0	299.0	383.0	486.0
Annual	38.3	513.5	275.0	275.9	497.0	489.2	563.0	562.8	709.0	710.3	541.0	538.0	538.0	538.0	1403.4	1088.0	1347.0	1454.0	1642.0

UNESCO Runoff Location
Sanmenxia, China

Lat 34.69° N
Long 111.27° E

Area Model	Area Model	Area Model	Area UNESCO
848F (km**2)	A51M (km**2)	C003 (km**2)	Milliman Mesole (km**2)
1130000	1060000	1060000	740000
			688421

COLORADO (Dry)

Runoff Obs	R(tot) 848F 1XCO2	R(tot) C903 1XCO2	R(m) C903 1XCO2	R(tot) B100 1XCO2	R(m) B100 1XCO2	R(tot) A51M 1XCO2	R(m) A51M 1XCO2	R(tot) 947B 2XCO2	R(m) 947B 2XCO2	Precip Obs Legates	Precip Obs Shees	Precip 848F 1XCO2	Precip C903 1XCO2	Precip B100 1XCO2	Precip A51M 1XCO2	Precip 947B 2XCO2
Jan	0.6	8.8	4.0	4.2	14.0	13.8	8.0	8.2	17.0	18.0	16.0	37.6	20.0	39.0	31.0	53.0
Feb	0.6	11.6	6.0	5.2	8.0	8.2	12.0	10.3	17.0	17.0	13.0	50.0	19.0	30.0	38.0	50.0
Mar	0.8	12.6	6.0	5.5	14.0	12.6	11.0	11.3	10.0	17.0	15.0	43.4	28.0	42.0	42.0	46.0
Apr	1.0	11.8	3.0	3.0	6.0	6.9	11.0	11.2	4.0	14.0	12.0	27.5	18.0	25.0	45.0	19.0
May	1.8	11.0	5.0	4.9	9.0	9.5	11.0	11.0	8.0	12.0	11.0	51.0	31.0	44.0	44.0	35.0
Jun	2.7	6.1	2.0	2.5	4.0	4.7	2.0	4.3	2.0	9.0	9.0	37.7	16.0	32.0	15.0	12.0
Jul	1.6	2.7	1.0	1.3	2.0	2.0	1.0	1.5	0.0	26.0	20.0	29.0	12.0	24.0	18.0	6.0
Aug	0.8	1.4	0.0	0.3	1.0	1.4	0.0	0.6	1.0	29.0	22.0	25.5	2.0	21.0	9.0	9.0
Sep	0.6	0.6	0.0	0.0	0.0	0.5	0.0	0.2	1.0	18.0	14.0	9.2	1.0	11.0	3.0	11.0
Oct	0.6	2.8	0.0	0.2	5.0	4.0	1.0	0.8	4.0	16.0	15.0	27.4	4.0	39.0	22.0	35.0
Nov	0.5	6.9	2.0	1.4	5.0	5.2	3.0	2.2	9.0	12.0	11.0	44.4	17.0	38.0	26.0	46.0
Dec	0.6	6.7	4.0	4.1	19.0	17.4	10.0	8.0	18.0	17.0	14.0	35.2	30.0	63.0	46.0	63.0
Winter	1.8	27.1	14.0	13.5	41.0	39.4	30.0	26.4	52.0	52.0	43.0	122.8	69.0	132.0	115.0	166.0
Spring	3.5	35.4	14.0	13.4	29.0	29.0	33.0	33.4	22.0	43.0	38.0	121.9	77.0	111.0	131.0	100.0
Summer	5.1	10.2	3.0	4.0	7.0	8.0	3.0	6.4	3.0	64.0	51.0	92.2	30.0	77.0	42.0	27.0
Fall	1.7	10.3	2.0	1.6	10.0	9.7	4.0	3.2	14.0	46.0	40.0	81.0	22.0	88.0	51.0	92.0
Annual	12.1	83.0	33.0	32.5	87.0	86.0	70.0	69.4	91.0	205.0	172.0	417.9	198.0	408.0	339.0	385.0

UNESCO Runoff Location
Yuma, Arizona

Lat 32.44' N
Long 114.55' W

Area Model	Area Model	Area Model	Area UNESCO
848F (km**2)	A51M (km**2)	C903 (km**2)	Milliman Merde (km**2)
650000	640000	640000	629100

LENA (High Latitude Dry)

Area Model	Area (km**2)	Runoff Obs	R(tot) 848F 1XCO2	R(tot) C003 1XCO2	R(m) B100 1XCO2	R(tot) B100 1XCO2	R(m) B100 1XCO2	R(tot) A51M 1XCO2	R(m) A51M 1XCO2	R(tot) 947B 2XCO2	R(m) 947B 2XCO2	Precip Obs Legates	Precip Obs Shea	Precip 848F 1XCO2	Precip C003 1XCO2	Precip B100 1XCO2	Precip A51M 1XCO2	Precip 947B 2XCO2	Precip 947B 2XCO2
Jan	7.0	7.0	0.0	1.0	1.9	0.0	0.2	0.0	0.3	0.0	1.2	32.0	25.0	36.3	51.0	49.0	50.0	56.0	56.0
Feb	4.6	4.6	0.0	1.0	1.3	0.0	0.0	0.0	0.0	0.0	0.4	23.0	19.0	39.8	49.0	37.0	39.0	49.0	49.0
Mar	3.7	3.7	0.2	8.0	2.1	0.0	0.0	8.0	0.2	23.0	1.2	26.0	20.0	57.4	90.0	65.0	68.0	82.0	82.0
Apr	2.9	2.9	79.7	81.0	16.4	81.0	14.5	164.0	19.2	262.0	39.9	46.0	37.0	97.1	133.0	112.0	103.0	125.0	125.0
May	12.0	12.0	219.6	271.0	123.4	296.0	130.4	148.0	142.9	158.0	222.7	72.0	66.0	169.9	200.0	192.0	166.0	212.0	212.0
Jun	191.3	191.3	76.2	186.0	259.0	88.0	226.3	48.0	140.6	52.0	161.3	121.0	118.0	200.8	255.0	222.0	203.0	237.0	237.0
Jul	104.7	104.7	62.0	115.0	160.6	62.0	98.3	66.0	66.4	68.0	72.5	163.0	164.0	241.1	330.0	255.0	270.0	288.0	288.0
Aug	72.3	72.3	64.2	32.0	113.5	66.0	66.0	70.0	63.5	66.0	69.2	164.0	157.0	220.6	270.0	236.0	238.0	241.0	241.0
Sep	63.2	63.2	30.0	63.0	97.0	35.0	57.1	23.0	60.7	31.0	59.0	109.0	101.0	129.4	193.0	162.0	116.0	145.0	145.0
Oct	38.6	38.6	7.3	16.0	57.9	9.0	29.9	8.0	29.8	17.0	33.1	74.0	65.0	94.8	129.0	125.0	105.0	106.0	106.0
Nov	8.5	8.5	0.3	3.0	18.0	1.0	10.0	0.0	9.9	3.0	15.7	54.0	45.0	66.8	75.0	81.0	69.0	86.0	86.0
Dec	7.3	7.3	0.1	2.0	4.5	0.0	2.0	0.0	2.0	0.0	5.1	42.0	33.0	53.2	64.0	54.0	59.0	85.0	85.0
Winter	18.8	18.8	0.1	4.0	7.7	0.0	2.2	0.0	2.3	0.0	6.7	97.0	77.0	129.3	164.0	140.0	148.0	190.0	190.0
Spring	18.6	18.6	299.5	360.0	141.9	377.0	145.0	320.0	162.3	443.0	263.7	144.0	123.0	324.4	423.0	369.0	337.0	419.0	419.0
Summer	368.3	368.3	202.4	333.0	533.1	216.0	390.5	184.0	270.4	186.0	302.9	448.0	439.0	662.5	855.0	713.0	711.0	766.0	766.0
Fall	110.3	110.3	37.6	82.0	172.9	45.0	97.0	31.0	100.4	51.0	107.8	237.0	211.0	291.0	397.0	368.0	290.0	337.0	337.0
Annual	516.1	516.1	539.6	779.0	855.5	638.0	634.7	535.0	535.4	680.0	681.1	926.0	850.0	1407.2	1839.0	1590.0	1486.0	1712.0	1712.0

UNESCO Runoff Location

Kussar, USSR

Lat 70.42' N
Long 127.39' W

Area Model	Area (km**2)	Area Model	Area (km**2)	Area Model	Area (km**2)	UNESCO	Area (km**2)
848F	2400000	A51M	2400000	C003	2400000	Milliman Meade	2500000
Annual	2310000					UNESCO	2430000

SEVERNAY DVINA (High Latitude Dry)

	Runoff Obs UNESCO	R(848F) 1XC02	R(tot) C003 1XC02	R(m) C003 1XC02	R(tot) B100 1XC02	R(m) B100 1XC02	R(tot) A51M 1XC02	R(m) A51M 1XC02	R(947B) 2XC02	R(m) 947B 2XC02	Precip Obs Legates	Precip Obs Shea	Precip 848F 1XC02	Precip C003 1XC02	Precip B100 1XC02	Precip A51M 1XC02	Precip 947B 2XC02
Jan	2.7	1.0	1.0	1.5	0.0	0.8	0.0	0.5	2.0	6.6	15.0	10.0	17.0	17.0	17.0	15.0	19.0
Feb	2.0	0.8	1.0	0.8	0.0	0.4	1.0	0.8	9.0	6.2	12.0	8.0	15.4	14.0	15.0	14.0	14.0
Mar	1.9	9.4	17.0	10.2	10.0	5.7	13.0	7.5	57.0	37.4	11.0	9.0	12.8	22.0	15.0	15.0	27.0
Apr	6.0	65.8	64.0	49.5	60.0	40.5	81.0	56.5	31.0	44.9	10.0	11.0	16.0	23.0	18.0	24.0	25.0
May	37.2	23.9	22.0	39.0	23.0	36.0	18.0	42.7	14.0	18.6	15.0	15.0	20.4	32.0	22.0	23.0	47.0
Jun	18.7	2.9	10.0	11.2	4.0	5.3	4.0	7.6	9.0	11.0	20.0	20.0	22.0	35.0	25.0	24.0	35.0
Jul	8.1	3.0	9.0	10.3	4.0	3.8	3.0	3.5	6.0	7.5	24.0	23.0	21.4	31.0	25.0	22.0	32.0
Aug	6.1	2.0	7.0	7.5	3.0	3.1	2.0	2.1	6.0	6.6	24.0	22.0	17.2	27.0	22.0	14.0	32.0
Sep	6.3	2.5	4.0	4.7	2.0	2.3	2.0	2.0	3.0	4.1	21.0	20.0	19.4	16.0	17.0	19.0	17.0
Oct	8.1	4.3	7.0	5.8	5.0	3.5	4.0	3.5	7.0	4.9	20.0	19.0	22.2	25.0	23.0	29.0	27.0
Nov	6.4	1.1	7.0	6.9	4.0	4.1	3.0	3.7	7.0	7.1	18.0	14.0	20.8	22.0	19.0	23.0	20.0
Dec	3.7	0.8	3.0	4.0	2.0	2.7	1.0	1.4	13.0	10.3	16.0	12.0	19.0	20.0	19.0	19.0	27.0
Winter	8.4	2.6	5.0	6.3	2.0	3.8	2.0	2.7	24.0	23.1	43.0	30.0	51.4	51.0	51.0	48.0	60.0
Spring	45.1	99.1	103.0	98.6	93.0	82.2	112.0	106.6	102.0	100.9	36.0	35.0	49.2	77.0	55.0	62.0	99.0
Summer	32.8	7.9	26.0	28.9	11.0	12.2	9.0	13.2	21.0	25.0	68.0	65.0	60.6	93.0	72.0	60.0	99.0
Fall	20.8	7.9	18.0	17.4	11.0	9.9	9.0	9.1	17.0	16.0	59.0	53.0	62.4	63.0	59.0	71.0	64.0
Annual	107.1	117.5	152.0	151.2	117.0	108.1	132.0	131.6	164.0	165.0	206.0	183.0	223.6	284.0	237.0	241.0	322.0

UNESCO Runoff Location
Ust-Pinega, USSR

Lat 64.06°N
Long 42.10°E

Area	Area	Area	Area	Area
Model	Model	Model	Milliman	UNESCO
848F	A51M	C003	Meade	(km**2)
(km**2)	(km**2)	(km**2)	(km**2)	(km**2)
330000	340000	340000	350000	348000

References

- Abramopoulos, F., C. Rosenzweig, and B. Choudhury, 1988: Improved ground hydrology calculations for global climate models (GCMs): Soil water movement and evapotranspiration. *Journal of Climate*, **1**, 921-941.
- Arakawa, A., 1972: Design of the UCLA General Circulation Model. Tech. Rep. No. 7. Dept. Meteor., University of California, Los Angeles, 116 pp.
- Ayers, M.A., G.D. Tasker, D.M. Wolak, G.J. McCabe, and L.E. Hay, 1990: Simulated effects of climatic change on runoff and drought in the Delaware river basin. *Annu Civ Eng Conv Expo*. Published by ASCE, New York, NY, 31-38.
- Baumgartner, A., E. Reichel, 1975: *The World Water Balance*. Elsevier, Amsterdam.
- Critchfield, H.J., 1974: *General Climatology*, Prentice-Hall, Englewood Cliffs, New Jersey, 446 pp.
- Flaschko, I., C.W. Stockton, and W.R. Boggess, 1987: Climate variation and surface water resources in the Great Basin Region. *Water Resources Bulletin*, **23**, 47-57.
- Gates, W.L., and A.B. Nelson, 1975: A new (revised) tabulation of the Scripps topography on a 1° global grid. Part I, Terrain heights, Rep. R-1276-1, Adv. Res. Proj. Agency, Rand Corporation, Santa Monica, California, 132 pp.
- Gleick, P.H., 1987: Regional hydrological consequences of increases in atmospheric CO₂ and other trace gases. *Clim. Change*, **10**, 137-160.
- Gordon, A.L., and W.F. Stern, 1982: A description of the GFDL Global Spectral Model. *Monthly Weather Review*, **110**, 625-644.
- Hansen, J., G. Russell, D. Rind, P. Stone, A. Lacis, S. Lebedeff, R. Ruedy, and L. Travis, 1983: Efficient three-dimensional global models for climate studies: Models I and II. *Monthly Weather Review*, **111**, 609-662.

- Hansen, J., A. Lacis, D. Rind, G. Russell, P. Stone, I. Fung, R. Ruedy, and J. Lerner, 1984: Climate sensitivity: Analysis of feedback mechanisms, in *Climate Processes and Climate Sensitivity. Geophys. Monogr.*, **29**, edited by J.E. Hansen and T. Takahashi, 130-163.
- John Bartholomew and Son, 1967: *Times Atlas of the World*, Comprehensive edition, 2nd ed., Houghton Mifflin, Boston, Mass.
- Korzoun, V.I., A.A. Sokolov, M.I. Budyko, K.P. Voskresensky, G.P. Kalinin, A.A. Konoplyantsev, E.S. Korotkevich, and M.I. Lovich, (Eds.), 1977: *Atlas of World Water Balance*. USSR National Committee for the International Hydrological Decade, UNESCO Press, Paris.
- Kuhl, S., 1990: Predicting Monthly River Runoff Using Atmospheric Global Circulation Models, M.S. Thesis, Rutgers University, New Brunswick, NJ.
- Kuhl, S.C., and J.R. Miller, 1992: Seasonal river runoff calculated from a global atmospheric model. *Water Resources Research*, **28**, 2029-2039.
- Legates, D., and C. Willmott, 1990: Mean seasonal and spatial variability in gauge-corrected, global precipitation. *Int. J. Climatol.*, **10**, 111-127.
- Lettenmaier, D.P., and T.Y. Gan, 1990: Hydrologic sensitivities of the Sacramento-San Joaquin River Basin, California, to global warming. *Water Resources*, **26**, 69-86.
- Manabe, S., and D.G. Hahn, 1981: Simulation of atmospheric variability. *Monthly Weather Review*, **109**, 2260-2286.
- Manabe, S., and R.J. Stouffer, 1980: Sensitivity of a global climatic model to an increase of CO₂ concentration on the atmosphere. *J. Geophys. Res.*, **85**, 5529-5554.
- Matthews, E., 1983: Global vegetation and land use: New high-resolution data bases for climate studies. *J. Climate Applied Meteorology*, **22**, 474-487.
- Miller, D., 1977: *Water at the Surface of the Earth*, Academic, San Diego, California, 191 pp.

- Miller, J.R., and G.L. Russell, 1992: The impact of global warming on river runoff. *Journal of Geophysical Research*, **97**, 2757-2764.
- Miller, J.R., G.L. Russell, G. Caliri, 1992: Continental scale river flow in climate models. To be submitted.
- Millman, J.D., and R.H. Meade, 1983: World-wide delivery of river sediment to the oceans, *J. Geology*, **91**, 1-21.
- Mitchell, J.F.B., 1989: The "greenhouse" effect and climate change. *Rev. Geophys.*, **27**, 115-139.
- Pitcher, E.J., R.C. Malone, V. Ramanathan, M.L. Blackmon, K. Puri, and W. Bourke, 1983: January and July simulations with a spectral general circulation model. *Journal of Atmospheric Science*, **40**, 580-604.
- Rind, D., R. Goldberg, J. Hansen, C. Rosenzweig, and R. Ruedy, 1990: Potential evapotranspiration and the likelihood of future drought. *Journal of Geophysical Research*, **95**, 9983-10,003.
- Rind, D., 1988: The doubled CO₂ climate and the sensitivity of the modeled hydrologic cycle. *Journal of Geophysical Research*, **93**, 5385-5412.
- Roos, M., 1989: Possible climate change and its impact on water supply in California. *Oceans I*, 247-249.
- Russell, Gary L., and J.R. Miller, 1990: Global river runoff calculated from a global atmospheric general circulation model. *Journal of Hydrology*, **117**, 241-254.
- Shea, D., 1986: Climatological Atlas: 1950-1979, Surface Air Temperature, Precipitation, Sea-Level Pressure and Sea-Surface Temperature (45°S-90°N), NCAR, Boulder Colorado, Tech. Note/TN-269+STR.
- Singh, V.P., 1989: *Hydrologic Systems, Vol. II, Watershed Modeling*, Prentice-Hall, Englewood Cliffs, New Jersey, 320 pp.

- Stockton, C.W., and W.R. Boggess, 1979: Geohydrological Implications of Climate Change on Water Resources Development. Report prepared for the U.S. Army Coastal Engineering Research Center, Fort Belvoir, Virginia, Contract Rpr. No. CACW 72-78-C-0031, 206 pp.
- Stouffer, R.J., S. Manabe, and K. Bryan, 1989: Interhemispheric asymmetry in climate response to a gradual increase of atmospheric CO₂. *Nature*, **342**, 660-662.
- Thornthwaite, C.W., and J.R. Mather, 1955: The Water Balance. Drexel Institute of Technology, Laboratory of Climatology, Publications in Climatology, **VIII**.
- UNESCO, 1969: Discharge of selected rivers of the world: Volume 1. General and regime characteristics of stations selected: UNESCO, 7 Place de Fontenoy, Paris.
- UNESCO, 1974: Discharge of selected rivers of the world: Volume 3, part 2. Mean monthly and extreme discharges (1969-1972): UNESCO, 7 Place de Fontenoy, Paris.
- UNESCO, 1985: Discharge of selected rivers of the world: Volume 3, part 4. Mean monthly and extreme discharges (1976-1979): UNESCO, 7 Place de Fontenoy, Paris.
- United States Geological Survey, 1987: USGS Daily Values, US West Optical Publishing, 90 Madison St., Suite 200, Denver Colorado.
- Vörösmarty, C.J., B. Moore, A.L. Grace, M.P. Gildea, J.M. Melillo, B.J. Peterson, E.B. Rastetter, and P.A. Steudler, 1989: Continental scale models of water balance and fluvial transport: An application to South America. *Global Biogeochem. Cycles*, **3**, 241-265.
- Williamson, D.L., 1983: Description of the NCAR Community Climate Model (CCM0B), NCAR Technical Report, NCAR/TN-210+STR, 88 pp.